University of Windsor
Scholarship at UWindsor

Electronic Theses and Dissertations | Theses, Dissertations, and Major Papers

1985

DEFORMATIONS OF HOLLOW STRUCTURAL SECTIONS SUBJECTED TO COLD BENDING.

MOKHTAR MAHMOUD. SEDDEIK
University of Windsor

Follow this and additional works at: https://scholar.uwindsor.ca/etd

Recommended Citation
SEDDEIK, MOKHTAR MAHMOUD., "DEFORMATIONS OF HOLLOW STRUCTURAL SECTIONS SUBJECTED TO COLD BENDING." (1985). *Electronic Theses and Dissertations*. 1617.
https://scholar.uwindsor.ca/etd/1617

This online database contains the full-text of PhD dissertations and Masters' theses of University of Windsor students from 1954 forward. These documents are made available for personal study and research purposes only, in accordance with the Canadian Copyright Act and the Creative Commons license—CC BY-NC-ND (Attribution, Non-Commercial, No Derivative Works). Under this license, works must always be attributed to the copyright holder (original author), cannot be used for any commercial purposes, and may not be altered. Any other use would require the permission of the copyright holder. Students may inquire about withdrawing their dissertation and/or thesis from this database. For additional inquiries, please contact the repository administrator via email (scholarship@uwindsor.ca) or by telephone at 519-253-3000ext. 3208.

CANADIAN THESES ON MICROFICHE

I.S.B.N.

THESES CANADIENNES SUR MICROFICHE

National Library of Canada
Collections Development Branch

Canadian Theses on
Microfiche Service

Ottawa, Canada
K1A 0N4

Bibliothèque nationale du Canada
Direction du développement des collections

Service des thèses canadiennes
sur microfiche

NOTICE

The quality of this microfiche is heavily dependent upon the quality of the original thesis submitted for microfilming. Every effort has been made to ensure the highest quality of reproduction possible.

If pages are missing, contact the university which granted the degree.

Some pages may have indistinct print especially if the original pages were typed with a poor typewriter ribbon or if the university sent us a poor photocopy.

Previously copyrighted materials (journal articles, published tests, etc.) are not filmed.

Reproduction in full or in part of this film is governed by the Canadian Copyright Act, R.S.C. 1970, c. C-30. Please read the authorization forms which accompany this thesis.

THIS DISSERTATION
HAS BEEN MICROFILMED
EXACTLY AS RECEIVED

AVIS

La qualité de cette microfiche dépend grandement de la qualité de la thèse soumise au microfilmage. Nous avons tout fait pour assurer une qualité supérieure de reproduction.

S'il manque des pages, veuillez communiquer avec l'université qui a conféré le grade.

La qualité d'impression de certaines pages peut laisser à désirer, surtout si les pages originales ont été dactylographiées à l'aide d'un ruban usé ou si l'université nous a fait parvenir une photocopie de mauvaise qualité.

Les documents qui font déjà l'objet d'un droit d'auteur (articles de revue, examens publiés, etc.) ne sont pas microfilmés.

La reproduction, même partielle, de ce microfilm est soumise à la Loi canadienne sur le droit d'auteur, SRC 1970, c. C-30. Veuillez prendre connaissance des formules d'autorisation qui accompagnent cette thèse.

LA THÈSE A ÉTÉ
MICROFILMÉE TELLE QUE
NOUS L'AVONS REÇUE

NL-339 (r. 82/08)

Canada

DEFORMATIONS OF HOLLOW STRUCTURAL SECTIONS SUBJECTED TO COLD BENDING

by
Mokhtar Mahmoud Seddeik

A Dissertation
submitted to the Faculty of Graduate Studies through the Department of Civil Engineering in Partial Fulfillment of the requirements for the Degree of Doctor of Philosophy at The University of Windsor

©

Windsor, Ontario, Canada
1985

© Mokhtar Mahmoud Seddeik 1985
All Rights Reserved

To my family

ABSTRACT

Cold bending of Hollow Structural Sections (HSS) of rectangular and square geometry results in permanent distortion of their cross-sections. The main objective of this study is to predict the relationship between the radius of bend imposed on the HSS and such distortions.

A theoretical study is carried out using the variational principle of the total potential energy and a Rayleigh-Ritz type procedure. Displacement functions in the form of Fourier series are employed to describe the deformed shape of the HSS after rolling. Non-linear strain-displacement relations are used to account for geometric non-linearity. Plastic deformations are assumed to be governed by the Von-Mises yield criterion and the total deformation theory of plasticity. The analysis also accounts for linear strain hardening of the material in the plastic range.

At any instant of the rolling process, the loading on the HSS member consists of a concentrated load applied at its mid-point as well as friction between the member and the rollers of the bending machine. To model the rolling process the load is assumed to be applied successively at different points along the length of the member causing it to deform plastically.

The resulting deflection at mid-span of the member is related to its relaxed radius of bend by studying its geometry during the rolling process. The results of the theoretical analysis is compared to that obtained from an experimental program. The good agreement between the results substantiates the validity of the proposed method of analysis.

The minimum radius of bend of an HSS is calculated by specifying an upper limit for the magnitude of distortions allowed in its cross-section. Two different parameters are assumed to define that upper limit. The minimum radii calculations could be based on either one depending on the engineering judgement of the designer. The recommended minimum radii based on this study are compared to those recommended by three different steel companies; little or no agreement was found. A possible reason for the disagreement is the lack of a common criterion defining the maximum distortion allowed in the cross-section.

ACKNOWLEDGEMENT

The author wishes to express his sincere thanks and gratitude to his advisor, Dr. J. B. Kennedy, for suggesting the topic of this research. Dr. Kennedy devoted his time and effort to make this study a success. Throughout the course of this work Dr. Kennedy maintained constant supervision and provided many valuable suggestions and recommendations. His confidence, support and encouragement were most invaluable in the completion of this work.

Thanks are also due to Dr. G. Abdel-Sayed and Dr. G. Monforton of the Civil Engineering Department, Dr. D. Watt of the Engineering Material Department and Dr. M. Shridher of the Electrical Engineering Department. Their willingness to assist at all times is most appreciated.

The financial assistance provided by CIDECT through the Steel Company of Canada (STELCO) is greatly appreciated.

The author is really indebted to his wife, Maha. Her understanding, encouragement and patience made the completion of the graduate program possible.

The author is also grateful to his parents and parents-in-law for their continued encouragement and support.

TABLE OF CONTENTS

ABSTRACT v

ACKNOWLEDGEMENT vii

LIST OF TABLES xi

LIST OF FIGURES xiii

NOMENCLATURE xv

CHAPTER

I. INTRODUCTION 1

1.1 General 1
1.2 Mechanism of the Rolling Process 2
1.3 Motivation and Objectives 5
1.4 Scope 7

II. LITERATURE REVIEW 10

2.1 General 10
2.2 Stability of Thin Walled Sections . . . 11
2.3 Non-Linear Analysis 13
2.4 Rolling Process 16

III. BASICS OF THE THEORETICAL ANALYSIS 18

3.1 General 18
3.2 Justification of the Analytical Method . 19
3.3 The Rayleigh-Ritz Method 21
3.4 Geometric Non-linearity 22
3.4.1 Methods of Calculation 22
3.4.2 Strain-Displacement Relations . . 25
3.5 Stress-Strain Curve 26
3.6 Elastic Stress-Strain Relations 26
3.7 Material Non-Linearity 28
3.7.1 Yield Criterion 29
3.7.2 Incremental and Deformation Theories 30
3.7.3 Plastic Stress-Strain Relations . 31

IV. ENERGY FORMULATION 34

4.1 General 34
4.2 Theoretical Model 35

4.3 Boundary Conditions 35
4.4 Displacement Functions 38
4.4.1 Overall Displacements 40
4.4.2 Local Displacements 42
4.4.3 Effect of Shear 44
4.4.4 Total Displacement Functions . . 45
4.4.5 Comments on the Displacement Functions 46
4.5 Total Potential Energy 47
4.5.1 Strain Energy 47
4.5.2 External Work 50
4.6 Evaluation of the Total Potential Energy (T.P.E.) 51
4.6.1 Numerical Calculations of the T.P.E. 51
4.6.2 Comments 53
4.7 Minimization of the Total Potential Energy 55
4.7.1 Introduction to Function Minimization 55
4.7.2 Minimization Techniques 57

V. MODELLING OF THE ROLLING PROCESS 60

5.1 General 60
5.2 Radius of Curvature 61
5.3 Effect of Friction 66
5.4 Residual Stresses 71
5.5 Analytical Procedure 74

VI. EXPERIMENTAL PROGRAM 78

6.1 General 78
6.2 Specimen Details 79
6.3 Machine Description 79
6.4 Testing Procedure 82
6.5 Analysis of the Experimental Results . . 85
6.6 Moment of Inertia of the Deformed Sections 105

VII. RESULTS OF THE THEORETICAL ANALYSIS 111

7.1 General 111
7.2 Convergence of the Displacement Functions 113
7.3 Comparison with Reference Example . . . 116
7.4 Displacement and Stress Distribution . . 119
7.5 Effect of the Number of Elements in the Mesh Subdivision 120

7.6 Effect of Friction 128

7.7 Distribution of Residual Stresses 130
7.8 Comparison Between Theoretical and Experimental Results 132
7.9 Parametric Study 140

VIII. MINIMUM RADIUS OF BEND 149

8.1 General 149
8.2 Minimum Radii Recommended by the Steel Companies 150
8.3 Recommended Minimum Radii 150
8.4 Comparison Between Recommended and Published Minimum Radii 155

IX. SUMMARY AND CONCLUSIONS 162

9.1 Summary 162
9.2 Conclusions 166

REFERENCES 169

APPENDIX

A 173
B 176
C 180
D 185
E 190

VITA AUCTORIS 195

LIST OF TABLES

Table		Page
6.1	Properties of the Hollow Sections	80
6.2	Cross-section Dimensions After Rolling	88
6.3	Percentage Change in Properties	94
6.4	Comparison Between the Measured and Estimated Values for p_b	99
6.5	Comparison Between the Measured and Estimated Values for p_e	102
6.6	Reduction in the Moment of Inertia	107
7.1	Conversion of the Displacement Functions . . .	114
7.2	Conversion of the Different Components of Stresses	115
7.3	Residual Stresses in Plates #1 and #2 for Different HSS Profiles	131
7.4	Comparison Between the Theoretical and Experimental Values for p_b	133
7.5	Comparison Between the Theoretical and Experimental Values for p_e	135
7.6	Comparison Between the Calculated and Estimated Values for p_b	141
7.7	Comparison Between the Calculated and Estimated Values for p_e	143
8.1	Minimum Radii of Bend Recommended by U.S. Steel	151
8.2	Minimum Radii of Bend Recommended by British Steel	152
8.3	Minimum Radii of Bend Recommended by Ferrotubi	153

Table		Page
8.4	Comparison Between Measured and Predicted Minimum Radii	156
8.5	Comparison of Recommended Minimum Radii and that of U.S. Steel	158
8.6	Comparison of Recommended Minimum Radii and that of British Steel	159
8.7	Comparison of Recommended Minimum Radii and that of Ferrotubi	160

LIST OF FIGURES

Figure		Page
1.1	Construction of the Pyramid Type Rolling Machine	3
1.2	Three-Roller Bending Machine	4
1.3	Cross-section Distortion Due to the Rolling Process	6
3.1	Co-ordinate axes	24
3.2	Stress-strain Relation	27
4.1	Local Axes of the Four Component Plates	36
4.2	Deformations of the Beam Model Due to the Rolling Process	39
5.1	Geometry of the Specimen at any Instant of the Rolling Process	63
5.2	Applied Forces on the Specimen During the Rolling Process	67
5.3	Bending Moment and Deflection Due to Friction Forces	68
5.4	Residual Stresses	72
6.1	Properties of the HSS	81
6.2	Typical Rolling Arrangement	83
6.3	Dimensions of the Rolls in the Rolling Machines	84
6.4	Longitudinal View of the HSS After Rolling	86
6.5	Side View of the HSS After Rolling	87
6.6	Cross-section Dimensions Before and After Bending	92
7.1	Flow Chart for the Computer Program	112

Figure		Page
7.2	Dimensions and Stress-strain Relations for the Reference Example	117
7.3	Load-deflection Curve	118
7.4	Out of Plane Displacement Profile	121
7.5	Distribution of the In-plane Displacement in the x-direction	122
7.6	Distribution of the In-plane Displacement in the y-direction	123
7.7	Distribution of σ_x for Two Sections at 1/8 and 3/8 the Span of the Model	124
7.8	Distribution of σ_y for two Sections at 1/8 and 3/8 the Span of the Model	125
7.9	Distribution of τ_{xy} for Two Sections at 1/8 and 3/8 the Span of the Model	126
7.10	Distribution of σ_e for Two Sections at 1/8 and 3/8 the Span of the Model	127
7.11	Effect of the Number of Elements on the Overall Deflection	129
7.12	Effect of the Ratio $\frac{h}{t}$ on the Deformations of the Compression Flange	145
7.13	Effect of the Ratio $\frac{h}{t}$ on the Deformations of the Web	146
7.14	Effect of the Ratio $\frac{h}{b}$ on the Deformations of the Compression Flange	147
7.15	Effect of the Ratio $\frac{b}{h}$ on the Deformations of the Web	148

NOMENCLATURE

A_r, B_k, C_{nm}, D_{pq}, G_{ij}, H_g, K_e	unknown coefficients in the displacement functions
A	area of the plate
b	width of the cross-section
b_1	width of the cross-section after rolling
D	membrane stiffness
e	deformation of the compression flange
E	modulus of elasticity
E_p	slope of the stress-strain curve in the plastic range
E_s	secant modulus
F	friction force
F_n	force perpendicular to the beam at the fixed roller
G	shear modulus
h	height of the cross-section
$I_{reduced}$	Moment of inertia after rolling
I_x	moment of inertia about the major axis
I_y	moment of inertia about the minor axis
$k_1(s)$	curvature of the specimen at the exit side of the machine
$k_2(s)$	curvature of the specimen at the entry side of the machine
k_r	relaxed radius of bend
ℓ	length of the beam model
M_f	moment due to friction forces

M_p	plastic moment
P	applied vertical load
P_b	percentage increase in width after bending
P_e	percentage bowing in the compression flange
P_i	percentage change in moment of inertia
R	radius of bend
r_e, r_u	radii of the outer and intermediate rollers, respectively
S	bending stiffness
s_1	distance between the fixed roller, on the exit side, and the middle roller along the center line of the beam
s_2	distance between the two fixed rollers along the center line of the beam
t	thickness of the cross-section
T	total potential energy
u	in-plane displacement in the x-direction
U_e	elastic strain energy
U	total strain energy
v	in-plane displacement in the y-direction
w	out-of-plane displacement
W	external work due to vertical load
W_f	external work due to friction
x,y,z	co-ordinate axes
γ_{xy}	shear strain
γ^t_{xy}	total shear strain
γ^p_{xy}	plastic shear strain

δ	deflection of the beam under rolling
$\varepsilon_x, \varepsilon_y$	strain in the x and y directions, respectively
$\varepsilon_x^t, \varepsilon_y^t$	total strain in the x and y directions, respectively
ε_e^t	effective total strain
$\varepsilon_x^p, \varepsilon_y^p$	plastic strain in the x and y directions, respectively
ε_e^p	effective plastic strain
ε_o	yield strain
η	coefficient of friction
ν	Poisson's ratio
σ_x, σ_y	stress in the x and y direction, respectively
σ_e	effective stress
σ_e'	effective stress at any point along the plastic region of the stress-strain curve
σ_o	yield stress in axial tension
σ_r	residual stresses
τ_{xy}	shear stress

Subscripts of the displacement components:

x,y	denotes differentiation with respect to x and y, respectively. Double subscripts denote second derivative
f	denotes effect of friction

CHAPTER I

INTRODUCTION

1.1 GENERAL

The use of Hollow Structural Sections (HSS) for construction purposes became very popular in the last twenty five years. HSS posses many structural, architectural and economic advantages as structural elements. A widely used type of HSS is one of square or rectangular geometry. These sections can be used in many structures as straight or curved members. There are many potential applications for curved HSS such as in domes, arched roofs, machine parts, subway tunnels, highway barriers, etc.

Mandrels as well as different types of rolling machines are used to produce curved HSS. The choice of any bending method is usually based on both economy and engineering judgement. Availability, cost and the use of the member after rolling are examples of the factors that should be considered when choosing the bending method. In the present study, cold bending by means of a three-roller machine of the pyramid type, was chosen. Compared to other bending methods, the three-roller machine

seemed to be available, economic and most suitable for the large bends required for construction purposes. Rolling machines are commonly used to bend plates or beams with solid sections. To the best knowledge of the author, this is the first study to be conducted on rolling of hollow structural sections.

1.2 MECHANISM OF THE ROLLING PROCESS

The three-roller machine of the pyramid type consists basically of three rollers; two fixed in place, the outer ones, and one movable roller in the middle, Fig. 1.1. The three rollers are mounted vertically in the machine as shown in Fig. 1.2. The specimen is fed into the machine from one side until it is supported on the two outer rollers. The load is applied to the specimen through the intermediate roller by changing its position with respect to the other ones. The load is applied until a certain position of the intermediate roller is achieved. The change in position of the middle roller is equal to the deflection produced in the specimen at their point of contact. The rolling process is then started to force the same deflection to all sections of the specimen as they pass under the middle roller. This deflection can be related to the radius of bend of the specimen by studying its geometry during the rolling process.

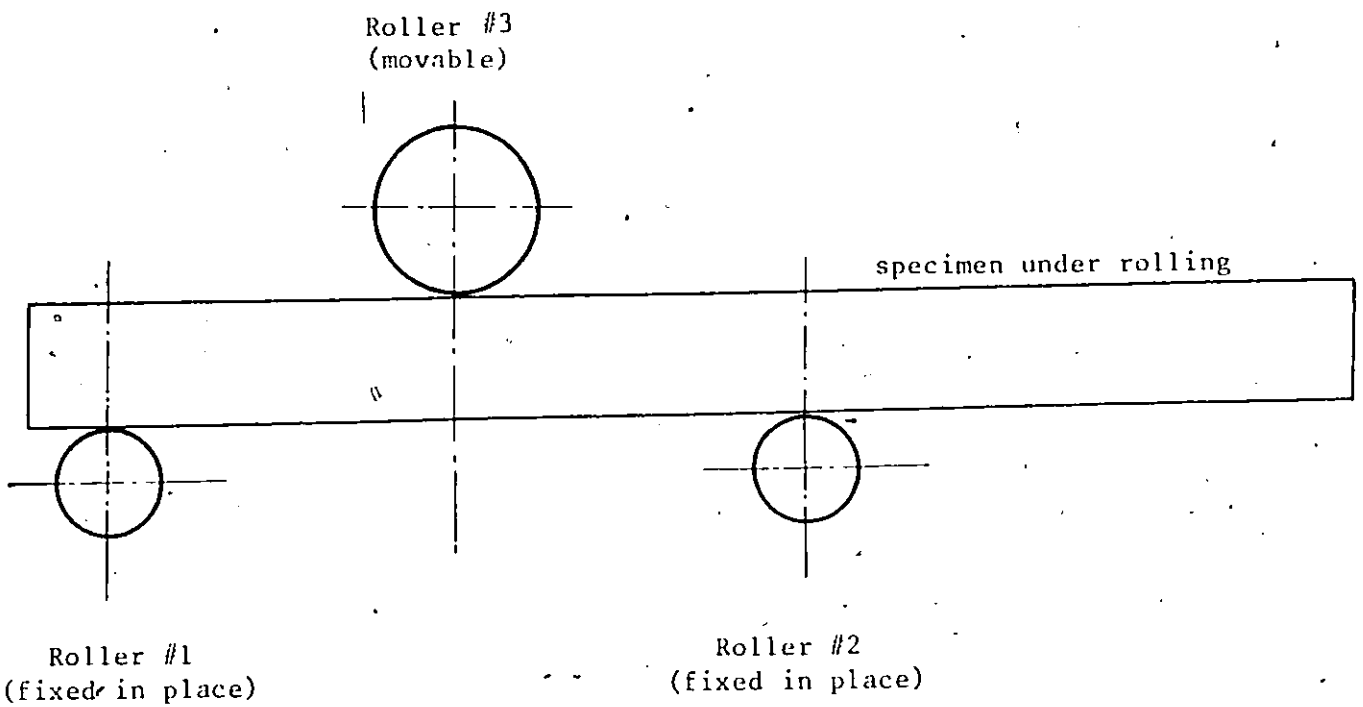

Fig. 1.1. Construction of the pyramid type rolling machine

Fig. 1.2. Three-roller bending machine

1.3 MOTIVATION AND OBJECTIVES

A hollow structural element of square or rectangular cross-section is composed of four thin plates. Because of its strength, rolling of such section requires relatively high loads to achieve a permanent radius of curvature. When these loads are applied during the rolling process, the different components composing the element undergo large permanent local deformations causing distortion in its cross-section as shown in Fig. 1.3. The amount of distortion resulting in an HSS section depends on its dimensions, material properties and the radius of bend imposed.

The distortion of the cross-section may affect its aesthetic appeal or integrity to carry loads when used after rolling. Therefore, conditions or criteria should be adopted to specify certain levels of distortion as the acceptable tolerable limits. Based on these conditions, the minimum radius of bend of an HSS element is determined. There are no common guidelines on which the different steel companies can base their choice of such conditions. The choice is usually arbitrary and can be based on either visual inspection or the structural capacity of the member after bending. Obviously different conditions result in different radii of bend for the same section.

The recommended values for the minimum radii of bend

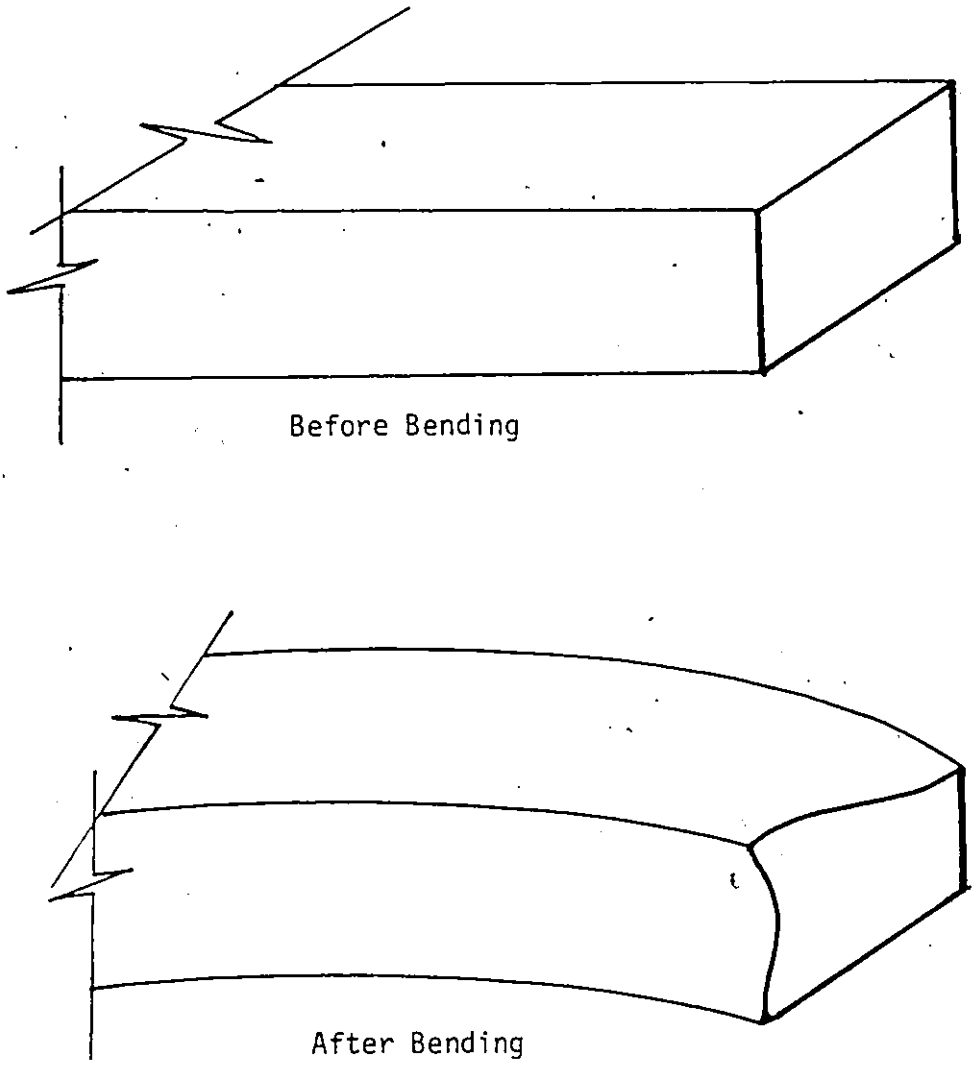

Fig. 1.3. Cross-section distortion due to the rolling process

published by U.S. Steel, British Steel Corporation and the Steel Company of Italy (Ferrotubi) are often contradictory. As these recommended values are based only on results obtained from experimental studies, the need for a theoretical analysis to establish a method to predict the minimum radius of bend for HSS is clear. Therefore, the objectives of the present study are:

1. To develop an analytical approach to calculate the relation between the radius of curvature of cold bent HSS and the resulting distortion in the cross-section.
2. To recommend different conditions that specify an acceptable level of distortion in the cross-section. Based on these conditions the minimum radii for the different HSS profiles can be calculated.
3. To predict the magnitude of the residual stresses resulting from the rolling process in the different parts of the HSS.
4. To verify the analytical solution by comparing its results to those obtained from an experimental study.

1.4 SCOPE

To achieve these objectives, a theoretical analysis is carried out using the variational principle of the total potential energy and a Rayleigh-Ritz type procedure. Displacement functions with unknown coefficients are

assumed to describe the deformed shape of the different components of the hollow section after bending. Expressions for the total potential energy in terms of these displacement functions in both the elastic and plastic ranges are developed. The unknown coefficients of the displacement functions are then evaluated by minimizing the total potential energy using Rosenbrock's method.

Non-linear strain-displacement relations are used to account for the effect of large deformations. A bilinear stress-strain relation with linear strain hardening is assumed to describe the material behaviour under loading. The Von-Mises yield criterion is adopted to determine the initiation of yielding at any point of the beam model and the total deformation theory of plasticity is used to obtain the stress-strain relations in the plastic range.

In the three-roller machine, the load is applied through the middle roller by changing its position with respect to the other two rollers. The relation between the radius of bend of the beam model and the middle roller position is presented. This relation can be obtained by studying the geometry of the model inside the machine during the rolling process. A method is proposed to model the rolling process, the effect of friction between the flanges of the model and the rollers is considered in the

analysis and an estimate of the residual stresses resulting from the rolling process is calculated at different points of the model.

To verify the theoretical analysis, the results are compared to those available from an experimental program. In this program, 54 tests were conducted on 27 different sizes of HSS. Each size was bent to four different radii of curvature. After rolling, sections bent to each of the four radii were accurately measured. Multiple regression analysis was used to obtain relations between the radius of bend, the cross-section properties and the deformations resulting in the cross-section due to the rolling process. A comparison between the theoretical and experimental results is presented.

To calculate the minimum radius of bend, two conditions which define the maximum allowable distortion in the cross-section are used:

(a) Percentage increase in the width of the cross-section after bending.

(b) Percentage bowing in the compression flange after bending.

A comparison between the minimum radii of bend obtained in this study and those published by three different steel companies is presented.

CHAPTER II

LITERATURE REVIEW

2.1 GENERAL

The increasing use of thin plate elements in many structures attracted many researchers towards the study of the different aspects of behaviour of such elements. Stability, large deformations and elasto-plastic analysis are some of these aspects that received most attention.

Closed form solutions for elastic plates subjected to small deflections are now available for many cases of loading and plate end conditions (2, 42, 44). However, numerical methods such as finite difference, finite element, finite strip or energy minimization are usually used if the analysis has to account for either geometric or material non-linearity. The rapid development in digital computers made the application of these numerical methods to many complicated problems possible.

In this chapter, some of the studies conducted on thin walled sections are reviewed. Most of these studies deal with the stability of the different components of the section. A review of the studies on the non-linear behaviour of plates is also presented. No published work is

available on the rolling of beams with hollow sections. However, some of the researches carried out to study the mechanics of the rolling process and the geometry of the deflected shape of plates and beams with solid sections during and after rolling are reviewed.

2.2 STABILITY OF THIN WALLED SECTIONS

Most of the studies carried on thin walled elements are directed towards studying the stability of the different components composing the element. To simplify the problem, many researchers considered only the case of pure moment applied to these elements. The typical approach in analyzing this type of structures was to study the buckling behaviour of the web element treating it as an isolated element constrained along its longitudinal boundaries by stiffness representing the flexural stiffness of the flanges (38). However, when the flanges are themselves relatively thin, the stiffness of the compression flange reduces during the bending process due to the instability under the compressive stresses. So, the problem is then one of interaction between the buckling strength of the compression flange and that of the web and either one can dominate in determining the critical load according to the dimensions of the element.

Graves Smith (12) reported that the first attempt to

analyze thin walled box girders as single integral structure was made by dividing the web of the section into a series of strips each under a locally constant stress. Graves Smith avoided this approximation by using the total potential energy approach. Assuming elastic and small deflection conditions, displacement functions with unknown coefficients were used to represent the out-of-plane deflection of each plate composing the section. Using the Lagrange multiplier method, the unknown coefficients of the displacement functions were obtained at the critical buckling load.

Rockey and Bagchi (39) used the finite element method to solve the problem of web buckling in plate girders under partial edge loading taking the stiffness of the flange into consideration. The study concludes by showing that the effect of the flange thickness on the load distribution in the web and on the buckling load is quite considerable. Tien and Wang (43) used the finite difference method to calculate the effect of stress gradient on the buckling load of thin walled box girders. Two loading cases were used: a uniformly distributed load and a central concentrated load. Higher buckling loads were obtained compared to those calculated from a case of constant stress. Other approaches such as finite element method (32, 37, 47) and finite strip method (14) have also

been used to study the buckling problem.

2.3 NON-LINEAR ANALYSIS

Non-linear analysis can include either geometric or material non-linearity effects depending on the behaviour of the structure under loading. If plastic and large amounts of deformations are expected, both non-linearities have to be considered in the analysis. Because of the complexity of such problems, most of the analysis was directed towards the study of single plates only. However, the general procedures used in the analysis of single plates can be applied to thin walled sections provided that the compatibility conditions at the corners of the section are satisfied.

Graves Smith (13) used the total potential energy approach to study the post-buckling behaviour of thin walled box girders subjected to pure moment. The effect of plasticity was accounted for by using Von-Mises yield criterion and Prandtl-Reuss relations.

Rhodes and Harvey (36) studied the buckling of lipped channel beams subjected to pure moment using the total potential energy approach. They studied the post-buckling of the same section using a semi-energy method in which the stresses and deflection throughout the section are linked by solving Von-Karman's compatibility equations.

The results of the analysis were compared to those obtained from an experimental investigation. The agreement of the results proved the validity of the approach used in the theoretical analysis.

Different approaches have been used by many researchers when studying the non-linear behaviour of plates. Graves Smith (11), Moxham (31) and Little (26) used the total potential energy approach but with different formulations. Graves Smith used sophisticated expressions to represent the deformed shape after elastic buckling. In order to integrate the energy function within the plate thickness, linear distribution of stresses was assumed. The analysis was restricted to situations where unloading from the yield surface did not occur. This usually requires high width to thickness ratios.

Moxham's displacement functions were straight Fourier series. He used the deformation theory to calculate the deformed shape. However, once that shape has been determined the flow theory was used to calculate the stresses and strains.

Little used the incremental flow theory. The number of iteration required to find the minimum of the total potential energy was much less in Little's solution than in the others. This was due to: (i) the use of both the energy function and its gradient vectors to search for the

minimum, and (ii) only the increase in the energy due to the loading increments was minimized as opposed to minimizing the total energy at each load increment. The difference is the value of the total energy at the end of the previous load increment which is constant.

Another approach was tried by Freize (9) and Harding (16) using the dynamic relaxation method. Although the flow theory was used in both studies, different yield criteria were adopted to determine the initiation of yield at the different points. Harding used Von-Mises yield criterion. He divided the plate thickness into a number of layers and the appropriate stress-strain relations were derived at each layer depending on its stress level. To avoid that, Freize used a full section yield criterion proposed by Ilyushin (19). This resulted in a great reduction in computer time and computational efforts.

Finite element method has also been used in many studies. Zienkiewicz (47) reviews most of the work done to consider plasticity and large deformation in the analysis using the finite element method.

Bradfield and Chladny (3) compared all the previous approaches with respect to the number of degrees of freedom, geometrical representation of the plate, stress-strain relations, representation of residual stresses and representation of initial out of flatness.

2.4 ROLLING PROCESS

Many researches are directed towards studying the rolling process of single plates and beams with solid cross-sections. However, due to the complexity of the problem, no studies have been carried out on the rolling of thin walled beams. The mechanics of the rolling process was the main concern of many researchers. Through different approaches, they were able to predict the load and torque required to roll any specimen of any material and dimensions as well as the pressure distribution between the rolls and the material under rolling (17, 20, 21, 41).

Few researches were directed to study the geometry of the specimen during and after rolling. Bassett and Johnson (1) analyzed the plate bending problem using a three-roller pyramid type machine. Two methods of analysis were proposed to predict the final shape of a plate after rolling:

1. Geometric analysis; based on the assumption that the deflected form of the plate is an arc of a circle.
2. A load analysis using the uniaxial stress-strain relation of the material of the plate.

The two methods were applied to the rolling of plates made of two different materials: aluminum and steel. The experimental results were best accounted for by the geometric analysis.

Hanson and Jannerup (15) studied the bending of steel beams with solid rectangular cross-sections by the three-roller machine. An iterative method is used to study the geometry of the deflected shape of the beam during rolling. The calculations based on this method led to a curvature function, for the beam under rolling, which differs from the often assumed function as an arc of a circle. Although shear and friction between the rollers and the beam were neglected in the analysis, agreement between the theoretical model and experimental results was reasonable.

CHAPTER III

BASICS OF THE THEORETICAL ANALYSIS

3.1 GENERAL

Different numerical methods can be used to analyze the HSS rolling problem. A comparison between the finite difference, the finite element and the total potential energy minimization methods yielded the conclusion that the minimization of the total potential energy is most suitable in this case.

As a result of the rolling process, the different components of the HSS member undergo large amounts of deformations in both the elastic and the plastic ranges. Therefore, both geometric and material non-linearities have to be considered in the analysis.

In this chapter a brief comparison between the basic concepts of the finite difference, the finite element and the total potential energy minimization is presented. The basic principles of the Rayleigh-Ritz method of analysis are also given and the methods for accounting for both geometric and material non-linearities are explained.

3.2 JUSTIFICATION OF THE ANALYTICAL METHOD

The equilibrium of linear elastic plates is controlled by one differential equation of the fourth order. Direct solution of this equation is possible for many cases with different boundary conditions and loading. Because of the simplicity of the problem, closed form solutions are available for many of these cases. On the other hand, the behaviour of elastic non-linear plates is described by two differential equations known as Von-Karman's equations (6). In this case, the deflection of the plate creates in-plane forces which in turn affect the magnitude of the deflection. Therefore, the solution of such a problem is often iterative where the in-plane forces in the plate are first assumed so that the deflection can be calculated. Using this deflection a second estimate of the in-plane forces can be obtained. The same procedure continues until the solution converges.

The presence of plasticity introduces a major complication as the stress-strain relation varies from point-to-point in the plate according to the stress level at each point. Only numerical techniques such as the energy minimization, finite difference or finite element methods can be used to obtain a solution for such a problem. To use the finite difference technique to analyze non-linear plastic plates, the two Von-Karman equations have to be

expressed in an incremental form at each point of the finite difference mesh. Using these equations a step-by-step solution can be obtained. Graves Smith (11) gave the complete derivation of these incremental equations. However, he concluded that for an unsymmetric problem that involves more than one plate, such as in the case of a channel or box sections, this method leads to a very large number of equations which make its use unfeasible.

In the finite element method continuous updating of the solution is required to account for both material or geometric non-linearity. The solution should be incremental, where at each increment the stiffness of the whole structure has to be adjusted depending on the magnitude of the applied load as well as the stress level at the different parts of the structure. This process requires large storage capacity and long execution time on the computer.

The energy minimization method is based on the assumption of displacement functions with unknown parameters that represent the deformed shape of the structure and satisfy its boundary conditions. These parameters can be evaluated by minimizing the total potential energy of the structure. This technique is known as Rayleigh-Ritz method. Compared to other methods, the energy minimization has many advan-

tages such as simplicity, small computer storage and, more importantly, the basic method of analysis does not change when material or geometric non-linearity is considered. Based on that, it was decided to use the energy minimization as the method of analysis .

3.3 THE RAYLEIGH-RITZ METHOD

One of the most used methods in solving many structural problems using the energy technique is the Rayleigh-Ritz method. This method can be used in the analysis of deformations, stability, non-linear behaviour and vibration. In this method, a structure having an infinitely large number of degrees of freedom is replaced by a model of finite degrees of freedom. Therefore, to evaluate the deformation of a structure under a system of loading, the deformed shape of the structure is approximated by different displacement functions with unknown coefficients. These displacement functions have to satisfy at least the geometric boundary conditions of the structure and insure compatibility between its different components.

The principle of minimum potential energy is then used to evaluate the magnitude of the unknown coefficients of the displacement functions. This principle states (34): "of all the displacements which satisfy the boundary conditions of a structural system, those corresponding to stable equilibrium configuration make the total potential

energy a relative minimum."

Therefore, the total potential energy is expressed in terms of the unknown coefficients of the displacement functions. These coefficients are then determined so that the total potential energy computed on the basis of these functions is a minimum.

It should be noted that the accuracy of the results obtained when using the Rayleigh-Ritz method depends mainly on the successful choice of the displacement functions that represent the deformed shape of the structure. One of the major drawbacks of this method is that although the displacements could be evaluated fairly accurately, the corresponding stresses may differ significantly from their exact values. This is due to the fact that the stresses are based on the derivatives of the displacements, and obviously the derivatives of an approximate function is less accurate than the function itself (34). Another important characteristic of the Rayleigh-Ritz method is that the differential equation of equilibrium does not enter into the analysis. However, equilibrium is satisfied in an average sense through the minimization of the total potential energy.

3.4 GEOMETRIC NON-LINEARITY

3.4.1 Methods of Calculation

The amount of deformations resulting in any structure

depends on its material characteristics, the magnitude of the applied load as well as on the dimensions and geometry of the structure. If a structure is expected to have small displacements compared to its dimensions, the additional deformation resulting from the change in the structure geometry is considered of secondary magnitude and can be neglected. However, if the structure undergoes large amounts of deformations these secondary deformations will have more dominant effects on the structure behaviour and have to be considered in the analysis. In this case the structure is described to have a geometric non-linear behaviour.

Different methods can be used to account for geometric non-linear behaviour of structures. Pogner (35) summarized these methods in three approaches.

1. Applying the load incrementally and solving a series of linear equations that describe the structure behaviour at each load increment.
2. Formulating a set of non-linear simultaneous equations that govern the behaviour of the structure and then seeking their solution by successive approximation.
3. Using non-linear strain-displacement relations in formulating the problem.

In the present study, since the minimization of the

total potential energy method of analysis is used, the third approach is most appropriate.

3.4.2 Strain-Displacement Relations

A cartisian coordinate system (x,y,z) is introduced such that x and y are the axes in the plane of the middle surface of the plate and z is the perpendicular axis to this plane as shown in Fig. 3-1. The displacement of any point in the middle plane in the x, y and z directions are u, v and w, respectively. The strain components at any point at a distance z from the middle plane are given by:

$$\varepsilon_x = u_x - z\, w_{xx}$$

$$\varepsilon_y = v_y - z w_{yy}$$

$$\gamma_{xy} = u_y + v_x - 2z w_{xy} \qquad (3.1)$$

where

ε_x, ε_y = strain components in the x and y directions, respectively;

γ_{xy} = shear strain;

u,v,w = displacements in the x, y and z directions, respectively; and

z = perpendicular distance between any point and the middle plane of the plate.

The subscripts x and y in the displacement components u, v and w denotes differentiation with respect to x and y, respectively, double subscripts denotes second derivative.

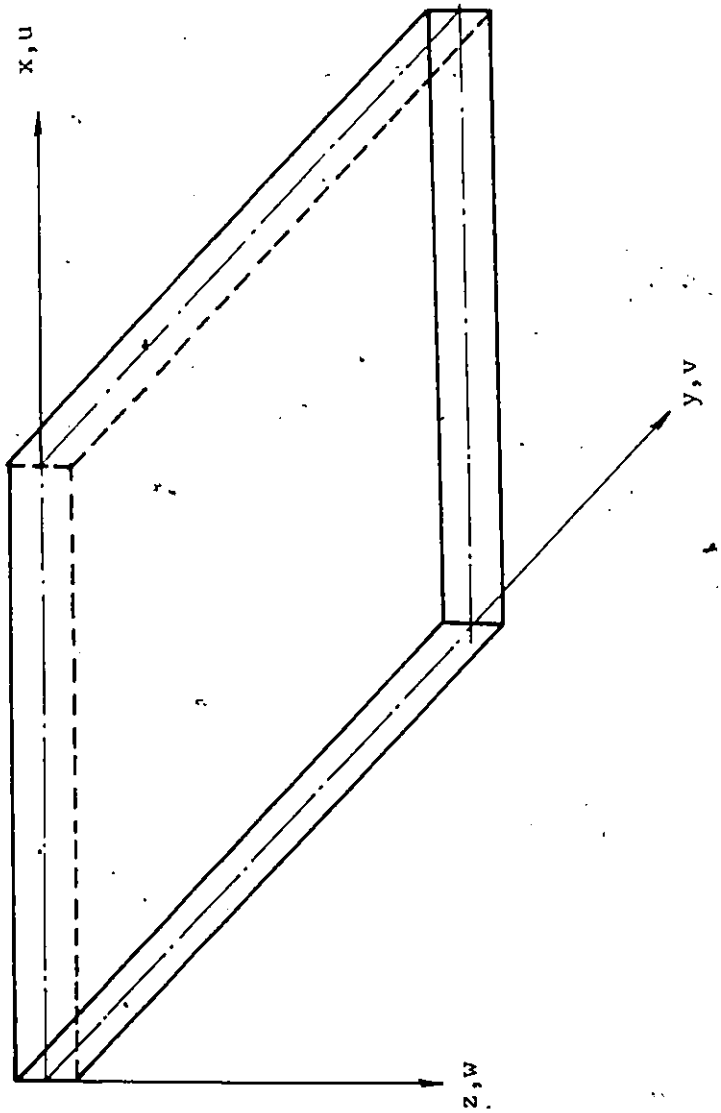

Fig. 3.1. Coordinate axes.

To account for geometric non-linearity, quadratic terms are introduced in the strain displacement relations. The quadratic terms in u and v are neglected because of their small values (25). Therefore, the resulting strain displacement relations can be written as (42):

$$\varepsilon_x = u_x - z\, w_{xx} + 0.5\, w_x^2$$

$$\varepsilon_y = v_y - z\, w_{yy} + 0.5\, w_y^2$$

$$\gamma_{xy} = u_y + v_x - 2z w_{xy} + w_x w_y \qquad (3.2)$$

3.5 STRESS-STRAIN CURVE

To study the material behaviour under loading, simple tension tests were carried out. A series of three tests were conducted using the universal testing machine. Two strain gauges were mounted on each specimen, one on each side, and the average readings of these gauges was used in the analysis. The average results of the stress-strain curves obtained from these tests are shown in Fig. 3.2. Based on the results of these tests, the stress-strain relation can be approximated by a bilinear curve with modulii of elasticity of 200,000 MPa and 5,000 MPa in the elastic and plastic ranges, respectively, as shown in Fig. 3.2 by the two straight lines.

3.6 ELASTIC STRESS-STRAIN RELATIONS

In the elastic range, Hooke's law is used; the

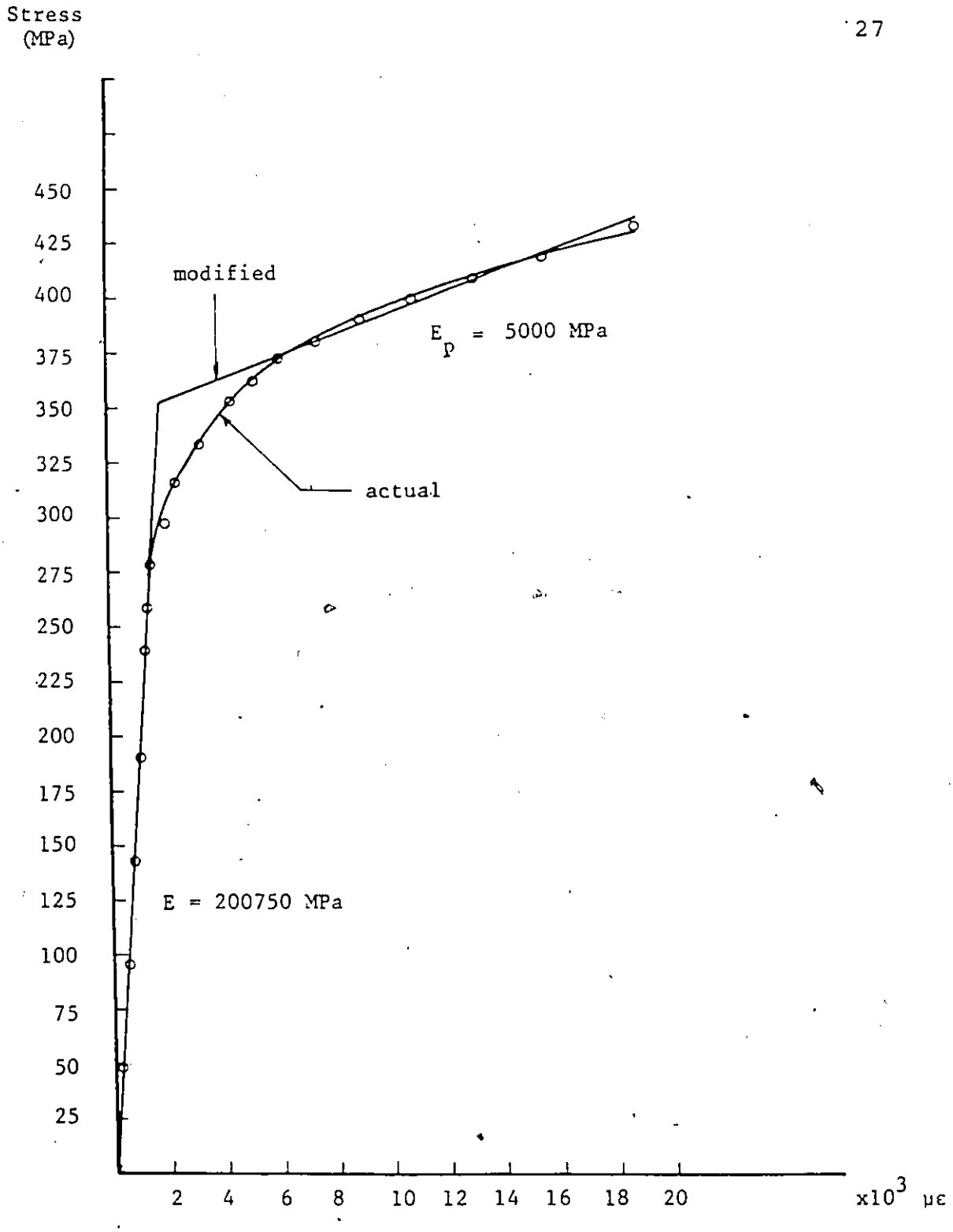

Fig. 3.2. Stress-strain relation.

stress-strain relations are given by:

$$\varepsilon_x = \frac{1}{E}(\sigma_x - \nu\sigma_y)$$

$$\varepsilon_y = \frac{1}{E}(\sigma_y - \nu\sigma_x)$$

$$\gamma_{xy} = \frac{1}{G}\tau_{xy} = \frac{2(1+\nu)}{E}\tau_{xy} \qquad (3.3)$$

where

σ_x, σ_y = stresses in the x and y directions, respectively;

τ_{xy} = shear stress;

ν = Poisson's ratio;

E = modulus of elasticity; and,

G = shear modulus.

If the stresses are expressed in terms of the strains, the stress-strain relations will become:

$$\sigma_x = \frac{E}{1-\nu^2}(\varepsilon_x + \nu\varepsilon_y)$$

$$\sigma_y = \frac{E}{1-\nu^2}(\varepsilon_y + \nu\varepsilon_x)$$

$$\tau_{xy} = \frac{E}{2(1+\nu)}\gamma_{xy} \qquad (3.4)$$

3.7 MATERIAL NON-LINEARITY

The expression material non-linearity is used to describe the non-linear behaviour of a material under loading. The steel material expresses such a behaviour in the plastic range. To account for that behaviour, the

plasticity theory has to be introduced. There are two main requirements to construct a plasticity theory:

a. A yield criterion.

b. A stress-strain relation.

3.7.1 Yield Criterion

In a case of a uniaxial stress, the yield point of the material can be easily determined. However, if several stresses are acting in different directions, only a specific combination of these stresses will cause yield. The criteria for deciding which combination of multiaxial stresses will cause yield are called yield criteria. Several yield criteria has been proposed since 1773. Maximum Stress Theory by Rankine, Maximum Strain Theory by Saint-Venant, Maximum Shear Theory by Tresca and Maximum Strain Energy Theory by Beltrami are some examples of these yield criteria (29).

One of the most accepted yield criteria is the one known as the Distortion Energy Theory or the Von-Mises Yield Criterion. This theory assumes that yielding begins when the distortion energy equals the distortion energy at yield in simple tension. For a case of plane stress it can be shown that yielding begins when (29):

$$\sigma_e = \sigma_o \qquad (3.5)$$

where

σ_o = the yield stress in axial tension;

and

σ_e = the effective stress which is defined as:

$$\sigma_e = (\sigma_x^2 + \sigma_y^2 - \sigma_x\sigma_y + 3\ \tau_{xy}^2)^{1/2} \qquad (3.6)$$

The Von-Mises yield criterion is widely used at the present time because it usually fits the experimental data of steel structures better than any of the other theories.

3.7.2 Incremental and Deformation Theories

In the plastic range, the amount of strain expressed by the material under any load depends on the loading path. To obtain a stress-strain relation in the plastic range, the yield criterion has to be used with one of the plasticity theories; namely, the incremental or the deformation theory. The incremental theory accounts for the effect of the loading path on the final stresses and, therefore, the load has to be applied incrementally. However, to simplify the process the deformation theory assumes that the plastic strains are functions of the current state of stresses and are independent of the history of loading, and hence the total load can be applied in one step.

It should be noted that there are some cases of loading where the incremental theory reduces to the deformation theory such as the case of proportional or radial

loading where all the stresses increase in ratio. Budiansky (5) proposed that there are ranges of loading paths other than the proportional loading for which the basic requirements of the plasticity theory are satisfied by the deformation theory. However, this has not been established experimentally yet. In stability problems Gerard (10) states that the deformation theory is in substantially good agreement with the experimental results. On the other hand, the incremental theory requires the introduction of initial imperfection in order to obtain a satisfactory degree of correlation with tests.

In the present study, because of the large size of the problem, the deformation theory is used. This helps in reducing the time required by the computer solution to solve the problem.

3.7.3 Plastic Stress-Strain Relations

The Von-Mises yield criterion and the total deformation theory are used to develop the plastic stress-strain relations. These relations are (29):

$$\sigma_x = \frac{4}{3} E_s(\varepsilon_x^t + 0.5\ \varepsilon_y^t)$$

$$\sigma_y = \frac{4}{3} E_s(\varepsilon_y^t + 0.5\ \varepsilon_x^t)$$

$$\tau_x = \frac{1}{3} E_s\ \gamma_{xy}^t \qquad (3.7)$$

where

$\varepsilon_x^t, \varepsilon_y^t$ = total strains in the x and y directions, respectively;

γ_{xy}^t = total shear strain; and,

E_s = secant modulus, defined as:

$$E_s = \frac{\sigma_e}{\varepsilon_e^t} \tag{3.8}$$

where

σ_e = the effective stress, given by Eq. 3.6

and

ε_e^t = the effective total strain, given by (29):

$$\varepsilon_e^t = \frac{2}{\sqrt{3}} \left(\varepsilon_x^{t^2} + \varepsilon_y^{t^2} + \varepsilon_x^t \varepsilon_y^t + 0.25\ \gamma_{xy}^{t^2}\right)^{1/2} \tag{3.9}$$

At any applied load, the displacement components at any point in the structure can be calculated through the minimization of the total potential energy. The total strain components are then calculated using equations 3.2. To calculate the different stress components at the same load, the effective stress σ_e must be first estimated to be able to use equations 3.7 and 3.8. A relation between ε_e^t and σ_e can be obtained from the stress-strain curve. This relation is given by (29):

$$\varepsilon_e^t = \varepsilon_e^p + \frac{2(1+\nu)}{3E}\ \sigma_e \tag{3.10}$$

where ε_e^p = the effective plastic strain, given by:

$$\varepsilon_e^p = \frac{2}{\sqrt{3}} \left(\varepsilon_x^{p^2} + \varepsilon_y^{p^2} + \varepsilon_x^p \varepsilon_y^p + 0.25\, \gamma_{xy}^{p^2}\right) \qquad (3.11)$$

where

$\varepsilon_x^p, \varepsilon_y^p$ = plastic strains in the x and y directions, respectively;

γ_{xy}^p = plastic shear strain

The plastic strain is the difference between the total strain and the elastic strain. To calculate the different plastic strain components, an iterative solution is required to estimate the elastic part in the total strain components. Mendelson (29) proposed a simpler relation to estimate ε_e^p. By expressing σ_e at any load increment as a series in terms of σ_e at the previous load increments, this relation is given by:

$$\varepsilon_e^p = \frac{\varepsilon_e^t - \frac{2}{3}\left[(1+\nu)/E\right]\grave{\sigma_e}}{1 + \frac{2}{3}\left[(1+\nu)/E\right] E_p} \qquad (3.12)$$

where

$\grave{\sigma_e}$ = effective stress at any point along the plastic region of the stress-strain curve;

and

E_p = slope of the stress-strain curve in the plastic range.

For materials with linear strain hardening, equation 3.12 yields the exact value of the plastic effective strain ε_e^p given by equation 3.11.

CHAPTER IV

ENERGY FORMULATION

4.1 GENERAL

The analytical solution is based on the energy minimization method using the Rayleigh-Ritz technique. Displacement functions with unknown coefficients are assumed to describe the deformed configuration of the HSS after rolling. The unknown coefficients are determined through the minimization of the total potential energy of the HSS using Rosenbrock's method of minimization.

In this chapter, a description of the theoretical model used in formulating the problem as well as the assumed displacement functions are given. Expressions for the total potential energy in both the elastic and plastic ranges are derived. The numerical calculations for evaluating the total potential energy and the minimization process are also explained.

4.2 THEORETICAL MODEL

Although the rolling process seems simple, the theoretical modelling for it is very complicated. In the rolling process, the load is applied continually to the

specimen under rolling through the middle roller. This process is modelled by assuming that the load is applied to the different sections of the specimen successively one after the other. Therefore, at any instant of the rolling process, the specimen is considered stationary and subjected to a concentrated load at its mid-point. The specimen under rolling is modelled as a simply supported beam with a span length equal to the distance between the centers of the fixed rollers of the bending machine. The beam model is decomposed into four plates: two flange plates and two web plates simply supported at their extremeties. The local axes of these plates are shown in Fig. 4.1; the number shown identifies the different plates as follows:

Plate #1 compression flange

Plate #2 web plate facing the top side of the rollers

Plate #3 tension flange

Plate #4 web plate facing the bottom side of the rollers (the base of the machine)

The positions of the different plates when the specimen is mounted in the machine are as shown in Fig. 6.5.

4.3 BOUNDARY CONDITIONS

It is assumed that at any instant of the rolling process, the model is a simply supported beam . The cross-section is decomposed into four plates simply supported at their extremities. Since the cross-section of the model

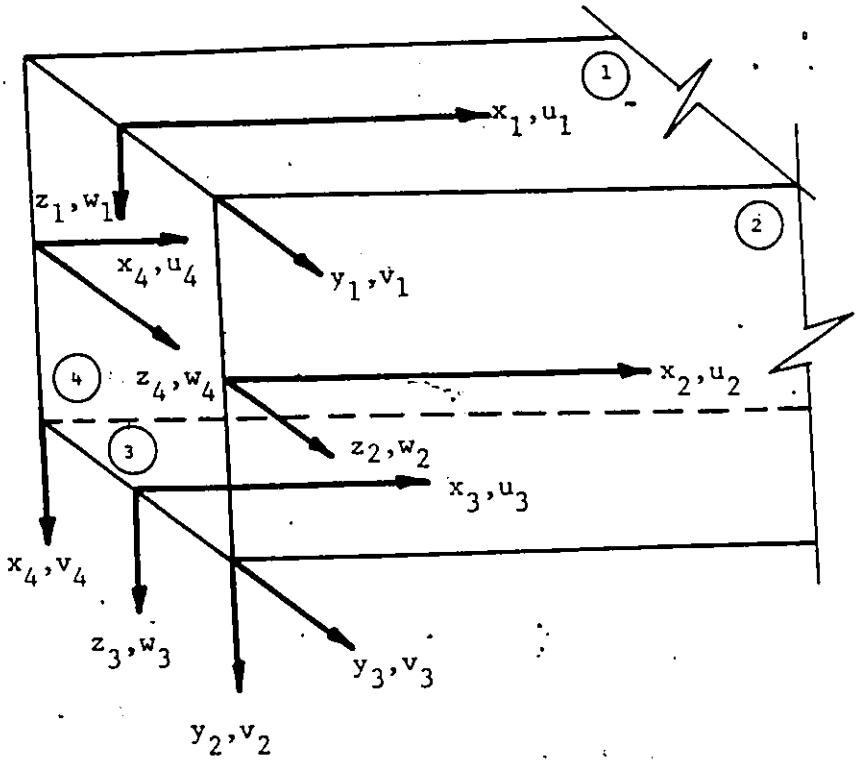

Fig. 4.1. Local axes of the four component plates.

is composed of relatively thin plates, plastic hinges tend to form at its corners at relatively small load. Therefore, the compatibility of rotations at the corners is disregarded. All other displacement boundary conditions are satisfied. These boundary conditions are:

(a) Longitudinal direction:

at $x = 0$ and at $x = \ell$

$$v_1 = w_1 = 0$$
$$v_2 = w_2 = 0 \qquad (4.5)$$
$$v_3 = w_3 = 0$$

(b) Transverse direction:

$$u_2 \text{ at } y = -\frac{h}{2} = u_1 \text{ at } y = \frac{b}{2}$$
$$u_4 \text{ at } y = -\frac{h}{2} = u_1 \text{ at } y = -\frac{b}{2}$$
$$u_2 \text{ at } y = \frac{h}{2} = u_3 \text{ at } y = \frac{b}{2}$$
$$u_4 \text{ at } y = \frac{h}{2} = u_3 \text{ at } y = -\frac{b}{2}$$
$$v_2 \text{ at } y = -\frac{h}{2} = w_1 \text{ at } y = \frac{b}{2}$$
$$v_4 \text{ at } y = -\frac{h}{2} = w_1 \text{ at } y = -\frac{b}{2} \qquad (4.6)$$
$$v_2 \text{ at } y = \frac{h}{2} = w_3 \text{ at } y = \frac{b}{2}$$
$$v_4 \text{ at } y = \frac{h}{2} = w_3 \text{ at } y = -\frac{b}{2}$$
$$w_2 \text{ at } y = -\frac{h}{2} = v_1 \text{ at } y = \frac{b}{2}$$
$$w_4 \text{ at } y = -\frac{h}{2} = v_1 \text{ at } y = -\frac{b}{2} = 0$$
$$w_2 \text{ at } y = \frac{h}{2} = v_3 \text{ at } y = \frac{b}{2}$$
$$w_4 \text{ at } y = \frac{h}{2} = v_3 \text{ at } y = -\frac{b}{2} = 0$$

The subscripts 1, 2, 3 and 4 in the displacement components denote plate's number.

4.4 DISPLACEMENT FUNCTIONS

The exact deformed configuration of any structure can be determined by solving its differential equation of equilibrium. In many cases, closed form solutions of such equilibrium equations do not exist. This is usually due to the complexity that arise from incorporating complicated types of loading, boundary conditions and/or nonlinear behaviour. In these cases assumed displacement functions that approximate the deformed configuration of the structure are used. These approximate functions can be chosen either directly based on a predicted deformed shape of the structure, or evaluated based on an assumed stress or strain state for the structure. In the present analysis, the displacement functions are assumed directly based on the deformed shape of the model obtained from the experimental program, a typical deformed section is shown in Fig. 4.2.

It should be noted that the assumed displacement functions should satisfy some conditions, the most important of which is that they should be geometrically admissible. Geometric admissibility implies two conditions:

(i) The assumed displacement functions should satisfy all displacement boundary conditions and insure compatibility between the different elements of the structure.

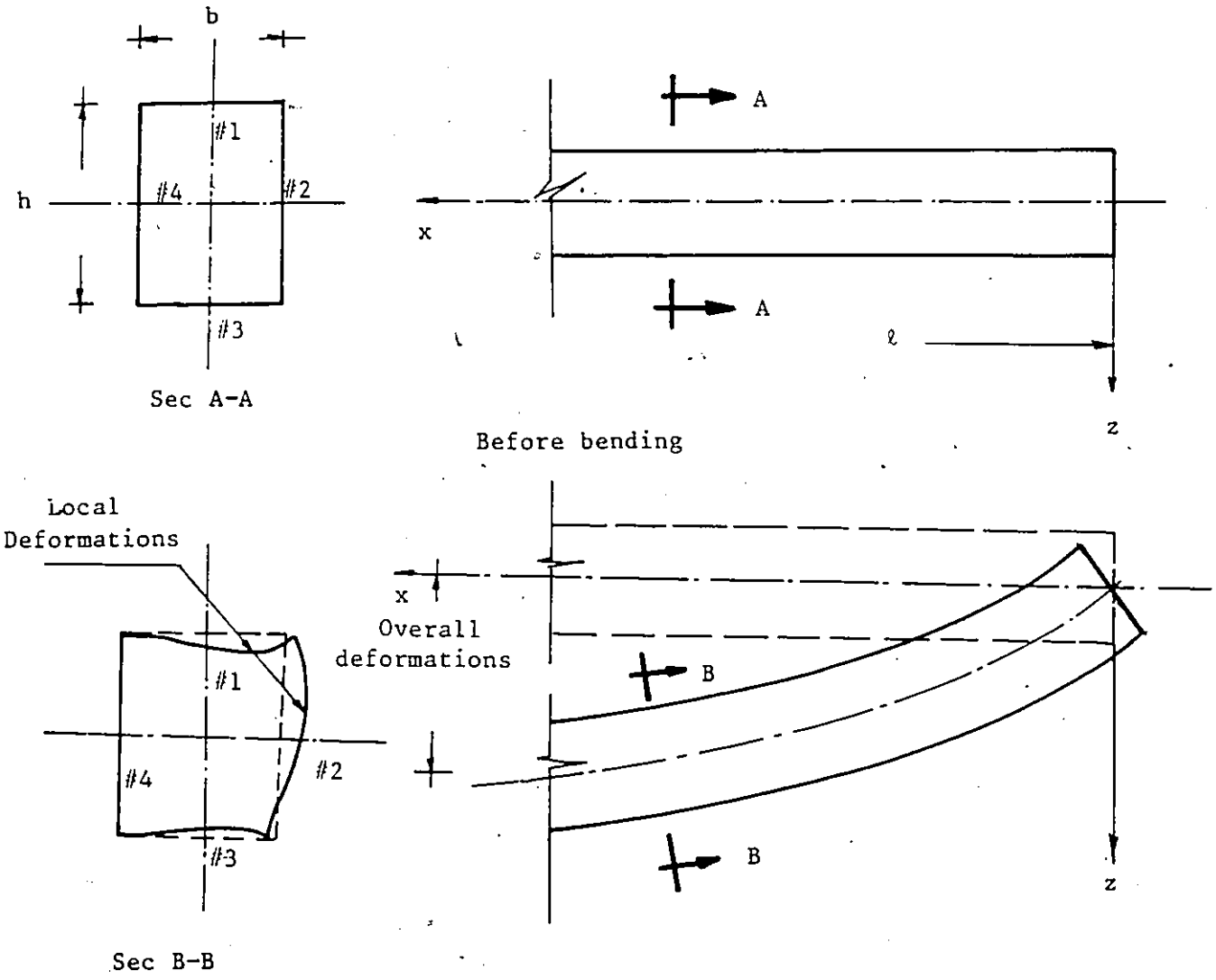

Fig. 4.2. Deformations of the beam model due to the rolling process.

(ii) The assumed displacement functions should improve the solution by bringing the value of the total potential energy closer to the true minimum as more higher order terms are added to the previously used ones in the displacement functions.

Other conditions such as completeness and the ability to represent rigid body displacements of the structure should also be observed (30).

Observing the deformations taking place in the HSS during the rolling process, it can be shown that the displacement consist mainly of two parts:

(a) Overall displacement; due to the deformation of the HSS as a beam.

(b) Local displacement, which varies in each plate depending on its location in the cross-section.

4.4.1 Overall Displacements

This part of the displacement functions describes the displacement of the center line of the model which is the same as that of the ends of each plate, i.e., the corners of the beam model. This displacement is basically due to the deformation of the model as a beam under concentrated load. As the beam model is assumed to be simply supported, a sine-function in the longitudinal direction of the model is chosen to represent this type of deformation. Denoting the longitudinal direction as the x-axis as shown in Fig. 4.1, the displacement functions of each plate will be as follows:

Plate #1

$$u = \sum_k B_k \frac{k\pi}{\ell} \frac{h}{2} \cos \frac{k\pi x}{\ell} \tag{4.1a}$$

$$v = 0 \tag{4.1b}$$

$$w = \sum_k B_k \sin \frac{k\pi x}{\ell} \tag{4.1c}$$

Plate #2

$$u = -\sum_k B_k \frac{k\pi}{\ell} y \cos \frac{k\pi x}{\ell} \tag{4.1d}$$

$$v = \sum_k B_k \sin \frac{k\pi x}{\ell} \tag{4.1e}$$

$$w = 0 \tag{4.1f}$$

Plate #3

$$u = -\sum_k B_k \frac{k\pi}{\ell} \frac{h}{2} \cos \frac{k\pi x}{\ell} \tag{4.1g}$$

$$v = 0 \tag{4.1h}$$

$$w = \sum_k B_k \sin \frac{k\pi x}{\ell} \tag{4.1i}$$

Plate #4

$$u = -\sum_k B_k \frac{k\pi}{\ell} y \cos \frac{k\pi x}{\ell} \tag{4.1j}$$

$$v = \sum_k B_k \sin \frac{k\pi x}{\ell} \tag{4.1k}$$

$$w = 0 \tag{4.1ℓ}$$

where

B_k = unknown coefficient; and

$k = 1,3,5,.....$

4.4.2 Local Displacements

This part of the displacement functions represents the additional deformations that take place locally in each plate. These local deformations vary in the different plates depending on the location of each plate in the cross-section. Fourier series functions in both the longitudinal and transverse directions are chosen to represent these deformations. The different components of displacement chosen for each plate are as follows:

Plate #1

$$u = \sum_r A_r \frac{h}{2} \sin \frac{r\pi x}{\ell} \tag{4.2a}$$

$$v = \sum_{mn} \sum C_{nm} (y+\frac{b}{2}) \sin \frac{n\pi (y+\alpha\frac{b}{2})}{b} \sin \frac{m\pi x}{\ell} \tag{4.2b}$$

$$w = \sum_{qp} \sum D_{pq} (y+\frac{b}{2}) \cos \frac{p\pi y}{b} \sin \frac{q\pi x}{\ell} \tag{4.2c}$$

Plate #2

$$u = -\sum_r A_r \, y \sin \frac{r\pi x}{\ell} \tag{4.2d}$$

$$v = 0 \tag{4.2e}$$

$$w = -\sum_{nm} \sum C_{nm} \, b \sin \frac{n\pi (y-\alpha\frac{h}{2})}{h} \sin \frac{m\pi x}{\ell} \tag{4.2f}$$

Plate #3

$$u = -\sum_r A_r \frac{h}{2} \sin \frac{r\pi x}{\ell} \tag{4.2g}$$

$$v = -\sum_{mn} \sum C_{nm} (y+\frac{b}{2}) \sin \frac{n\pi (y-\alpha\frac{b}{2})}{b} \sin \frac{m\pi x}{\ell} \tag{4.2h}$$

$$w = -\sum_{ij}\sum G_{ij}(y+\frac{b}{2}) \cos \frac{i\pi y}{b} \sin \frac{j\pi x}{\ell} \qquad (4.2i)$$

Plate #4

$$u = -\sum_{r} A_r \, y \sin \frac{r\pi x}{\ell} \qquad (4.2j)$$

$$v = 0 \qquad (4.2k)$$

$$w = 0 \qquad (4.2\ell)$$

where A_r, C_{nm}, D_{pq}, G_{ij} are the unknown coefficients; $i=j=m=n=p=q = 1, 3, 5, \ldots$; and $r = 2, 4, 6, \ldots$.

The coefficient α is used to define the point of zero out-of-plane displacement in the web plate. If the two webs were free to deform, the resulting deformed section would have been symmetric with the zero out of plane deformation of the web at mid-point. However, plate #4 did not express any out-of-plane displacement as shown in Fig. 4.2. Preventing the out-of-plane motion of one of the webs (plate #4) is the same as if the whole section was pushed sideways until the deformation of that web (plate #4) is zero. This will result in increasing the deformations of the other web (plate #2) and relocating its point of zero deflection below its mid-depth.

To determine the magnitude of the coefficient α, two factors have to be considered: firstly, the common shape of the different sections resulting from the experimental program, and secondly, the value of the total potential

energy at any specified coefficient α. In other words, the chosen value for α should result in deformations that comply with that obtained in the experiments and should yield the lowest value possible for the total potential energy. To satisfy the deformed shape of the cross-sections, the point of zero out-of-plane deflection should be in the middle third of the lower half of the web plate, i.e., at a distance of $y = 0.33\ (\frac{h}{2})$ to $y = 0.67\ (\frac{h}{2})$. This range is determined mainly by visual inspection of the deformed sections. The total potential energy of three different sections: 101.6 x 101.6 x 4.78 mm, 177.8 x 127.0 x 6.35 mm and 203.0 x 203.0 x 9.53 mm, is calculated at different values of $\alpha = 0.30$, 0.40, 0.50 and 0.60, and in all cases $\alpha = 0.60$ yielded the least value for the total potential energy. Therefore, α=0.6 is chosen and kept constant throughout the theoretical analysis.

4.4.3 Effect of Shear

The previously mentioned displacement functions assumes that plane section before deformation remains plane after deformation. Due to the short span of the beam and the large amount of load used during the rolling process, that assumption will not be valid. A displacement function is assumed to account for the non-linear deformation of the web plate in the longitudinal direction. This displacement function is the same for both web plates and is given

by:

$$u = -\sum_g H_g \sin \frac{g\pi y}{h} \tag{4.3}$$

where H_g is an unknown coefficient and g = 1, 3, 5, ...

This displacement will also affect the longitudinal in-plane displacement of the two flanges; the additional displacement of the compression and tension flanges can be obtained after substituting $y = -\frac{h}{2}$ and $y = \frac{h}{2}$, respectively, in equation 4.3.

It should be noted that expression 4.3 is valid only for one half of the beam model. The sign of the expression should be reversed to describe the shear displacement of the second half.

4.4.4 Total Displacement Functions

Since each of the previously mentioned displacement functions satisfies all the boundary conditions, the total displacement functions are the summation of their respective components. Therefore, the total displacement functions are:

Plate #1

$$u = \sum_k B_k \frac{k\pi}{\ell} \frac{h}{2} \cos \frac{k\pi x}{\ell} + \sum_r A_r \frac{h}{2} \sin \frac{r\pi x}{\ell} + \sum_g H_g \tag{4.4a}$$

$$v = \sum_m \sum_n C_{nm} (y+\frac{b}{2}) \sin \frac{n\pi (y+\alpha\frac{b}{2})}{b} \sin \frac{m\pi x}{\ell} \tag{4.4b}$$

$$w = \sum_k B_k \sin \frac{k\pi x}{\ell} + \sum_q \sum_p D_{pq} (y+\frac{b}{2}) \cos \frac{p\pi y}{b} \sin \frac{q\pi x}{\ell} \tag{4.4c}$$

Plate #2

$$u = -\sum_k B_k \frac{k\pi}{\ell} y \cos\frac{k\pi x}{\ell} - \sum_r A_r y \sin\frac{r\pi x}{\ell} - \sum_g H_g \sin\frac{g\pi y}{h} \quad (4.4d)$$

$$v = \sum_k B_k \sin\frac{k\pi x}{\ell} \quad (4.4e)$$

$$w = -\sum_m \sum_n C_{nm} b \sin\frac{n\pi(y-\alpha\frac{h}{2})}{h} \sin\frac{m\pi x}{\ell} \quad (4.4f)$$

Plate #3

$$u = -\sum_k B_k \frac{k\pi}{\ell}\frac{h}{2} \cos\frac{k\pi x}{\ell} - \sum_r A_r \frac{h}{2} \sin\frac{r\pi x}{\ell} - \sum_g H_g \quad (4.4g)$$

$$v = -\sum_m \sum_n C_{nm} (y+\frac{b}{2}) \sin\frac{n\pi(y-\alpha\frac{b}{2})}{b} \sin\frac{m\pi x}{\ell} \quad (4.4h)$$

$$w = \sum_k B_k \sin\frac{k\pi x}{\ell} - \sum_j \sum_i G_{ij}(y+\frac{b}{2}) \cos\frac{i\pi y}{b} \sin\frac{j\pi x}{\ell} \quad (4.4i)$$

Plate #4

$$u = -\sum_k B_k \frac{k\pi}{\ell} y \cos\frac{k\pi x}{\ell} - \sum_r A_r y \sin\frac{r\pi x}{\ell} - \sum_g H_g \sin\frac{g\pi y}{h} \quad (4.4j)$$

$$v = \sum_k B_k \sin\frac{k\pi x}{\ell} \quad (4.4k)$$

$$w = 0 \quad (4.4\ell)$$

These displacement functions should also be modified to account for the effect of the friction between the beam model and the rollers. This will be considered in Chapter 5.

4.4.5 Comments on the Displacement Functions

It should be noted that the displacement functions deduced above are chosen specifically to describe the

deformed shape of the HSS in the present problem, i.e., using a specific machine and certain procedure of rolling. In choosing these displacement functions, three assumptions are made:

(i) The web plates are considered very stiff in their own plane, i.e., local deformations in the y-direction are neglected.

(ii) The flange plates of the model are considered narrow strips, therefore, u, is assumed to be constant for all points located at the same distance x.

(iii) The shift of the neutral axis after deformation is considered to be small and, therefore, neglected.

Figure 4.2 shows that web plate #4 did not express any out of plane displacement. That is due to the fact that during the rolling process this plate was facing the base of the rolling machine which acts as a support to the specimen under rolling.

4.5 TOTAL POTENTIAL ENERGY

4.5.1 Strain Energy

The strain energy is defined as the capability of the internal forces (stresses) to perform work during the deformation process of the body. The strain energy density, i.e. the strain energy per unit volume, is equal to the area under the stress-strain curve. For an elastic

linear stress-strain relation and a case of plane stress, the strain energy U_e can be expressed in terms of the different components of displacements u, v and w as follows (Appendix A):

$$U_e = \frac{D}{2}\int_A \{[u_x^2 + v_y^2 + \frac{1}{2}(1-\nu)(u_y+v_x)^2 + 2\nu u_x v_y]$$

$$+ [u_x w_x^2 + v_y w_y^2 + (1-\nu)\, w_x w_y\, (u_y+v_x) + \nu(u_x w_y^2 + v_y w_x^2)]$$

$$+ 0.25\ (w_x^4 + 2w_x^2 w_y^2 + w_y^4)\}\ dA$$

$$+ \frac{S}{2}\int_A [w_{xx}^2 + w_{yy}^2 + 2(1-\nu)w_{xy}^2 + 2\nu w_{xx} w_{yy}]\ dA \qquad (4.7)$$

where

D = membrane stiffness = $\frac{Et}{1-\nu^2}$;

S = bending stiffness = $\frac{Et^3}{12(1-\nu^2)}$;

t = thickness of the plate, and

A = area of the plate

In the plastic range, the effective stress and the effective strain are used instead of the one dimensional stress and strain used in the elastic range. The relation between the effective stress and the effective strain is taken from the uniaxial stress-strain curve. Therefore, the abscissa and the ordinate of the uniaxial stress-strain curve are replaced by ε_e^t and σ_e, respectively (28,29). In this case and for a material with linear strain hardening, the total strain energy, elastic and plastic strain energy, for a case of plane stress can be expressed in terms of the displacement components as follows (Appendix B).

$$U = 0.5\ (E_p\varepsilon_o^2 - \sigma_o\varepsilon_o)\ V$$

$$+ \left(\frac{2}{3}E_p t \int_A \{[u_x^2 + v_y^2 + u_x v_y + 0.25\ (u_y+v_x)^2]\right.$$

$$+ [u_x w_x^2 + v_y w_y^2 + 0.5\ w_x w_y (u_y+v_x)$$

$$+ 0.5\ (v_y w_x^2 + u_x w_y^2)]$$

$$\left. + [0.25\ (w_x^2+w_y^2)^2]\right\}\ dA$$

$$+ \frac{1}{18}\ E_p t^3 \int_A [w_{xx}^2 + w_{yy}^2 + w_{xy}^2 + w_{xx} w_{yy}]\ dA)$$

$$+ \left(\frac{2}{\sqrt{3}}\ (\sigma_o - E_p \varepsilon_o)\right)\int_V \{[u_x^2 + v_y^2 + u_x v_y + + 0.25(u_y+v_x)^2]$$

$$+ [u_x w_x^2 + v_y w_y^2 + 0.5\ w_x w_y\ (u_y+v_x) + 0.5(u_x w_y^2 + v_y w_x^2)]$$

$$+ [0.25(w_x^2+w_y^2)^2]$$

$$+ z^2[w_{xx}^2 + w_{yy}^2 + w_{xy}^2 + w_{xx}w_{yy}]$$

$$- z[2u_x w_{xx} + 2v_y w_{yy} + w_{xy}(u_y+v_x) + u_x w_{yy} + v_y w_{xx}]$$

$$- z[w_{xx}w_x^2 + w_{yy}w_y^2 + w_{xy}w_x w_y + 0.5\ w_{xx}w_y^2$$

$$+ 0.5\ w_{yy}w_x^2]\}^{1/2}\ dV) \qquad (4.8)$$

where

σ_o, ε_o = yield stress and strain, respectively; and

V = volume of the plate

4.5.2 External Work

External work is defined as the work done by the external forces during the deformation process. The formulation of the external work in terms of the different dis-

placement components of the structure depends on the mechanism of applying the loads as well as the deformed configuration of the structure. For a transverse concentrated load, P, causing an out of plane deflection, w, the external work, W, is the product of the applied load, i.e., W = Pw. This is an approximation leading to conservative results. To be exact the area and the P-w curve should be integrated to obtain the appropriate external work done on the system. This is not possible since the deflection w is yet to be determined from the minimization process.

The total potential energy of the structure is the summation of the strain energy U and the external work done W ; i.e.

$$T = U - W \qquad (4.9)$$

4.6 EVALUATION OF THE TOTAL POTENTIAL ENERGY (T.P.E.)

4.6.1 Numerical calculations of the T.P.E.

In modelling the rolling process problem the load is assumed to be applied incrementally through the middle movable roller. Applying the load incrementally is necessary to trace the progress of yielding in the different plates of the model. This does not cancel the advantage of using the deformation theory of plasticity because adopting this theory allows the use of fewer load increments each of larger magnitude.

Evaluation of the total potential energy is performed

using a computer program that was developed by the author as a part of modelling the rolling process. At each load increment, the total potential energy is calculated. Through the minimization of that energy the corresponding deformed configuration of the HSS can be determined. To calculate the strain energy of the beam model, the derivatives of the displacement functions with respect to x and y for each of the four plates composing the model are calculated. These derivatives are given in Appendix C.

In order to obtain the strain energy of any structure, the strain energy density is integrated over the volume of that structure. As shown in Appendix A the elastic strain energy can be integrated easily with respect to the plate thickness. However, a deliberate effort is needed to integrate it over the area of the plate especially if the number of terms in the series representing the displacement of the model is large. Therefore, a numerical integration method proposed by Weddle is used (33). This method requires at least seven integration points and gives exact results for functions of any degree up to the sixth.

The total strain energy cannot be integrated with respect to the thickness of the plate as easily as the elastic one since a part of the expression is under the square root. Therefore, numerical integration is performed here also. Since the highest power of the thickness in the

total strain energy expression is only the second degree, Simpson's rule of integration is used. However, Weddle's rule is still utilized when integrating over the area of the plate.

As all specimens are stress relieved after manufacturing, the beam model will have no initial stresses at the beginning of the loading process. Therefore, only elastic strain energy is considered. As the load increases, part of the model begins to plasticize while the other parts are still elastic. To account for such behaviour, each plate in the model is descretized into a number of elements. The strain energy of each element is calculated depending on the stress level in that element. Each element is assumed to have constant stresses equal to that at its center. The total strain energy of the model is the summation of the individual elements strain energies.

4.6.2 Comments

The use of the total potential energy minimization method in the analysis offered many advantages. In addition to those stated in Chapter 3, the method facilitates the choice of different displacement functions for each plate of the model to suit its deformation. However, accounting for both geometric and material non-linearities introduced some difficulties in the analysis. Geometric non-linearity resulted in long and difficult expression

for the total potential energy. Material non-linearity forced the use of a mesh subdivision for the different elements of the model to account for its elasto-plastic behaviour. This eliminated one of the main advantages of using trigonometric functions to represent the deformed shape of the model, namely the orthogonality characteristic. This characteristic would have reduced the total potential energy expression when integrated over the volume of the structure and made the exact integration of the function possible. As a result of the above difficulty, numerical integration had to be used to evaluate the total potential energy at each load increment.

The minimization process requires the evaluation of the total potential energy function several times at each load increment, each time having a certain set of coefficients, until the function reaches its minimum value at the correct solution. Because of the non-linearity of the problem, the number of iterations required to obtain the solution can be very high. If the integration of the total potential energy function is performed for each iteration the minimization process would have required a very long execution time. To avoid this the total potential energy expression is divided into smaller terms where the unknown coefficients of these terms can be taken as common factors outside the integration sign. The integra-

tion is then performed once and its results is stored in the computer. At each iteration only a multiplication process of the trial coefficients by the stored integrated values is performed.

4.7 MINIMIZATION OF THE TOTAL POTENTIAL ENERGY

4.7.1 Introduction to Function Minimization

The minimization of the total potential energy is based on the principle of stationary potential energy which states (34):

"Among all the possible displacements which satisfy the boundary conditions of a structural system, those corresponding to equilibrium configurations make the total potential energy assume a stationary value".

The total potential energy assumes a stationary value at the so-called critical points of the functions. The critical points of a function may be points at which the function is a relative maximum or minimum. Utilizing the principle of minimum potential energy, the structural problems can be described mathematically as: there is a certain function $T(\{c\})$ where $\{c\}$ are some unknown parameters, and it is required to evaluate $\{c\}$ such that $T(\{c\})$ is minimum. In the present problem, T is the total potential energy, and $\{c\}$ are the unknown coefficients of the displacement

functions that describe the deformed shape of the structure.

The necessary condition for the occurrence of a local minimum is that the variation in the total potential energy due to a small variation in any of the unknown coefficients is equal to zero, i.e.,

$$\delta T = 0 \tag{4.10}$$

For linear problems, the unknown coefficients of the displacement functions will be quadratic in the total potential energy expression. Therefore, equation 4.9 will lead to a system of linear independent simultaneous equations in these coefficients. These equations are the first derivatives of the total potential energy with respect to each of the unknown coefficients. Solving these equations, the magnitude of these coefficients can be determined. For non-linear problems, equation 4.9 leads to a system of non-linear equations in which the unknown coefficients will be coupled. In most cases the task of solving this system of non-linear equations is very difficult. Therefore, a better approach is to make use of the mathematical programming techniques to minimize the total potential energy and hence obtain the magnitude of the unknown coefficients at which the total potential energy is minimum.

4.7.2 Minimization Techniques

Different minimization techniques can be used to evaluate the solution of any structural problem through the minimization of its potential energy. Some of these techniques are known as non-gradient methods where only the numerical value of the function is required to search for the function minimum. Other techniques are classified as gradient methods where both the function as well as its first derivatives with respect to each of the unknown coefficients are required for the minimization process.

Many of these minimization techniques are programmed and stored in the computer library in the form of subroutines that can be used directly in solving any problem. In the present study three different techniques were tried: the conjugate gradient method (7), the quasi-Newton method (8) and the Rosenbrock method (40). The first two methods are classified as gradient methods while the third one is non-gradient. The computer subroutines based on the first two methods are provided by the International Mathematical & Statistical Libraries Inc. (IMSL) while that based on the third method is provided by the University of Waterloo computer library. The three methods were successful in obtaining the solution as long as the beam model was still elastic and deformations were relatively small. However, the first two methods failed to yield the minimum of the

total potential energy when non-linearity started to affect the solution. The failure of these methods could be due to the following reasons:

(i) The shape of the energy function in space. In non-linear problems, irregular shape of the function under minimization is expected.

(ii) The accuracy of evaluating both the function and its gradient. As both the function and the gradient were evaluated by numerical integration a certain level of accuracy is lost in the calculations.

It was decided then to use a non-gradient method to obtain the minimum of the function. Therefore, the Rosenbrock's method was successfully employed in the analysis. The method can handle both constraint and non-constraint minimization problems. The complete algorithm of the method is given in reference (40). A computer subroutine, named CLIMB, which is based on this method is used to perform the minimization process.

The minimization technique is an iterative process in which the value of the function to be minimized is calculated at different points in space until it reaches its minimum at the true solution. The coordinates of each of these points represent a set of values for the unknown coefficients of the function. To start the search

for the minimum, initial values have to be assumed for the unknown coefficients as a starting point. If these values were too far from the true solution, more iterations will be required to obtain that solution. This will considerably increase the execution time, of the computer program because in each iteration the value of the function has to be calculated again.

In the computer program, there is a limit on the number of evaluations of the total potential energy functions. Based on the analysis of many HSS models, this limit was set to 200 times the number of the unknown coefficients in the function. The computer program will indicate if the minimization process consumed all the specified number of iteration without reaching the minimum of the function. In this case, a better choice for the initial values of the unknown coefficients should be made. In all the cases solved this limit was found to be adequate to complete the minimization when any reasonable initial values were assumed.

CHAPTER V

MODELLING OF THE ROLLING PROCESS

5.1 GENERAL

Plastic bending of beams using rolling machines is an often-used process in industry. Although the process seems rather simple, a thorough analysis of it is very complicated. Shear stresses, friction between the beam and the rollers and the continuously changing geometry of the beam during the rolling process are some of the factors that defy an accurate analytical modelling of the process. The problem is even more complicated if the analysis has to account for the cross-section deformation of the beam under rolling.

The number of publications studying the cross-section deformation of beams subjected to plastic bending is very limited. The main concern of most of the studies is the cross-secion strength rather than its local deformations (18). Also very few publications have reported studies on the geometry of the beams during the rolling process. Such publications either report experimental tests or make several restrictive

assumptions to simplify the analytical modelling of the problem.

In this chapter, the method used to model the rolling process is explained. The relation between the radius of bend of the specimen and its deflection is derived. The effect of the frictional forces between the specimen and the rollers and the method to account for that effect are explained. Finally, the calculations of the residual stresses resulting in the model from the rolling process is presented.

5.2 RADIUS OF CURVATURE

The main objective of studying the geometry of the beam model during the rolling process is to find the relation between the middle roller position, i.e. the deflection of the beam, and the relaxed radius of bend. The relaxed radius of curvature is equal to the radius of curvature of the specimen while inside the machine, i.e. the plastic radius of curvature, minus the effect of the specimen springback.

One of the main assumption adopted by many researchers is that the deflected shape of the beam during rolling is circular. In this case the plastic radius of curvature can be calculated by simple geometry of the machine set up (20).

The assumption of constant radius of curvature contradicts the actual loading conditions which produce a linearly varying bending moment as shown in Fig. 5.1.b. Therefore, the present analysis adopts a solution, developed by Hanson and Jannerup (15), in which the actual bending moment is accounted for. It is assumed that the bending moment is a linear function of the length of the arc, s, between the rollers.

Assuming that the beam attains its plastic moment Mp at the point of contact with the middle roller, the beam will have different curvatures on either side of the point of contact. These curvatures can be represented by (15):

$$k_1(s) = k_r + \frac{M_p}{EI_x}\frac{s}{s_1} \qquad o<s<s_1 \qquad (5.1)$$

$$k_2(s) = \frac{M_p}{EI_x}\frac{s_2-s}{s_2-s_1} \qquad s_1<s<s_2 \qquad (5.2)$$

where: s_1 = distance between the fixed roller, on the exit side, and the middle roller along the center line of the beam;

s_2 = distance between the two fixed rollers along the center line of the beam;

k_r = relaxed radius of bend;

M_p = plastic moment; and

I_x = moment of inertia about the major axis.

The second term in equation 5.1 represents the effect

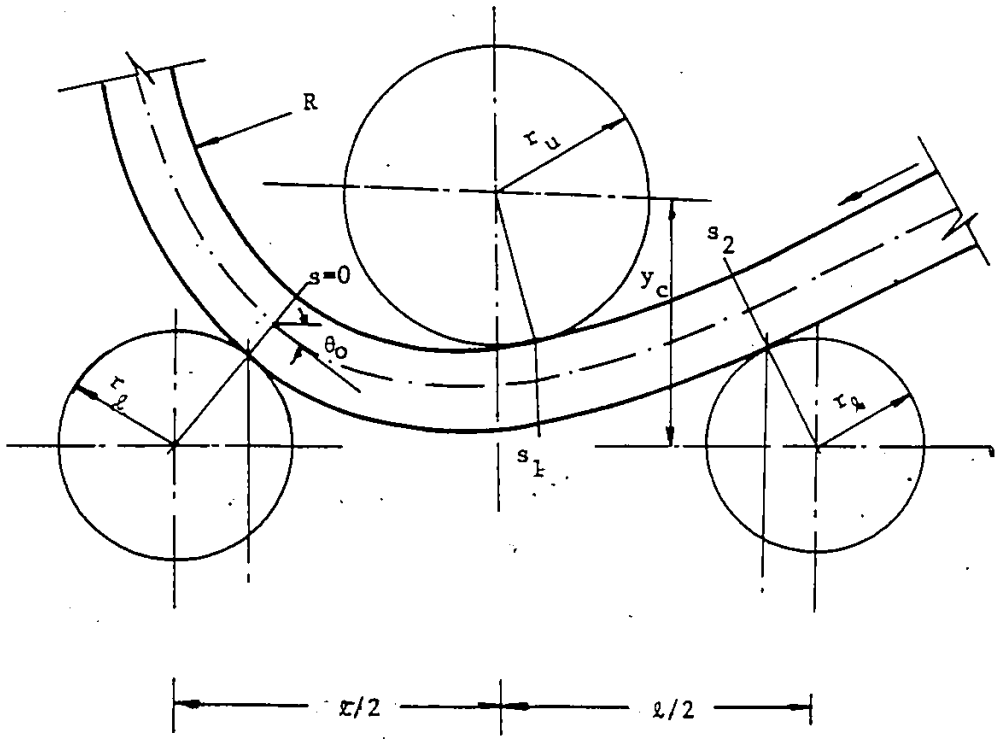

(a) Parameters determining the geometry of the specimen

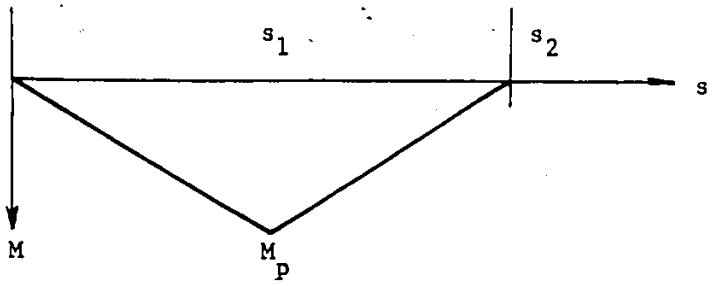

(b) Bending moment diagramm

Fig. 5.1 Geometry of the specimen at any instant of the rolling process.

of the beam springback. The plastic moment calculations for a hollow-section made of a material having linear strain hardening are given in Appendix D.

Using equations 5.1 and 5.2 four relations that describe the geometry of the specimen under rolling can be obtained (Appendix E). These relations are:

$$r_1 \sin(-\theta_o) + \int_o^{s_1} \cos\left(\theta_o + \int_o^s k_1(s)\,ds\right) ds - r_2 \sin\left(\theta_o + \int_o^{s_1} k_1(s)\,ds\right) = \ell/2 \qquad (5.3)$$

$$r_2 \sin\left(\theta_o + \int_o^{s_1} k_1(s)\,ds\right) + \int_{s_1}^{s_2} \cos\left(\theta_o + \int_o^{s_1} k_1(s)\,ds + \int_{s_1}^{s} k_2(s)\,ds\right) ds + r_1 \sin\left(\theta_o + \int_o^{s_1} k_1(s)\,ds\right) + \int_{s_1}^{s_2} k_2(s)\,ds = \ell/2 \qquad (5.4)$$

$$r_1 \cos\left(\theta_o + \int_o^{s_1} k_1(s)\,ds + \int_{s_1}^{s_2} k_2(s)\,ds\right) - r_1 \cos\theta_o - \int_o^{s_1} \sin\left(\theta_o + \int_o^{s} k_1(s)\,ds\right) ds - \int_{s_1}^{s_2} \sin\left(\theta_o + \int_o^{s_1} k_1(s)\,ds + \int_{s_1}^{s} K_2(s)\,ds\right) ds = 0 \qquad (5.5)$$

$$\delta = r_1 + r_2 - y_c \tag{5.6}$$

where

δ = deflection of the beam under rolling;

y_c = distance between the fixed rollers and the middle roller during rolling;

$r_1 = r_\ell + h/2$;

$r_2 = r_u + h/2$; and

h is the depth of the beam. All the other parameters are as defined in Fig. 5.1.a.

Equations 5.1 and 5.2 are then substituted in equations 5.3 to 5.6. Therefore for a specified value of k_r, the four unknowns in equations 5.3 to 5.6 are s_1, s_2, θ_o and δ. Since it is not possible to separate these unknowns and solve the equations directly, an iterative procedure must be used to obtain the solution. A multiple iterative procedure using the chord method together with linear interpolation iterative method, is utilized (27). In this procedure initial values are assumed for each of the four unknowns; the solution then iterates to obtain a value for each unknown while the other three variables are kept constant. The procedure continues until convergence is reached for all the values of the four unknowns.

A special computer program was developed to carry out the steps of the solution. Using this program the movement of the middle roller, which is equal to the deflection

of the beam under rolling δ, corresponding to any specific radius of bend can be calculated.

5.3 EFFECT OF FRICTION

One of the major forces resulting from the rolling process is the friction force between the specimen under rolling and the rollers. These friction forces result from the movement of the specimen during the rolling process. Noting that the two fixed rollers are driving, the friction forces will be as shown in Fig. 5.2. The bending moment and deflections resulting from this system of forces are as shown in Fig. 5.3.

To represent the effect of friction on the final deformations of the cross-section, new terms have to be added to the original displacement functions chosen to describe the deformations resulting from the vertical loads only. If the deflection of the center line of the specimen is as shown in Fig. 5.3.c, the displacement functions that represent the effect of friction are:

Plate #1

$$u_f = \sum_e k_e \frac{4e\pi}{\ell} \frac{h}{2} \cos \frac{4e\pi x}{\ell} \qquad (5.7a)$$

$$w_f = \sum_e k_e \sin \frac{4e\pi x}{\ell} \qquad (5.7b)$$

Plates #2 and #4

$$u_f = -\sum_e k_e \frac{4e\pi}{\ell} y \cos \frac{4e\pi x}{\ell} \qquad (5.7c)$$

$$v_f = \sum_e k_e \sin \frac{4e\pi x}{\ell} \qquad (5.7d)$$

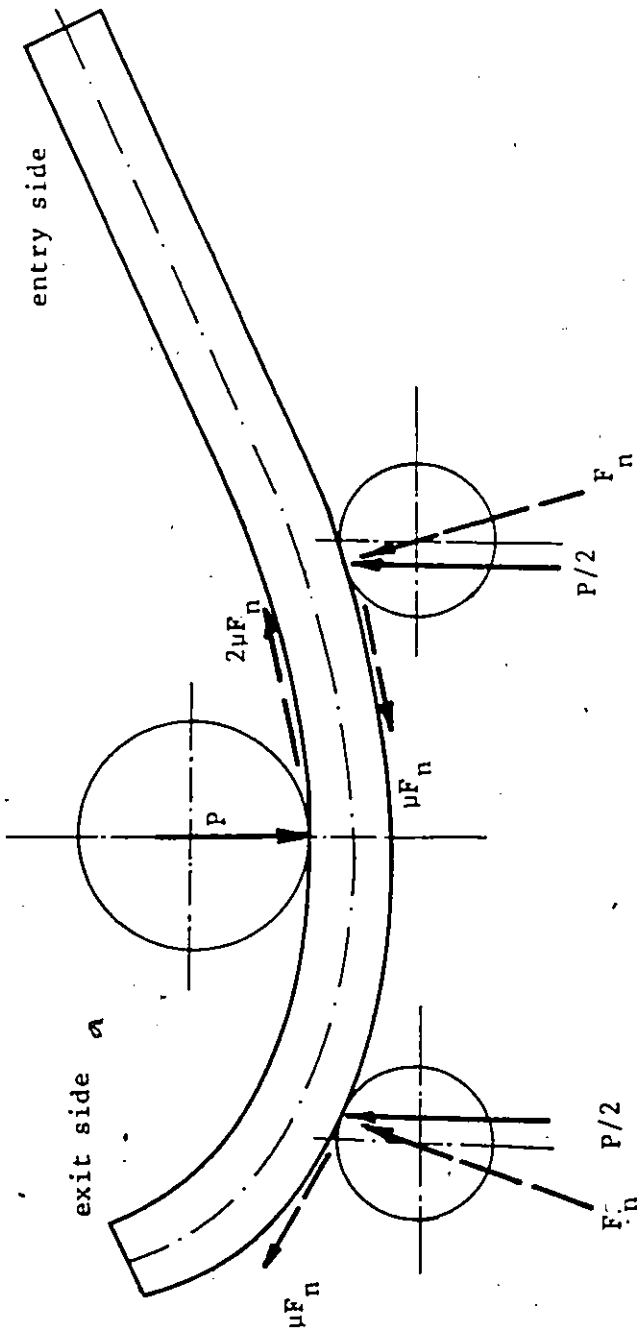

Fig. 5.2 Applied forces on the specimen during the rolling process.

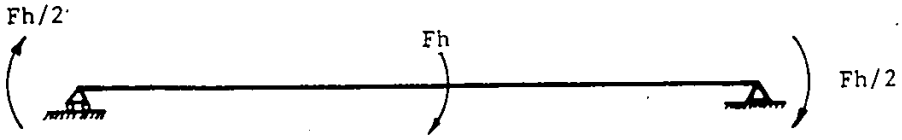

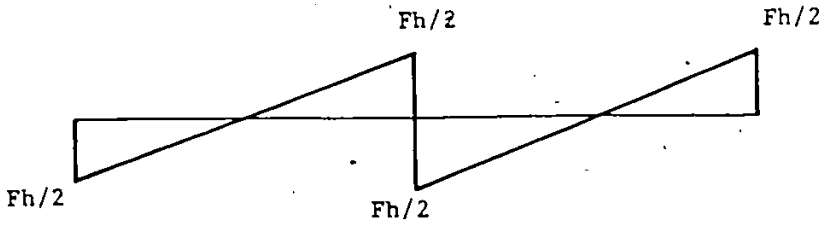

(a) Bending moment

(b) Deflection

Fig. 5.3. Bending moment and deflection due to Friction forces.

Plate #3

$$u_f = - \sum_e k_e \frac{4e\pi}{\ell} \frac{h}{2} \cos \frac{4e\pi x}{\ell} \qquad (5.7e)$$

$$w_f = \sum_e k_e \sin \frac{4e\pi x}{\ell} \qquad (5.7f)$$

where k_e is an unknown coefficient and e = 1, 3, 5, ... These functions have to be added to the original displacement functions given in section 4.3.4 to produce the total expression for the displacement functions.

The total potential energy is modified to account for the effect of friction. Using the derivatives of the additional terms due to friction, the strain energy can be calculated. The external work done by the friction forces is given by:

$$W_f = \Sigma M_f \theta \qquad (5.8a)$$

where

$\theta = (w_f)_x$;

F = friction force;

M_f = moment due to friction forces, given in Fig. 5.3.

Therefore,

$$w_f = F \frac{h}{2}(w_f)_x \Big|_{x=o} + Fh(w_f)_x \Big|_{x=\frac{\ell}{2}} + F \frac{h}{2}(w_f)_x \Big|_{x=\ell} \qquad (5.8b)$$

$$w_f = Fh \left(\Sigma k_e \frac{4t\pi}{\ell}\right) \qquad (5.8c)$$

The magnitude of the friction force, F, is given by:

$$F = \eta F_n \tag{5.9}$$

where η is the coefficient of friction and F_n = normal force as shown in Fig. 5.2.

For the rolling process of steel sections, a coefficient of friction of 0.07 - 0.09 is usually assumed (45). In the present analysis, a value of 0.08 is used. The value of F_n depends on the deflected shape of the specimen during the rolling process. To simplify the problem this shape is considered symmetric with respect to the middle roller to produce the same friction at each of the outer rollers. Therefore, the friction force F_n is given by:

$$F_n = \frac{P}{2} \cos \theta_o . \tag{5.10}$$

where P is the vertical load applied through the middle roller and θ_o as defined in Fig. 5.1.a. The two driving forces, F_n, at the outside roller have to overcome the friction force at the point of contact between the specimen and the middle roller.

It should be noted that as the sequence of the rolling process is to first apply the load while the specimen is stationary until it attains certain deflection under the middle roller and then to start rolling, the friction

forces do not contribute to the total potential energy until the specimen starts to move during the rolling process.

5.4 RESIDUAL STRESSES

When a structure is loaded beyond its elastic limit, some parts of the structure are permanently deformed while the others are still elastic. If the applied load is removed, the plastically deformed parts prevent the remaining elastic parts from returning to their initial positions causing some residual stresses (46). The magnitude of these residual stresses depends on the stress-strain relation of the material as well as on the stresses in the material before the release of the load. In the present study, the material behaviour under loading is best described by a bilinear stress-strain relation with linear strain hardening in the inelastic range. It is assumed that the stress-strain relation of the material is the same in tension and compression and the effect of Bauschinger is neglected.

Assuming that the material is axially loaded in tension beyond the yield point, i.e. loaded to point d in Fig. 5.4, the load required to produce a tensile stress equal to σ_d is P_d. If the load is removed, unloading will take place along the line d e f g which is parallel to the elastic line a b c. This process is equivalent to applying a load of the same magnitude, P_d, at the same position but

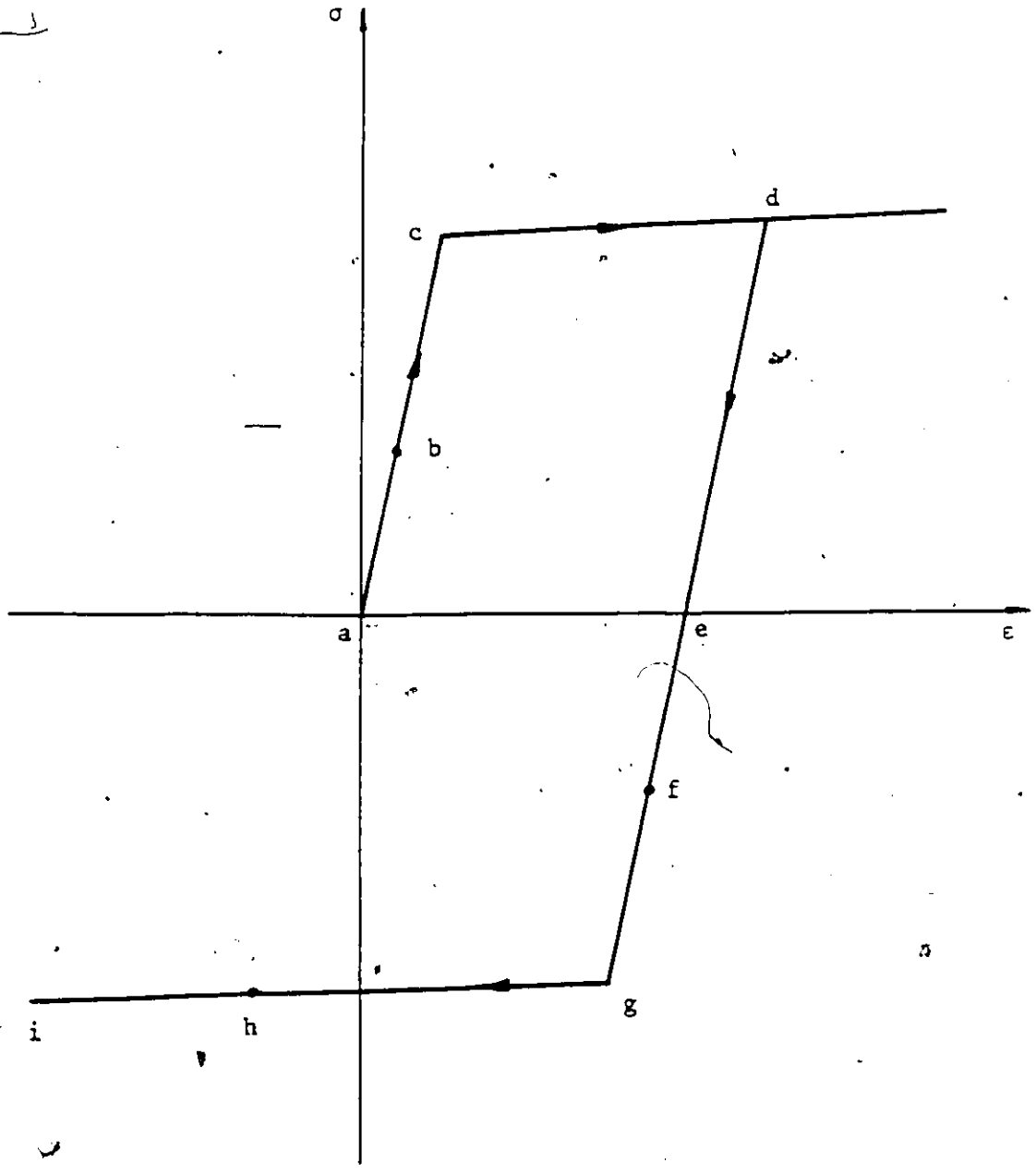

Fig. 5.4. Residual stresses.

in opposite direction. This load will produce compressive stresses to balance the existing tensile ones. The load, P_o, required to nullify the tensile stresses in the element can be calculated by simple proportion:

$$P_o = -P_b \frac{\sigma_d}{\sigma_b} \qquad (5.11)$$

where

P_b = the load required to produce stress equal to σ_b;

σ_b = the stress at any point along the line a-c; and

σ_d = the stress in the element before unloading.

Obviously P_o is smaller than P_d. If the unloading process continues until the value of P_d becomes zero, compressive stresses will start to develop causing residual stresses. The magnitude of these stresses depends on the value of P_d, therefore two separate cases should be considered:

1. If $P_d \leq P_o + P_c$ where P_c is the load required to produce the yield stress in the material and P_o is as defined before, the unloading range will be entirely elastic and the residual stresses will be equal to σ_f where f is any point along the line e g.

2. If $P_d > P_o + P_c$, the unloading range will be elasto-plastic since the stresses resulting from the unloading process are larger than that of the yield stresses of the material in compression. In this case the residual stresses are equal to σ_h where h is any point on the line gi.

The magnitude of the residual stresses can be estimated by assuming that a material having a stress-strain relation represented by the lines d gi is subjected to an applied load equal to P_d. If the resulting stress is σ_s, the residual stresses σ_r will be given by:

$$\sigma_r = \sigma_d - \sigma_s \qquad (5.12)$$

However, in the first case, where $P_d \leq P_o + P_c$, the stress σ_s can be calculated directly by simple proportion with the elastic stress at any point b. The concepts and procedures explained above are also valid for a case of a material subjected to stresses in more than one direction (46,22).

5.5 ANALYTICAL PROCEDURE

At any instant of the rolling process, the specimen under rolling is assumed to be a simply supported beam subjected to concentrated load at mid-span. The load is applied through the middle roller by changing its position with respect to the fixed ones. The position of the middle roller is calculated based on the radius of bend of the specimen required after rolling. Therefore, given the required radius of bend, the position of the middle roller can be calculated by solving equations 5.3 to 5.6. The distance moved by the middle roller to reach its new posi-

tion is equal to the deflection of the beam model at mid-point.

The load is applied incrementally until the model attains the same value of deflection calculated before. This is done through an iterative process that is used to search for that value of the deflection. In each iteration a new value of the deflection is calculated and then compared to that calculated based on the required radius of bend. The search ends if the difference between the two deflections is less than 10% of the magnitude of the required one. The deflection and the deformed shape of the cross-section are then calculated in each iteration by minimizing the total potential energy of the model calculated at that load increment.

Once this deflection is achieved the rolling process starts to force the same deflection at all the other sections of the model when they pass under the load. Therefore, the model is assumed to be moving to allow the load to be applied at another point. As the rolling is a continuous process in which every section of the model has to pass under the load, the more the number of load applications, the closer will the modelling be to the actual process. The present computer program allows the load to be applied at all the mesh points along the longitudinal axis of plate #1.

When the specimen moves with respect to the rollers, the stresses in each element of the model change according to the change in its position with respect to the load. All the elements moving closer to the point of application of the load become subjected to increasing stresses while those moving away from it experience an unloading process. Therefore, when the specimen moves, new stresses in the different elements of the model are calculated. These stresses act as initial stresses in the elements for the next loading step.

Since the position of the middle roller does not change during the rolling process, all sections of the model should have the same deflection when they pass under the load. Therefore, the iteration process to reach for the magnitude of the deflection is performed again when the load is at ~~its~~ new point of application. At this point the friction forces starts to enter the analysis. Because the elements of the model have some initial stresses, the load required to achieve the same deflection will be less than that used initially. It should be noted that the present analysis assumes that the rolling process is completed in one pass of rolling. A full pass of rolling is completed when at least a length equal to the distance between the fixed rollers pass under the load. This length is enough to give all the required information for any longer specimen.

When a part of the model leaves the machine, complete unloading occurs leaving some residual stresses in that part. The magnitude of these stresses is calculated using the procedure explained in the previous section. Therefore, for a specific radius of bend that is required after rolling, the cross-section deformed shape and an estimate of the residual stresses resulting from the rolling process are obtained.

CHAPTER VI

EXPERIMENTAL PROGRAM

6.1 GENERAL

The test program was carried out at Hodgson's Steel and Iron Works in Niagara Falls, Ontario, Canada, by some of the staff members of the Steel Company of Canada (STELCO). A detailed report that describes the experimental program was published in May 1978(4). Since the present theoretical analysis is based on the results obtained from the experimental program, it was felt that a brief summary of that program should be included here for completeness and for the benefit of the reader.

Bending of the HSS is carried out on a three-roller bending machine of the pyramid type similar to that shown in Fig. 1.2. This method of bending was chosen because, when compared to other methods, it was available, economical and ideally suited for large graduate bends required for construction purposes. Because of the cost involved, no considerations were given to heating the members before bending or to packing them with any filler material.

6.2 SPECIMEN DETAILS

A series of 54 tests were conducted on 27 different sizes of square and rectangular HSS. Two specimens of 2.5 m length were tested from each size. Profiles tested varied from 101.6 x 50.8 x 3.81 mm to 254.0 x 254.0 x 9.53 mm. All materials conformed to CSA Standard G40.21, Grade 50W, Class H. This specification calls for a minimum yield strength of 345 MPa, a tensile strength in the range of 450 MPa to 620 MPa and a minimum elongation of 22% in 50 mm. The chemical ingradients of this type of steel are described elsewhere (4). Sizes up to 610 mm in circumference were produced by a continuous weld process, while larger sizes were produced by an electric resistance weld process and were subsequently stress relieved.

A list of all HSS sizes tested and their cross-section properties are given in Table 6.1. The variables in this table are defined in Fig. 6.1.

6.3 MACHINE DESCRIPTION

The arrangement of the rollers in the pyramid type three-roller machine are as shown in Fig. 1.1. Rollers 1 and 2 are fixed in place while roller 3 is movable and is used to apply the load to the specimen. This arrangement makes the member under bending analogous to a simple beam with point supports at the fixed rollers, with the

Table 6-1

Properties of Cross-Sections

Member Size			A	C	$I_x \times 10^6$	$I_y \times 10^6$
h (mm)	b (mm)	t (mm)	(mm^2)	(mm)	(mm^4)	(mm^4)
101.6	50.8	3.81	1060	304.8	1.17	0.40
101.6	50.8	6.35	1640	304.8	1.95	0.64
101.6	50.8	7.95	1950	304.8	2.21	0.71
101.6	76.2	4.78	1530	355.6	2.18	1.39
101.6	76.2	6.35	1960	355.6	2.69	1.71
101.6	101.6	4.78	1770	406.4	2.75	2.75
101.6	101.6	9.53	3200	406.4	4.45	4.45
127.0	76.2	6.35	2280	406.4	4.70	2.10
127.0	76.2	9.53	3200	406.4	6.13	2.58
127.0	127.0	4.89	2280	508.0	5.60	5.60
127.0	127.0	9.53	4240	508.0	9.48	9.48
152.4	101.6	4.78	2280	508.0	7.28	3.89
152.4	101.6	9.53	4240	508.0	12.40	6.51
152.4	152.4	6.35	3610	609.6	12.60	12.60
177.8	127.0	4.78	2760	609.6	12.40	7.41
177.8	127.0	6.35	3610	609.6	15.80	9.40
177.8	177.8	4.78	3250	711.2	16.10	16.10
177.8	177.8	7.95	5240	711.2	24.80	24.80
203.2	101.6	4.78	2760	608.8	14.70	5.03
203.2	101.6	6.35	3610	608.8	18.80	6.35
203.2	101.6	9.53	5210	608.8	25.80	8.57
203.2	203.2	6.35	4900	812.8	31.30	31.30
203.2	203.2	9.53	7150	812.8	43.90	43.90
254.0	152.4	6.35	4900	812.8	42.90	19.50
254.0	152.4	9.53	7150	812.8	60.40	27.20
254.0	254.0	6.35	6190	1016.0	62.70	62.70
254.0	254.0	9.53	9080	1016.0	89.30	89.30

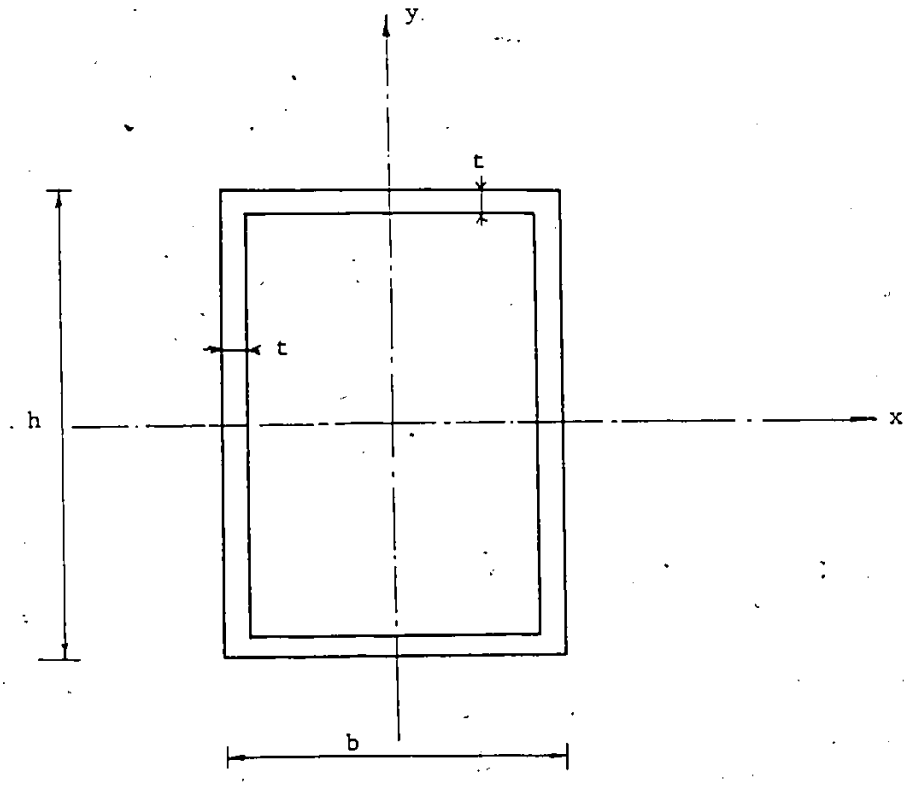

$$A = hb - (h-2t)(b-2t)$$

$$C = 2(h+b)$$

$$I_x = [bh^3 - (b-2t)(h-2t)^3]/12$$

$$I_y = [hb^3 - (h-2t)(b-2t)^3]/12$$

Fig. 6.1 Properties of the HSS.

load being applied to the beam at mid-span through the movable roller. A typical test arrangement is shown in Fig. 6.2. All tests were carried out on two separate machines. The details of the rolls diameters of these machines are shown in Fig. 6.3. Specimens up to and including 152.4 mm in depth were bent on machine No. 1 while machine No. 2 was used to bend the larger sections.

6.4 TESTING PROCEDURE

Two specimens of each of the 27 profiles were used in the test. Each specimen was bent to two different radii of curvature giving information about four levels of cross-section distortions with the corresponding radii of curvature for each profile used. The first specimen was bent to a radius at which minor distortion of the cross-section was apparent. A section was marked near one end of the specimen and this section was subjected to no further rolling. The remainder part of the specimen was then bent tighter until the level of distortion was considered unacceptably large. The specimen was then removed from the machine and accurate measurements of the radius of bend at each end of the specimen was made.

The rolling procedure was then repeated with the second specimen of the same profile. In this case, the radii of bend imposed had intermediate values between those measured from the first one. Cross sections were

Fig. 6.2. Typical rolling arrangement

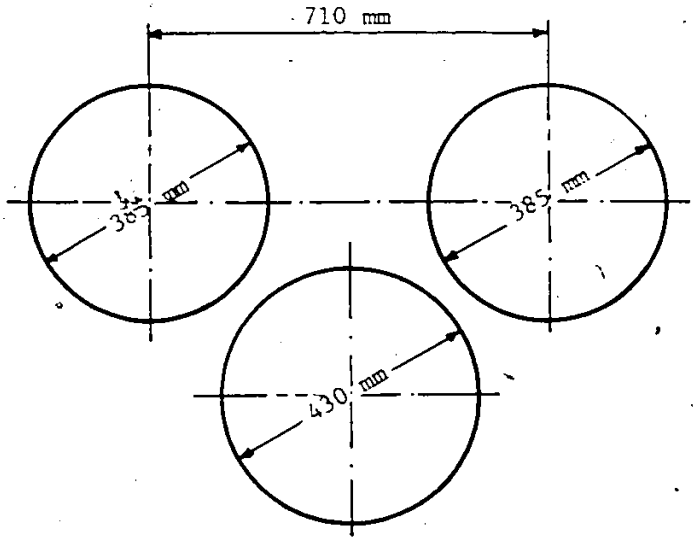

Bending Machine #1

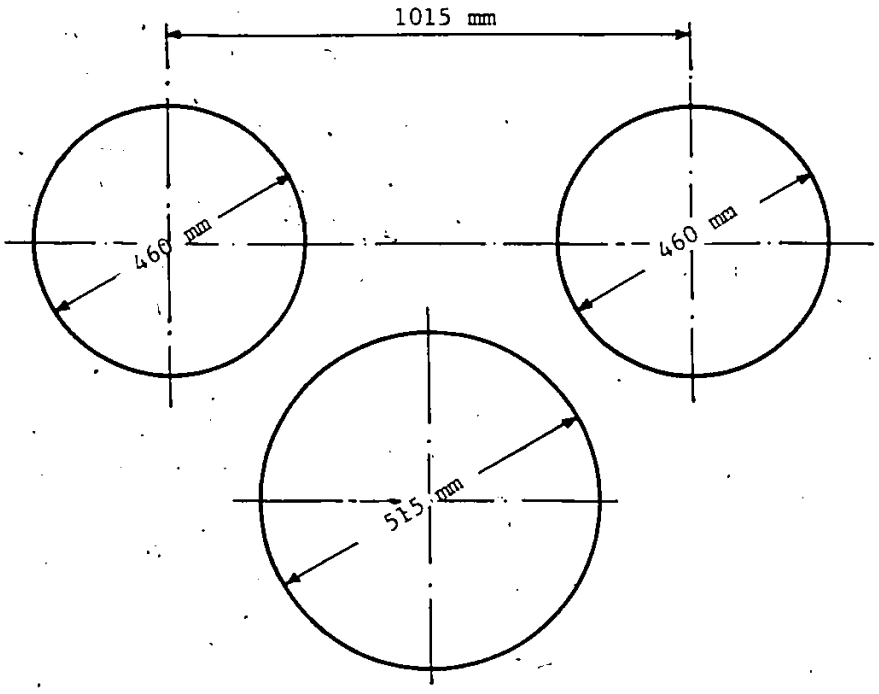

Bending Machine #2

Fig. 6.3. Dimensions of the rolls in the rolling machines

then cut from the portions bent to each of the four radii and these were subsequently accurately measured.

6.5 ANALYSIS OF THE EXPERIMENTAL RESULTS

Results from a total number of 108 cross-sections representing the 27 different HSS sizes were analyzed. In all cases, the distortions resulting from the rolling process had almost the same pattern, i.e., major deformations in both the compression flange and web plate facing the top of the rolling machine while minor distortions resulted in the tension flange and the other web. The effect of the rolling process on the cross-section profile is shown in Figs. 6.4 and 6.5, and a list of all dimensions of the distorted cross-section is given in Table 6.2 (see Fig. 6.6).

Based on these results two different parameters were calculated:

(i) Percentage increase in width after bending (P_b)

$$P_b = \frac{b_1 - b}{b} \times 100 \qquad (6.1)$$

(ii) Percentage bowing in compression flange after bending (P_e):

$$P_e = \frac{e}{h} \times 100 \qquad (6.2)$$

where b, b_1, e, h are as shown in Fig. 6.6. A list of

COLOURED PICTURES
Images en couleur

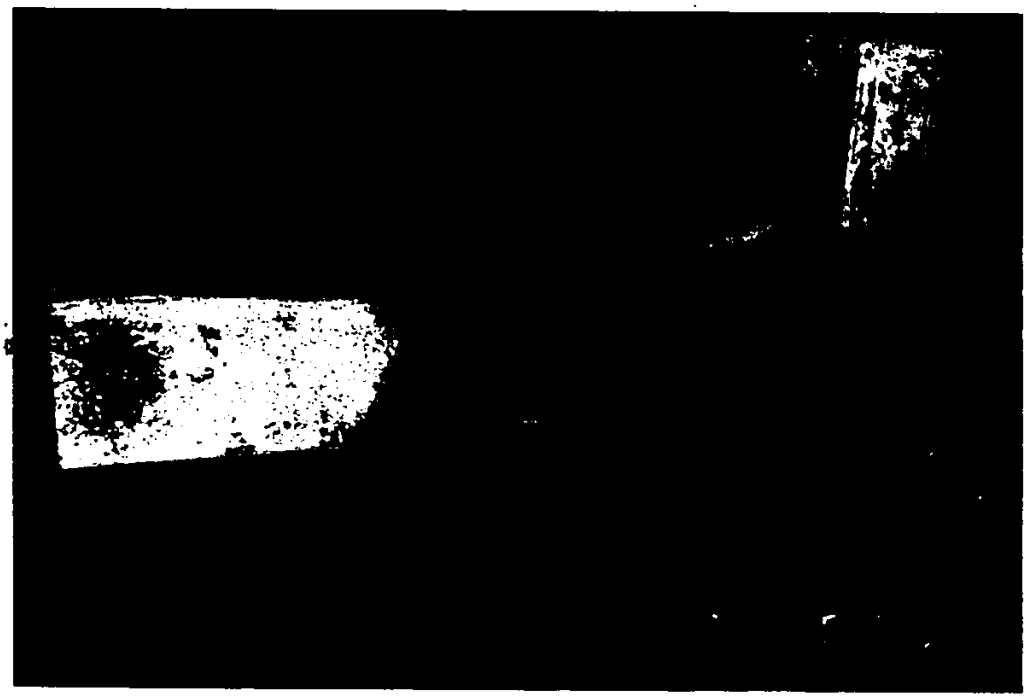

Fig. 6.4. Longitudinal view of the HSS after rolling

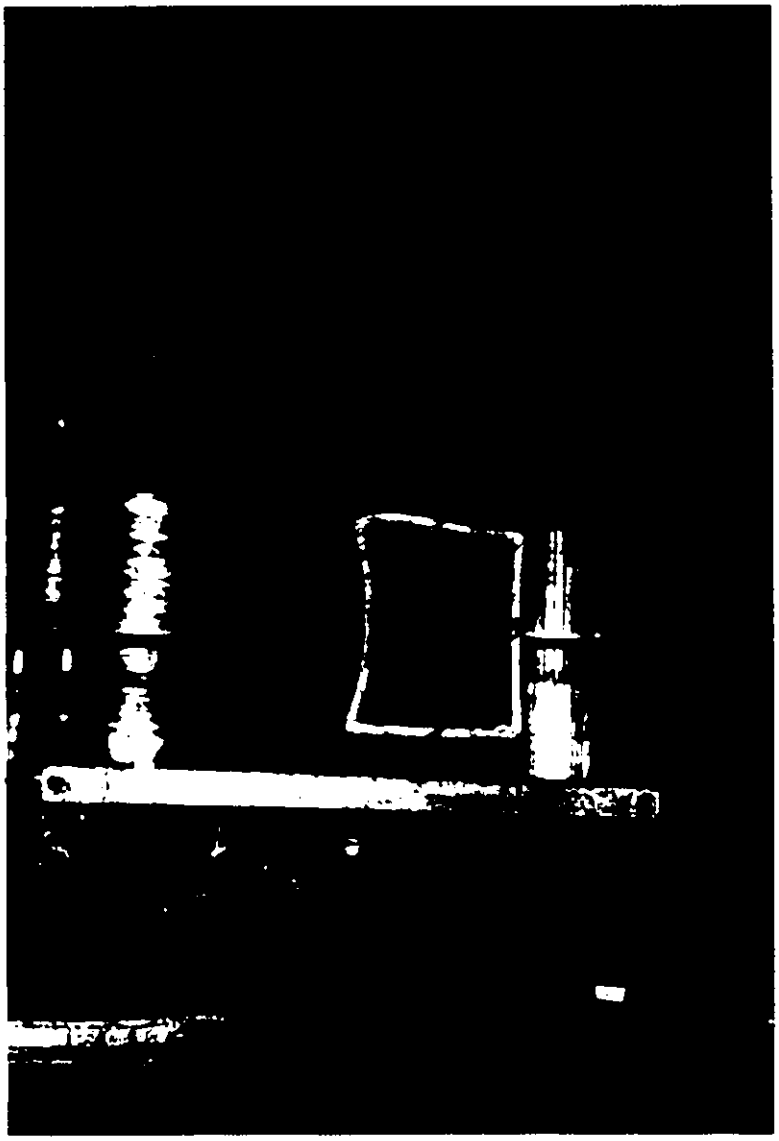

Fig. 6.5. Side view of the HSS after rolling.

Table 6-2

Cross-Secions Dimensions After Bending

Member Size			Radius	Dimensions After Bending			
h (mm)	b (mm)	t (mm)	R (m)	h_1 (mm)	h_2 (mm)	b_1 (mm)	e (mm)
101.6	50.8	3.81	0.84	95.2	90.5	55.6	2.4
			1.22	96.9	93.7	54.0	1.6
			1.83	98.4	95.2	54.0	0.8
			2.44	100.0	97.6	53.2	0.1
101.6	50.8	6.35	0.76	96.9	95.2	54.0	1.6
			0.91	98.4	96.9	53.2	1.2
			1.52	101.6	100.0	52.4	0.8
			2.13	101.6	100.0	52.4	0.8
101.6	50.8	7.95	0.51	98.4	96.9	54.0	0.8
			0.66	98.4	97.6	54.0	0.8
			1.07	100.0	99.2	53.2	0.1
			1.52	101.6	100.8	53.2	0.1
101.6	76.2	4.78	0.91	95.2	88.9	81.0	4.8
			1.22	96.9	91.3	80.2	3.2
			1.52	97.6	93.7	80.2	2.8
			2.44	98.4	96.9	78.6	0.8
101.6	76.2	6.35	1.14	95.2	89.7	82.5	2.4
			1.52	98.4	93.7	79.0	1.6
			2.13	98.4	95.2	77.8	0.8
			2.44	100.0	96.0	77.8	0.8
101.6	101.6	4.78	1.52	88.9	77.8	110.3	9.5
			2.44	92.1	85.7	106.8	7.1
			3.66	98.4	95.2	106.4	1.6
			4.88	98.4	96.9	104.8	0.8
101.6	101.6	9.53	0.66	88.9	84.2	109.6	3.2
			0.91	95.2	92.1	104.8	2.8
			1.37	96.9	95.2	104.0	0.8
			2.74	98.4	98.4	103.2	0.1
127.0	76.2	6.35	0.91	112.7	106.4	86.5	4.8
			1.14	114.3	112.7	84.2	4.8
			1.83	120.6	119.1	81.0	1.2
			2.44	121.4	120.6	79.4	0.8

Table 6-2 (cont'd)

Member Size			Radius	Dimensions After Bending			
h (mm)	b (mm)	t (mm)	R (m)	h_1 (mm)	h_2 (mm)	b_1 (mm)	e (mm)
127.0	76.2	9.53	0.91	115.1	111.1	83.3	2.0
			1.22	119.9	115.9	81.4	1.6
			1.68	120.6	119.1	79.8	0.8
			2.44	121.4	120.6	79.4	0.1
127.0	127.0	4.78	1.37	101.6	65.1	141.3	31.7
			3.05	111.1	96.9	138.1	12.7
			3.68	114.3	101.6	135.0	11.1
			4.27	120.6	112.7	133.3	4.8
			5.49	120.6	115.9	133.3	4.0
127.0	127.0	9.53	1.37	112.7	101.6	136.5	5.6
			1.52	111.1	104.0	134.1	4.0
			2.44	114.3	112.7	130.2	3.2
			4.27	120.6	115.9	130.2	0.8
152.4	101.6	4.78	2.44	138.1	120.6	115.9	8.0
			3.66	139.7	125.4	112.7	4.8
			6.10	144.5	138.9	107.9	2.8
152.4	101.6	9.53	1.22	133.3	127.0	115.1	4.0
			1.52	133.3	127.0	114.3	3.2
			2.44	141.3	136.5	108.7	2.8
			3.66	146.0	141.3	105.6	1.6
152.4	152.4	6.35	2.44	136.5	117.5	163.5	18.3
			3.66	139.7	120.6	161.9	15.9
			4.27	139.7	125.4	161.9	9.5
			4.88	141.3	131.8	159.9	6.3
177.8	127.0	4.78	2.44	162.7	146.0	136.5	17.5
			4.57	168.3	147.7	135.0	9.5
			7.32	169.9	157.2	134.1	4.8
			13.72	174.6	168.3	127.0	1.6
177.8	127.0	6.35	2.44	165.1	152.4	136.5	11.1
			4.27	166.7	158.7	136.5	6.3
			6.71	168.3	161.9	133.3	3.2
			10.97	171.4	168.3	130.2	2.8
177.8	177.8	4.78	7.32	158.7	127.0	188.9	28.6
			10.97	165.1	158.7	185.8	6.3
			18.29	171.4	165.1	183.4	2.4
			19.81	171.4	168.3	181.0	1.6

Table 6-2 (cont'd)

Member Size			Radius	Dimensions After Bending			
h (mm)	b (mm)	t (mm)	R (m)	h_1 (mm)	h_2 (mm)	b_1 (mm)	e (mm)
177.8	177.8	7.95	2.44	158.7	133.3	188.9	20.7
			7.32	161.9	152.4	186.9	8.0
			10.97	165.1	158.7	185.8	4.0
			15.24	171.4	168.3	181.8	2.8
203.2	101.6	4.78	4.88	186.5	171.4	100.6	11.1
			8.23	192.1	181.0	109.6	8.0
			12.19	195.3	190.5	107.2	1.6
			15.24	196.8	192.1	104.8	1.6
203.2	101.6	6.35	2.44	181.0	169.9	112.7	13.5
			3.66	184.1	177.8	111.1	7.1
			5.49	190.5	184.1	109.6	2.8
			13.72	195.3	188.9	103.2	1.6
203.2	101.6	9.53	2.44	184.1	181.0	112.7	3.2
			3.66	187.3	184.1	111.1	2.8
			4.57	190.5	185.8	109.6	2.4
			6.10	193.7	187.3	106.8	1.6
203.2	203.2	6.35	9.14	180.2	161.1	214.3	20.7
			13.72	184.1	169.9	213.1	12.7
			18.29	192.1	187.3	211.2	3.2
			24.38	193.7	188.1	209.5	1.6
203.2	203.2	9.53	7.32	177.8	171.4	214.3	5.6
			9.14	184.1	176.2	213.5	5.3
			10.97	184.9	182.6	213.1	4.8
			13.72	187.3	184.1	211.2	2.4
254.0	152.4	6.35	10.97	228.6	206.4	163.5	19.0
			15.24	231.8	214.3	163.5	15.9
			24.38	238.1	228.5	161.9	6.3
			30.48	238.1	233.4	161.9	2.4
254.0	152.4	9.53	7.32	225.4	217.5	165.1	4.0
			10.97	228.6	223.9	165.1	3.2
			13.72	228.6	225.4	165.1	3.2
			16.76	231.8	227.0	165.1	1.6

Table 6-2 (cont'd)

Member Size			Radius	Dimensions After Bending			
h (mm)	b (mm)	t (mm)	R (m)	h_1 (mm)	h_2 (mm)	b_1 (mm)	e (mm)
254.0	254.0	6.35	15.24	219.1	185.8	273.0	32.5
			24.38	215.9	185.8	272.3	33.4
			30.48	222.2	200.0	269.9	15.9
			36.58	228.6	215.9	269.9	12.7
254.0	254.0	9.53	10.97	212.7	196.8	273.0	12.7
			13.72	215.9	208.0	273.0	9.5
			18.29	222.2	212.7	258.3	6.3
			30.48	229.4	227.0	268.3	4.8

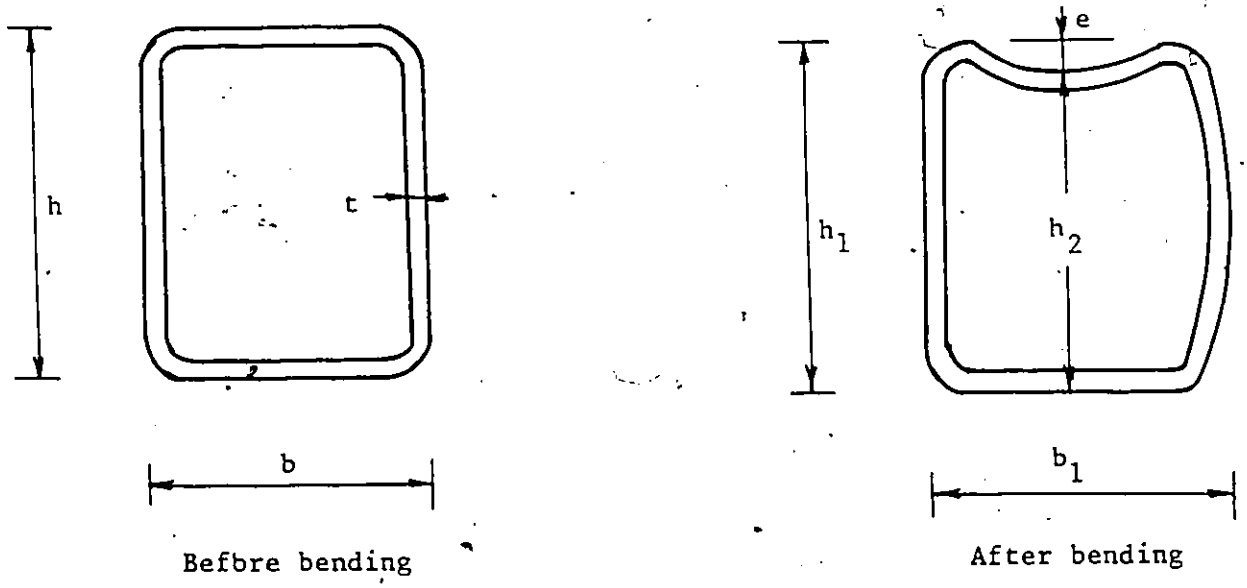

Fig. 6.6. Cross-section dimensions before and after bending.

these parameters for each radius of bend measured is given in Table 6.3.

The results presented in Table 6.3 are spread over a very wide range. It was apparent that there is no simple theoretical relationship between the radius of bend and any of the previous parameters. Therefore, it was decided to seek such a relationship by using a multiple regression analysis. The dependent variables were p_b and p_e while the independent variables were the radius of bend (R), the dimensions of the cross-section (h,b,t) and the moments of inertia of the section (I_x,I_y). Several regression relations were obtained using several possible combinations of the independent variables. The two relations which gave the highest multiple correlation coefficient were chosen to describe the two parameters p_b and p_e.

For the relation predicting the parameter p_b two models gave the same multiple correlation coefficient. The first model included R, h, b, t, I_x and I_y and the second one included R, h^2/t, h^2/t^2, bh/t, I_x and I_y. The multiple correlation coefficients of the two models were 0.844. The relationship predicting the parameter p_e was best described by a model which included R, h, b, t, I_x and I_y. This model gave a multiple correlation coefficient of 0.906. Therefore, the two relations used in the analysis were:

Table 6-3

Percentage Change in Properties

Member Size			Radius	Percentage Change in Properties	
h (mm)	b (mm)	t (mm)	R (m)	p_b (%)	p_e (%)
101.6	50.8	3.81	0.84	9.40	4.70
			1.22	6.25	3.15
			1.83	6.25	1.55
			2.44	4.70	0.25
101.6	50.8	6.35	0.76	6.25	3.15
			0.91	4.70	2.35
			1.52	3.15	1.55
			2.13	3.15	1.55
101.6	50.8	7.95	0.51	6.25	1.55
			0.66	6.25	1.55
			1.07	4.70	0.25
			1.52	4.70	0.25
101.6	76.2	4.78	0.91	6.27	6.27
			1.22	5.20	4.17
			1.52	5.20	3.63
			2.44	3.13	1.03
101.6	76.2	6.35	1.14	8.33	3.13
			1.52	3.63	2.10
			2.13	2.10	1.03
			2.44	2.10	1.03
101.6	101.6	4.78	1.52	8.60	9.38
			2.44	5.10	7.02
			3.66	4.70	1.57
			4.88	3.12	0.77
101.6	101.6	9.53	0.66	7.82	3.13
			0.91	3.12	2.72
			1.37	2.35	0.77
			2.74	1.57	0.12
127.0	76.2	6.35	0.91	13.53	6.27
			1.14	10.43	6.27
			1.83	6.27	1.57
			2.44	4.17	1.03

Table 6-3 (cont'd)

Member Size			Radius	Percentage Change in Properties	
h (mm)	b (mm)	t (mm)	R (m)	p_b (%)	p_e (%)
127.0	76.2	9.53	0.91	9.37	2.63
			1.22	6.80	2.10
			1.68	4.70	1.03
			2.44	4.17	0.17
127.0	127.0	4.78	1.37	11.26	25.00
			3.05	8.76	10.00
			3.68	6.26	8.76
			4.27	5.00	3.76
			5.49	5.00	3.12
127.0	127.0	9.53	1.37	7.50	4.38
			1.52	5.62	3.12
			2.44	2.50	2.50
			4.27	2.50	0.62
152.4	101.6	4.78	2.44	14.07	7.82
			3.66	10.95	4.70
			6.10	6.25	2.72
152.4	101.6	9.53	1.22	13.27	3.90
			1.52	12.50	3.13
			2.44	7.02	2.72
			3.66	3.90	1.57
152.4	152.4	6.35	2.44	7.30	11.98
			3.66	6.25	10.42
			4.27	6.25	6.25
			4.88	4.95	4.17
177.8	127.0	4.78	2.44	7.50	13.76
			4.57	6.26	7.50
			7.32	5.62	3.76
			13.72	0.00	1.26
177.8	127.0	6.35	2.44	7.50	8.76
			4.27	7.50	5.00
			6.71	5.00	2.50
			10.97	2.50	2.18

Table 6-3 (cont'd)

Member Size			Radius	Percentage Change in Properties	
h (mm)	b (mm)	t (mm)	R (m)	P_b (%)	P_e (%)
177.8	177.8	4.78	7.32	6.26	16.07
			10.97	4.47	3.57
			18.29	3.13	1.34
			19.81	1.79	0.90
177.8	177.8	7.95	2.44	6.26	11.61
			7.32	5.13	4.47
			10.97	4.47	2.23
			15.24	2.23	1.56
203.2	101.6	4.78	4.88	7.82	10.95
			8.23	7.82	7.82
			12.19	5.47	1.57
			15.24	3.12	1.57
203.2	101.6	6.35	2.44	10.95	13.27
			3.66	9.37	7.02
			5.49	7.82	2.72
			13.72	1.57	1.57
203.2	101.6	9.53	2.44	10.95	3.13
			3.66	9.37	2.72
			4.57	7.82	2.35
			6.10	5.10	1.57
203.2	203.2	6.35	9.14	5.47	10.16
			13.72	4.89	6.25
			18.29	3.91	1.56
			24.38	3.12	0.79
203.2	203.2	9.53	7.32	5.47	2.74
			9.14	5.07	2.61
			10.97	4.89	2.35
			13.72	3.91	1.17
254.0	152.4	6.35	10.97	7.30	12.50
			15.24	7.30	10.42
			24.38	6.25	4.17
			30.48	6.25	1.57

Table 6-3 (cont'd)

Member Size			Radius	Percentage Change in Properties	
h (mm)	b (mm)	t (mm)	R (m)	p_b (%)	p_e (%)
254.0	152.4	9.53	7.32	8.33	2.60
			10.97	8.33	2.08
			13.72	8.33	2.08
			16.76	8.33	1.05
254.0	254.0	6.35	15.24	7.50	12.81
			24.38	7.19	13.13
			30.48	6.25	6.25
			36.58	6.25	5.00
254.0	254.0	9.53	10.97	7.50	5.00
			13.72	7.50	3.75
			18.29	5.63	2.50
			30.48	5.63	1.88

$$p_b\% = (R^{-0.8}) \times (h^{-0.0014}) \times (b^{2.97}) \times (t^{-0.66}) \times (I_x^{1.42}) \times (I_y^{-1.594}) \times (0.00034) \quad (6.3)$$

$$p_e\% = (R^{-1.513}) \times (h^{-0.098}) \times (b^{-14.173}) \times (t^{-6.943}) \times (I_x^{-1.332}) \times (I_y^{7.251}) \times (0.000225) \quad (6.4)$$

The first model describing p_b was chosen over the second one only because of its simplicity and similarity to the model describing p_e. The standard error in equations 6.4 and 6.5 were 0.275% and 0.448%, respectively.

To test the significance of the multiple correlation coefficient (r) the critical value for r is calculated. For the number of observations = 92, 6 independent variables and a 95% level of significance, the critical value for r = 0.331 (23). Since the multiple correlation coefficients obtained for the relations 6.3 and 6.4 are greater than 0.331 the hypothesis that there is no association between the variables is rejected and the relations are considered significant.

Comparisons between the measured distortion of the cross-section and those predicted by equations 6.3 and 6.4 are given in Tables 6.4 and 6.5, respectively.

Equations 6.3 and 6.4 are only valid for sections with web depth in the range 110.0 mm to 205.0 mm. The

Table 6-4

Comparison Between the Measured and Estimated Values for p_b

Member Size			Radius	p_b %		
h (mm)	b (mm)	t (mm)	R (m)	Measured	Estimated*	Difference (%)
101.60	50.80	3.81	0.84	9.40	9.22	-1.94
			1.22	6.25	6.84	9.41
			1.83	6.25	4.94	-20.90
			2.44	4.70	3.93	-16.44
101.60	50.80	6.35	0.76	6.25	6.88	10.03
			0.91	4.70	5.95	26.68
			1.52	3.15	3.95	25.39
			2.13	3.15	3.02	-4.27
101.60	50.80	7.95	0.51	6.25	8.19	30.96
			0.66	6.25	6.66	6.55
			1.07	4.70	4.52	-3.73
			1.52	4.70	3.42	-27.30
101.60	76.20	4.78	0.91	6.27	8.15	29.96
			1.22	5.20	6.44	23.94
			1.52	5.20	5.41	3.95
			2.44	3.13	3.77	20.58
101.60	76.20	6.35	1.14	8.33	5.46	-34.40
			1.52	3.63	4.34	19.60
			2.13	2.10	3.31	57.83
			2.44	2.10	2.97	41.57
101.60	101.60	4.78	1.52	8.60	5.95	-30.77
			2.44	5.10	4.08	-20.05
			3.66	4.70	2.95	-37.28
			4.88	3.12	2.34	-24.94
101.60	101.60	9.53	0.66	7.82	6.77	-13.45
			0.91	3.12	5.23	67.78
			1.37	2.35	3.77	60.58
			2.74	1.57	2.17	38.05
127.00	76.20	6.35	0.91	13.53	10.41	-23.05
			1.14	10.43	8.70	-16.62
			1.83	6.27	5.96	-5.02
			2.44	4.17	4.73	13.46

*by Eq. 6.3

Table 6-4 (cont'd)

Member Size			Radius	p_b%		
h (mm)	b (mm)	t (mm)	R (m)	Measured	Estimated	Difference (%)
127.00	76.20	9.53	0.91	9.37	7.78	-16.94
			1.22	6.80	6.16	-9.48
			1.68	4.70	4.77	1.39
			2.44	4.17	3.54	-15.22
127.00	127.00	4.78	1.37	11.26	11.09	-1.53
			3.05	8.76	5.85	33.28
			3.68	6.26	5.03	-19.65
			4.27	5.00	4.47	-10.69
127.00	127.00	9.53	1.37	7.50	6.42	-14.45
			1.52	5.62	5.90	5.06
			2.44	2.50	4.04	61.74
			4.27	2.50	2.58	3.37
152.40	101.60	4.78	2.44	14.07	9.34	-33.61
			3.66	10.94	6.75	-38.32
			6.10	6.25	4.49	-28.19
152.40	101.60	9.53	1.22	13.27	9.67	-27.13
			1.52	12.50	8.11	-35.12
			2.44	7.02	5.55	-20.88
			3.66	3.90	4.02	2.96
152.40	152.40	6.35	2.44	7.30	8.64	18.40
			3.66	6.25	6.25	0.00
			4.27	6.25	5.52	-11.62
			4.88	4.95	4.96	0.29
177.80	127.00	4.78	2.44	7.50	13.82	82.25
			4.57	4.57	6.26	8.36
			7.32	7.32	5.62	5.74
177.80	127.00	6.35	2.44	7.50	11.06	47.49
			4.27	7.50	7.07	-5.74
			6.71	5.00	4.91	-1.77
			10.97	2.50	3.32	32.93
177.80	177.80	4.78	7.32	6.26	6.56	4.72
			10.97	4.47	4.74	6.11
			18.29	3.13	3.15	0.67
			19.81	1.79	2.96	65.14

Table 6-4 (cont'd)

Member Size			Radius	p_b%		
h (mm)	b (mm)	t (mm)	R (m)	Measured	Estimated	Difference (%)
177.80	177.80	7.95	2.44	6.25	10.47	67.21
			7.32	5.13	4.35	-15.27
			10.97	4.47	3.14	-29.65
			15.24	2.23	2.42	8.41
203.20	101.60	4.78	4.88	7.82	9.66	23.50
			8.23	7.82	6.36	-18.70
			12.19	5.47	4.64	15.12
			15.24	3.12	3.88	24.47
203.20	101.60	6.35	2.44	10.95	13.64	24.52
			3.66	9.37	9.86	5.21
			5.49	7.82	7.13	-8.86
			13.72	1.57	3.43	118.17
203.20	101.60	9.64	2.44	10.95	10.14	-7.42
			3.66	9.37	7.33	-21.78
			4.57	7.82	6.14	-21.53
			6.10	5.10	4.87	-4.50
203.20	203.20	6.35	9.14	5.47	6.03	10.15
			13.72	4.89	4.35	-10.97
			18.29	3.91	3.46	-11.53
			24.38	3.12	2.75	-11.91
203.20	203.20	9.53	7.32	5.47	5.19	-5.12
			9.14	5.07	4.35	-14.29
			10.97	4.89	3.76	-23.21
			13.72	3.91	3.14	-19.70

Table 6-5

Comparison Between the Measured and Estimated Values for P_e

Member Size			Radius	P_e		
h (mm)	b (mm)	t (mm)	R (m)	Measured	Estimated*	Difference (%)
101.60	50.80	3.81	0.84	4.70	3.75	-20.13
			1.22	3.15	2.13	-32.25
			1.83	1.55	1.16	-25.44
			2.44	0.25	0.75	200.00
101.60	50.80	6.35	0.76	3.15	2.03	-35.45
			0.91	2.35	1.55	-34.11
			1.52	1.55	0.71	-54.03
			2.13	1.55	0.43	-72.41
101.60	50.80	7.95	0.51	1.55	1.46	-5.69
			0.66	1.55	0.99	-36.15
			1.07	0.25	0.48	90.57
			1.52	0.25	0.28	12.04
101.60	76.20	4.78	0.91	6.27	8.48	35.25
			1.22	4.17	5.44	30.51
			1.52	3.63	3.90	7.50
			2.44	1.03	1.87	81.79
101.60	76.20	6.35	1.14	3.13	2.85	-8.96
			1.52	2.10	1.84	-12.19
			2.13	1.03	1.11	7.45
			2.44	1.03	0.90	-12.51
101.60	101.60	4.78	1.52	9.88	6.84	-30.81
			2.44	7.02	3.34	-52.42
			3.66	1.57	1.81	15.20
			4.88	0.77	1.17	52.00
101.60	101.60	9.53	0.66	3.13	3.46	10.68
			0.91	2.72	2.13	-21.66
			1.37	0.77	1.15	49.01
			2.74	0.12	0.40	235.02
127.00	76.20	6.35	0.91	6.27	8.27	31.90
			1.14	6.27	5.88	-6.20
			1.83	1.57	2.87	83.05
			2.44	1.03	1.86	80.05

*by Eq. 6.4

Table 6-5 (cont'd)

Member Size			Radius	P_e		
h (mm)	b (mm)	t (mm)	R (m)	Measured	Estimated	Difference (%)
127.00	76.20	9.53	0.91	2.63	2.14	-18.51
			1.22	2.10	1.38	-34.50
			1.68	1.03	0.85	-17.70
			2.44	0.17	0.48	183.49
127.00	127.00	4.78	1.37	25.00	22.29	-10.83
			3.05	10.00	6.64	-33.58
			3.68	8.76	5.00	-42.93
			4.27	3.76	3.99	6.17
127.00	127.00	9.53	1.37	4.38	4.18	-4.65
			1.52	3.12	3.57	14.39
			2.44	2.50	1.74	-30.24
			4.27	0.62	0.75	20.62
152.40	101.60	4.78	2.44	7.82	10.85	38.77
			3.66	4.70	5.88	25.02
			6.10	2.72	2.71	-0.27
152.40	101.60	9.53	1.22	3.90	5.29	35.76
			1.52	3.13	3.80	21.29
			2.44	2.72	1.86	-31.79
			3.66	1.57	1.00	-36.02
152.40	152.40	6.35	2.44	11.98	11.67	-2.58
			3.66	10.42	6.32	-39.36
			4.27	6.25	5.00	-19.93
			4.88	4.17	4.09	-1.94
177.80	127.00	4.78	2.44	13.76	23.81	73.00
			4.57	7.50	9.21	22.82
			7.32	3.76	4.52	20.12
177.80	127.00	6.35	2.44	8.76	13.47	53.71
			4.27	5.00	5.77	15.48
			6.71	2.50	2.42	-3.15
			10.97	2.18	1.39	-36.46

Table 6-5 (cont'd)

Member Size			Radius	P_e		
h (mm)	b (mm)	t (mm)	R (m)	Measured	Estimated	Difference (%)
177.80	177.80	4.78	7.32	16.07	7.52	-53.20
			10.97	3.57	4.08	14.24
			18.29	1.34	1.88	40.43
			19.81	0.90	1.67	85.30
177.80	177.80	7.95	2.44	11.61	14.95	28.80
			7.32	4.47	2.84	-36.53
			10.97	2.23	1.54	-31.02
			15.24	1.56	0.94	-40.03
203.20	101.60	4.78	4.88	10.97	9.35	-14.80
			8.23	7.82	4.24	-45.80
			12.19	1.57	2.34	50.00
			15.24	1.57	1.67	6.28
203.20	101.60	6.35	2.44	13.27	14.50	9.23
			3.66	7.02	7.85	11.80
			5.49	2.72	4.25	56.24
			13.72	1.57	1.06	-32.29
203.20	101.60	9.53	2.44	3.13	4.99	59.41
			3.66	2.72	2.70	-0.67
			4.57	2.35	1.93	-17.84
			6.10	1.57	1.25	-20.55
203.20	203.20	6.35	9.14	10.16	5.69	-43.97
			13.72	6.25	3.08	-50.73
			18.29	1.56	1.99	27.76
			24.38	0.79	1.29	63.32
203.20	203.20	9.53	7.32	2.74	3.52	28.51
			9.14	2.61	2.52	-3.59
			10.97	2.35	1.91	-18.76
			13.72	1.17	1.36	16.33

results of the four deeper specimens (254.0 mm) were so inconsistent that they tended to distort the values obtained in the regression analysis. When these results are included in the previous models the multiple correlation coefficients dropped to 0.616 and 0.647 for equations 6.3 and 6.4, respectively. Therefore, these results were excluded from the analysis. A possible reason for this inconsistency is that during the rolling of these deeper sections, the bending machine seemed to be working at its maximum capacity and frequent adjustment of the movable roller was required in order to complete the process.

6.6 MOMENT OF INERTIA OF THE DEFORMED SECTIONS

The deformation resulting from the rolling process also reduce the moment of inertia of the section. This reduction increases with decrease in the radius of bend. The percentage reduction, p_i, in the moment of inertia I_x, is described by

$$p_i = \frac{I_x - I_{reduced}}{I_x} \times 100 \qquad (6.5)$$

where $I_{reduced}$ is the moment of inertia of the deformed section. Values of p_i for all the specimens tested in the experimental program are given in Table 6.6. Thirty six specimens expressed reduction in the moment of inertia of less than 10%; while 47 specimens showed a reduction

between 10% and 20%, and the remaining 25 specimens exhibited reduction of more than 20%.

It should be noted that since the rolling process induces residual stresses in the different parts of the rolled specimens, the moment of inertia of the deformed section will no longer be directly proportional to its strength.

Table 6.6

Reduction in the Moment of Inertia

Member Size			Radius	Percentage Change in $I_x(p_i)$
h (mm)	b (mm)	t (mm)	R (m)	
101.6	50.8	3.81	0.84	11.78
			1.22	8.81
			1.83	5.94
			2.44	2.96
101.6	50.8	6.35	0.76	8.09
			0.91	5.57
			1.52	0.00
			2.13	0.00
101.6	50.8	7.95	0.51	5.09
			0.66	4.54
			1.07	1.90
			1.52	0.00
101.6	76.2	4.78	0.91	13.73
			1.22	10.67
			1.52	8.22
			2.44	5.88
101.6	76.2	6.35	1.14	12.87
			1.52	7.94
			2.13	7.43
			2.44	4.93
101.6	101.6	4.78	1.52	27.09
			2.44	19.70
			3.66	6.48
			4.88	5.93
101.6	101.6	9.53	0.66	24.97
			0.91	13.57
			1.37	9.67
			2.74	5.75
127.0	76.2	6.35	0.91	20.06
			1.14	16.28
			1.83	8.25
			2.44	7.35

Table 6.6 (cont'd)

Member Size			Radius R (m)	Percentage Change in I_x (p_i)
h (mm)	b (mm)	t (mm)		
127.0	76.2	9.53	0.91	17.26
			1.22	10.85
			1.68	9.08
			2.44	7.62
127.0	127.0	4.78	1.37	47.87
			3.05	26.91
			3.68	22.50
			4.27	11.74
			5.49	10.16
127.0	127.0	9.53	1.37	24.78
			1.52	25.61
			2.44	19.22
			4.27	11.46
152.4	101.6	4.78	2.44	20.12
			3.66	17.79
			6.10	9.94
152.4	101.6	9.53	1.22	22.18
			1.52	22.39
			2.44	13.71
			3.66	8.82
152.4	152.4	6.35	2.44	24.60
			3.66	21.26
			4.27	19.35
			4.38	15.91
177.8	127.0	4.78	2.44	18.78
			4.57	15.04
			7.32	10.90
			13.72	5.51
177.8	127.0	6.35	2.44	15.31
			4.27	12.05
			6.71	10.59
			10.97	6.95

Table 6.6 (cont'd.)

Member Size			Radius	Percentage Change in
h (mm)	b (mm)	t (mm)	R (m)	I_x (p_i)
177.8	177.8	4.78	7.32	27.89
			10.97	13.63
			18.29	7.87
			19.81	7.11
203.2	101.6	4.78	4.88	17.00
			8.23	11.05
			12.19	6.96
			15.24	6.23
203.2	101.6	6.35	2.44	20.02
			3.66	16.26
			5.49	11.12
			13.72	8.67
203.2	101.6	9.53	2.44	15.25
			3.66	12.82
			4.57	10.88
			6.10	9.31
203.2	203.2	6.35	9.14	24.34
			13.72	19.78
			18.29	10.33
			24.38	9.39
203.2	203.2	9.53	7.32	23.15
			9.14	18.25
			10.97	15.91
			13.72	14.31
254.0	152.4	6.35	10.97	20.96
			15.24	17.72
			24.38	11.77
			30.48	10.61
254.0	152.4	9.53	7.32	19.90
			10.97	16.94
			13.72	16.56
			16.76	14.72

Table 6.6 (cont'd.)

Member Size			Radius R (m)	Percentage Change in I_x (p_i)
h (mm)	b (mm)	t (mm)		
254.0	254.0	6.35	15.24	29.81
			24.38	31.16
			30.48	25.53
			36.58	19.16
254,0	254.0	9.53	10.97	30.49
			13.72	26.60
			18.29	23.18
			30.48	16.61

CHAPTER VII

RESULTS OF THE THEORETICAL ANALYSIS

7.1 GENERAL

The procedures explained in Chapters 4 and 5 are applied to the different profiles of the HSS. The calculations are carried out using a computer program that was developed by the author. A flow chart that describes the main operations of the computer program is given in Fig. 7.1.

In this chapter, general results such as the distribution of both the local and overall displacements and the distribution of the different component of stresses at different sections are given. The effect of friction between the specimen and the rollers is discussed and the distribution of the residual stresses resulting from the rolling process is shown. Comparison between the results of the present analysis and that of a reference example is given and comparison between the experimental and theoretical results is also presented. Finally, a parametric study is carried out to show the effect of the change in the cross-section dimensions on the resulting distortions in the section at various constant radii of bend.

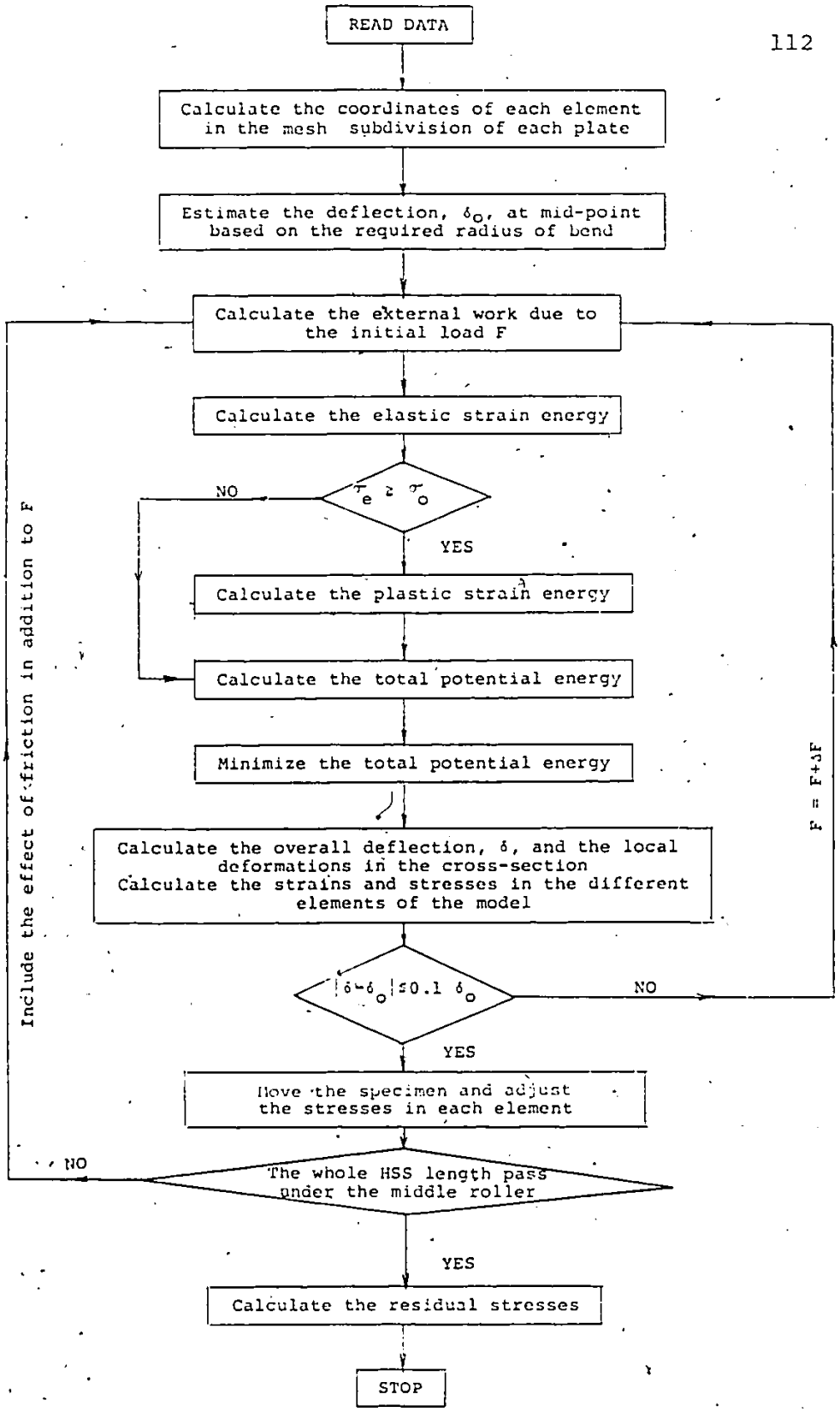

Fig. 7.1. Flow chart for the computer program.

7.2 CONVERGENCE OF THE DISPLACEMENT FUNCTIONS

The number of terms used in each series to describe the deformed shape of the HSS after bending is one of the main factors that affect the accuracy of the theoretical results. The larger the number of terms, the closer the solution to the true one. In the present study, because of the limitation on the storage capacity of the available computer, only three terms are considered in each series. Although the number of terms is limited to three, it is felt from the convergence of both the displacements and the stresses that three terms are adequate to give reasonably accurate estimates for both the deformations and the stresses. According to Oden (34), three terms of the series that is used to represent the overall deflection of the beam model, equation 4.1, will result in almost the exact value for the displacement and with an error of less than 10% in the stresses which is practically acceptable. The convergence of the different displacement functions as well as the stresses is demonstrated by solving a beam model of 203.20 x 203.2 x 9.53 mm cross-section dimensions. The solution was carried out using one, two and three terms. The results of the three different solutions are given in Table 7.1 and 7.2.

Table 7.1

Convergence of the Displacement Functions

Displ.	u			v			w		
No. of terms	1	2	3	1	2	3	1	2	3
Compression flange at $x = 3\ell/8$, $y = b/4$	1.263	1.287	1.291	0.061	0.064	0.065	6.139	6.146	6.149
Web at $x = 3\ell/8$, $y = h/4$	-0.764	-0.775	-0.776	6.055	6.063	6.065	0.012	0.013	0.014
Tension flange at $x = 3\ell/8$, $y = b/4$	-.267	-1.287	-1.291	0.009	0.012	0.013	6.039	6.050	6.054

Table 7.2

Convergence of the Stresses Components

Stresses	σ_x			σ_y			τ_{xy}		
No. of terms	1	2	3	1	2	3	1	2	3
Compression flange at $x = 3/8\ell$ $y = b/4$	-107.50	-109.51	-109.94	-26.60	-26.85	-27.16	0.65	0.71	0.79
Web at $x = 3/8\ell$ $y = h/4$	54.74	55.63	55.88	16.42	16.59	16.66	-45.55	-47.54	-47.56
Tension flange at $x = 3/8\ell$ $y = b/4$	103.00	105.11	105.78	11.17	12.12	12.43	0.02	0.16	0.27

7.3 COMPARISON WITH REFERENCE EXAMPLE

All efforts failed to find a similar problem for the purpose of comparison. It is believed that this is the first study on rolling of hollow structural sections. Therefore, the local deformations are only compared to those obtained from the experimental program in section 7.7. However, to prove the validity and the accuracy of the operations carried out by the computer program, the maximum overall displacement of the center line of the model, at mid-span, while still stationary is compared to that obtained by the finite element method (24) in both the elastic and plastic range.

The dimensions of the beam and the stress-strain relation used in this example are as shown in Fig. 7.2a and 7.2b, respectively. The stress-strain relation is approximated as shown in the figure to suit the present computer program. In the finite element method a total number of 768 elements were used while only 265 elements in the present study gave reasonable agreement as shown in Fig. 7.3. Because of the symmetry of the problem only one-quarter of the model was solved.

The difference in the results between the finite element method and the present study could be due to one or more of the following reasons:

(a) The difference in the number of elements used.

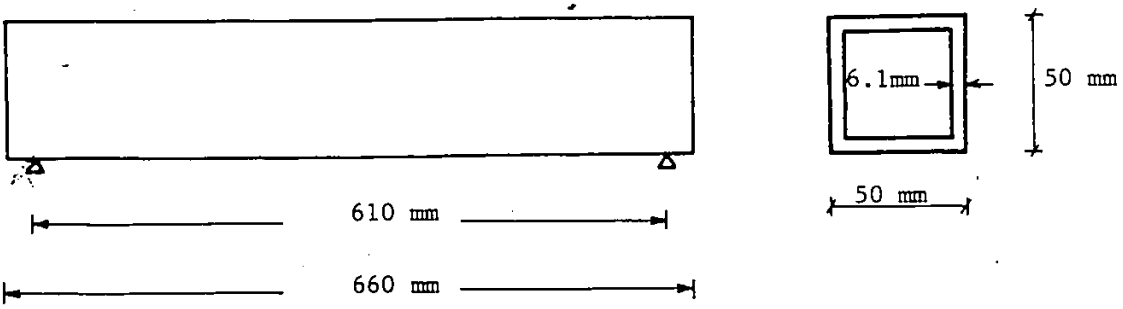

(a) Dimensions

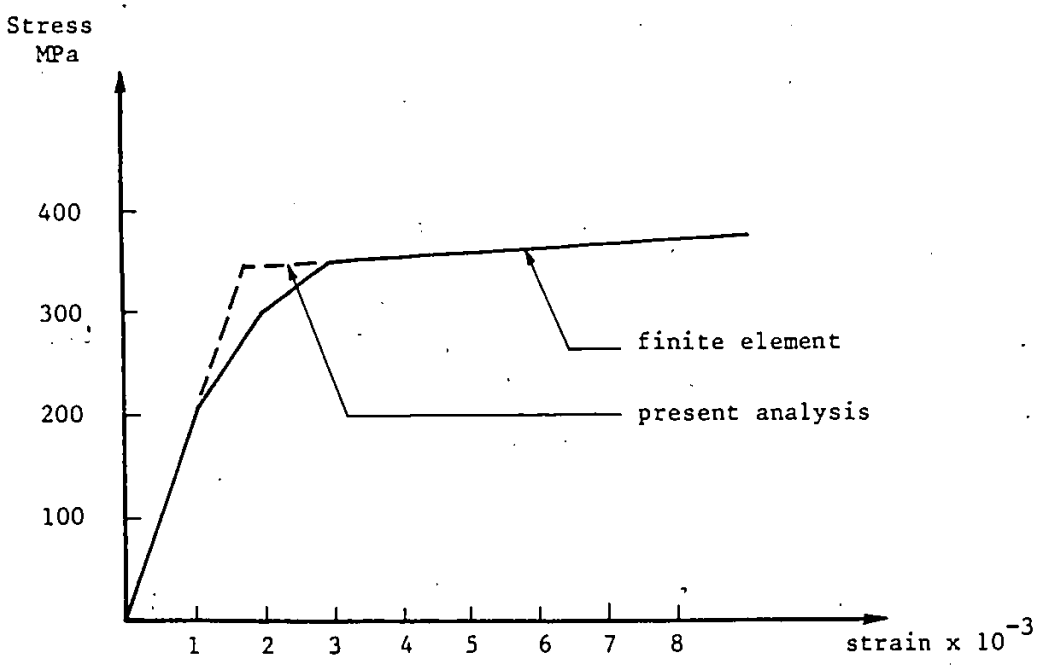

(b) Stress-strain relations

Fig. 7.2. Dimensions and stress-strain relation for the reference example.

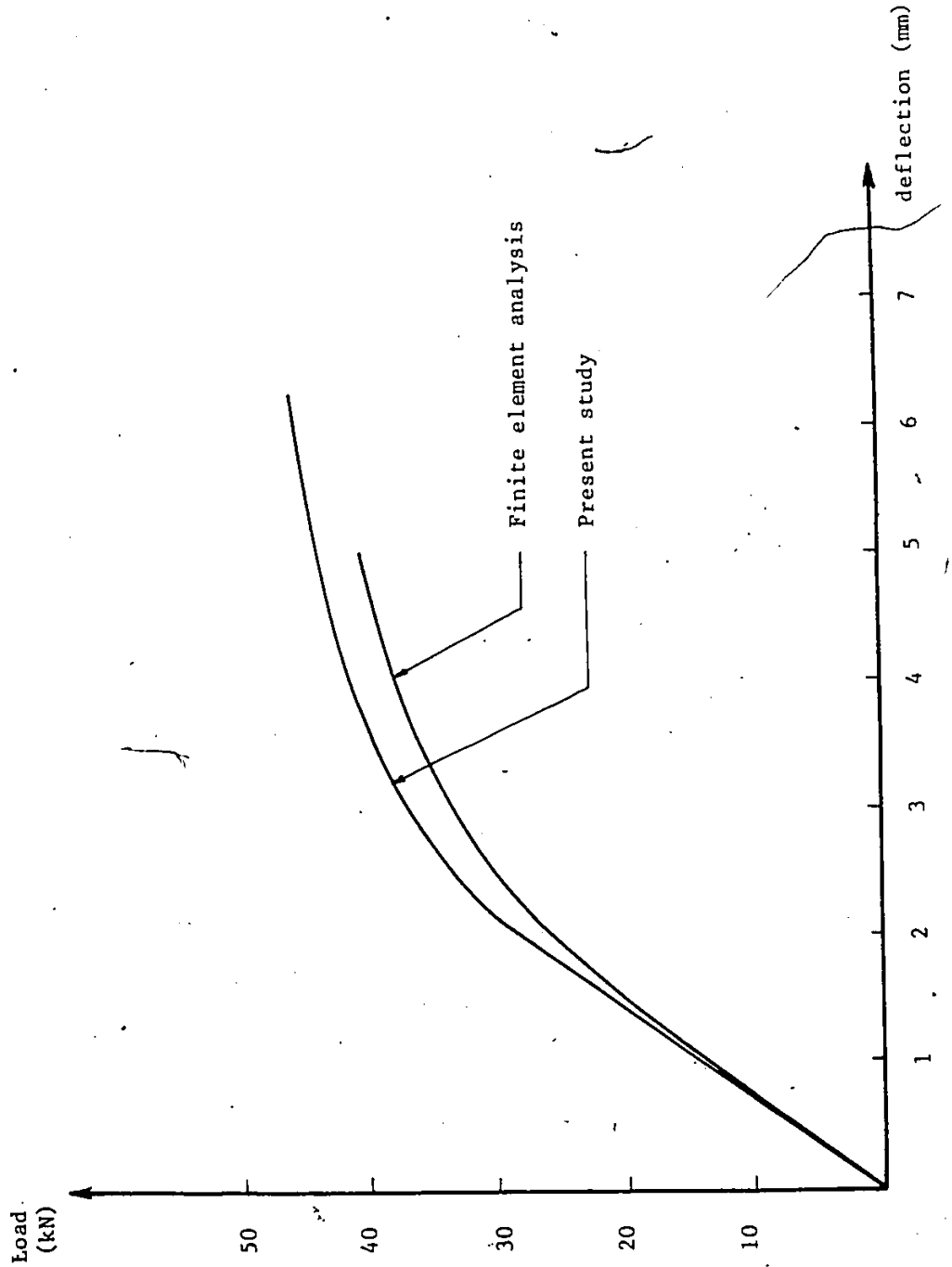

Fig. 7.3. Load-deflection curve

(b) The approximation in the stress-strain relation (see Fig. 7.2b).

(c) The approximation in estimating the magnitude of the stresses that results from using the Rayleigh-Ritz method.

7.4 DISPLACEMENT AND STRESS DISTRIBUTIONS

The displacement of any point in the beam model consists of two parts: overall and local displacements. The magnitude of such displacements depends on the applied load, the stress level at the point at the time of the load application as well as on the position of the point with respect to the load. At any section, the displacement profile is obtained from the respective assumed displacement function. The magnitude of the applied load and the stress level at the different points of the model will only affect the magnitude of such displacement.

A cross-section of dimensions 177.8 x 127.0 x 6.35 m is used to demonstrate the different displacement profiles obtained from the assumed displacement functions. Each plate in the model was divided into 16 elements. The model was subjected to different loads of 200, 300, 400, 500, 525 and 550 kN. All elements were elastic until the 500 kN load was applied. This load initiated yield in 8 elements in each of the compression and tension flanges. In each web, 12 elements followed in yielding at a load of 525 kN. The profile of the out-of-plane displacement in the trans-

verse and longitudinal directions are as shown in Fig. 7.4a and 7.4b, respectively. Also the distribution of the in-plane displacement in the x and y directions are shown in Figs. 7.5 and 7.6, respectively.

The distribution of the stresses σ_x, σ_y, τ_{xy} and σ_e are shown in Figs. 7.7, 7.8, 7.9 and 7.10, respectively. The distribution of these stresses are shown in two sections along the beam model; at $x = \ell/8$ and $x = 3\ell/8$. It should be noted that the stresses resulting from the overall deformations are more dominant when compared to that resulting from the local deformations. Therefore, although the tension flange has relatively small local deformations compared to that of the compression flange, both flanges yield almost at the same load.

In the web element, bending stresses are dominant at its ends while shear stresses are much larger than that of bending in the middle part of the web. That is the reason for the nearly even distribution of the effective stresses along the web elements.

7.5 EFFECT OF THE NUMBER OF ELEMENTS IN THE MESH SUBDIVISION

The number of elements in the mesh subdivision of each component of the beam model has an important influence on the theoretical results. Since the stresses are calculated at the center of each element, a larger number of smaller

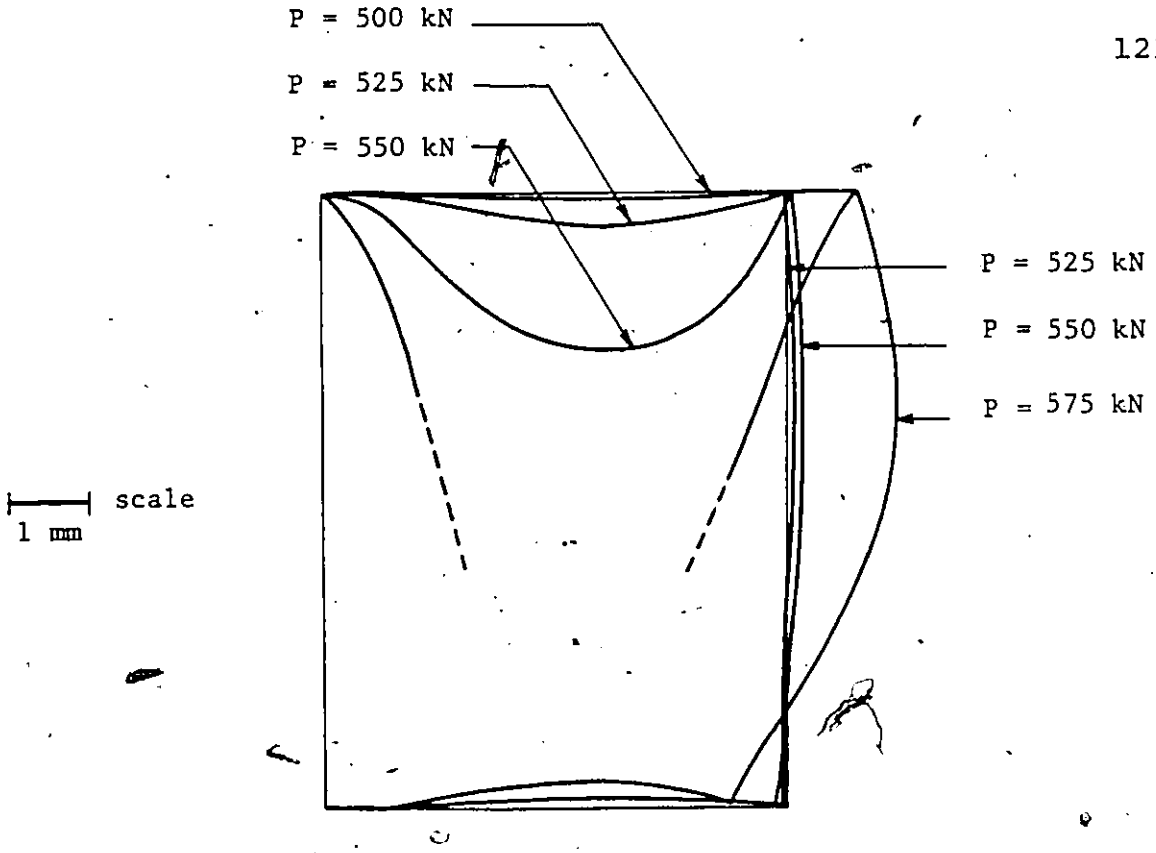

(a) Transverse profile at x=3ℓ/8

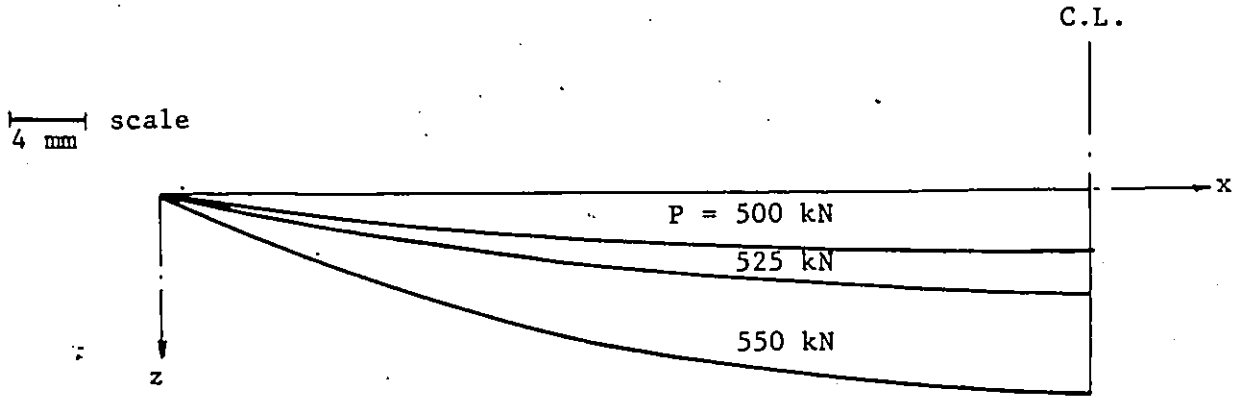

(b) Longitudinal profile along the centre of the compression flange

Fig. 7.4. Out-of-plane displacement profile.

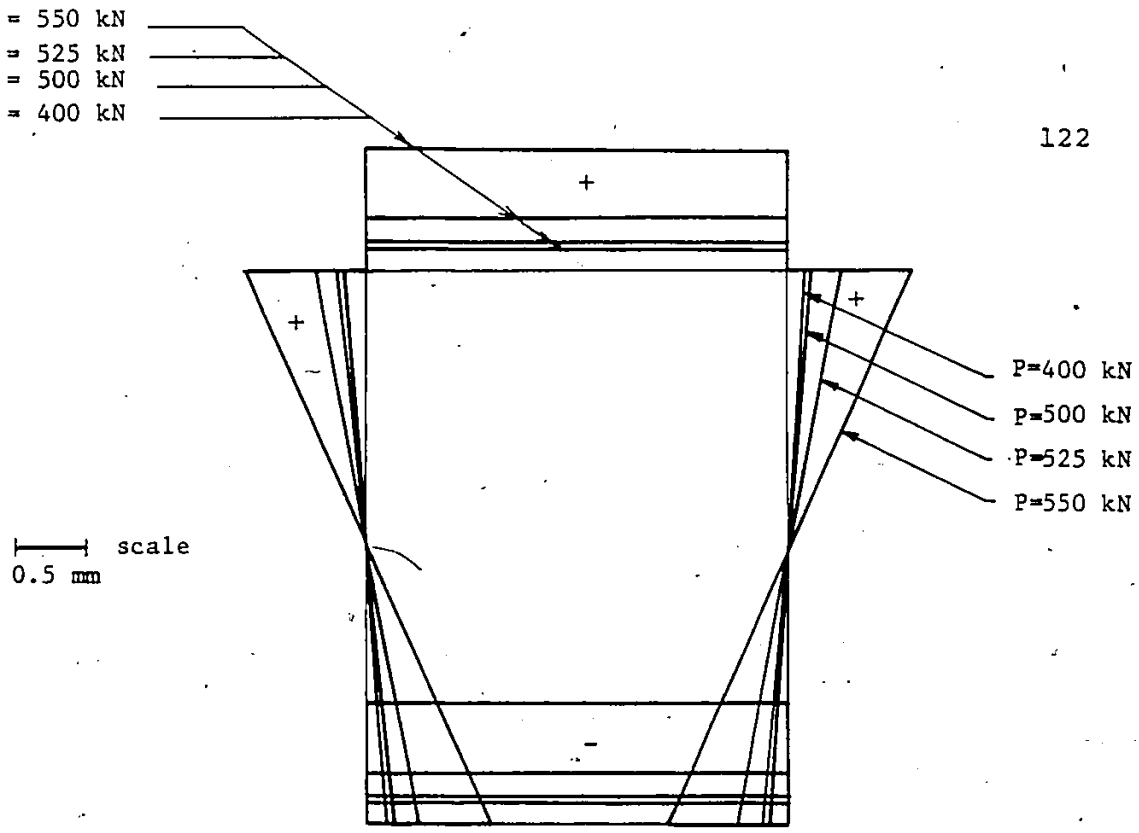

(a) Transverse distribution at x = ℓ/8

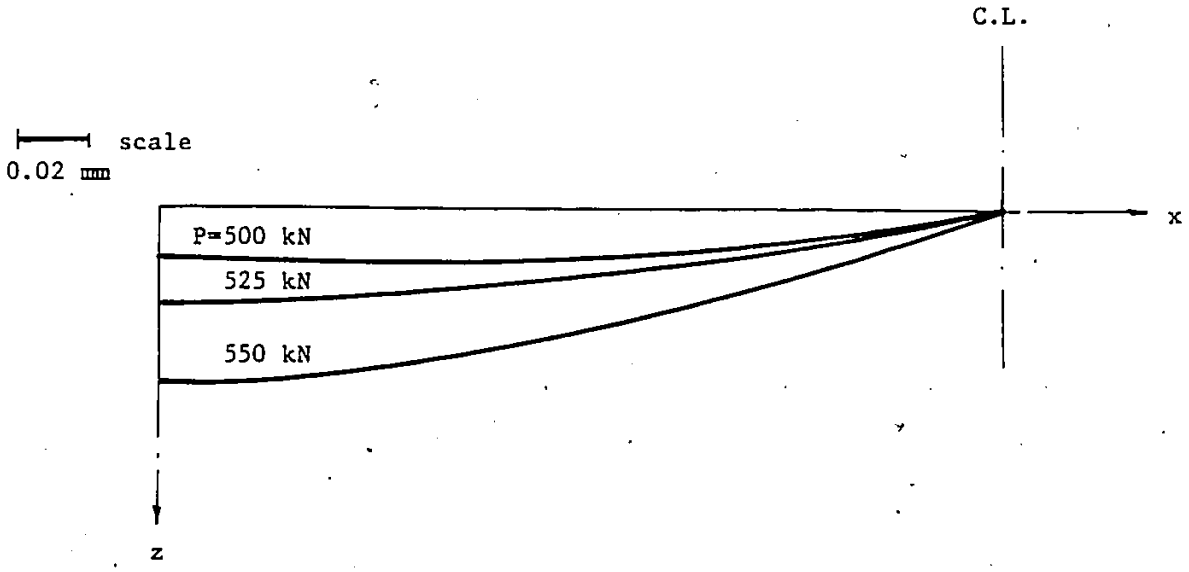

(b) Longitudinal distribution along the center of the compression flange.

Fig. 7.5 Distribution of in-plane displacement in the x-direction.

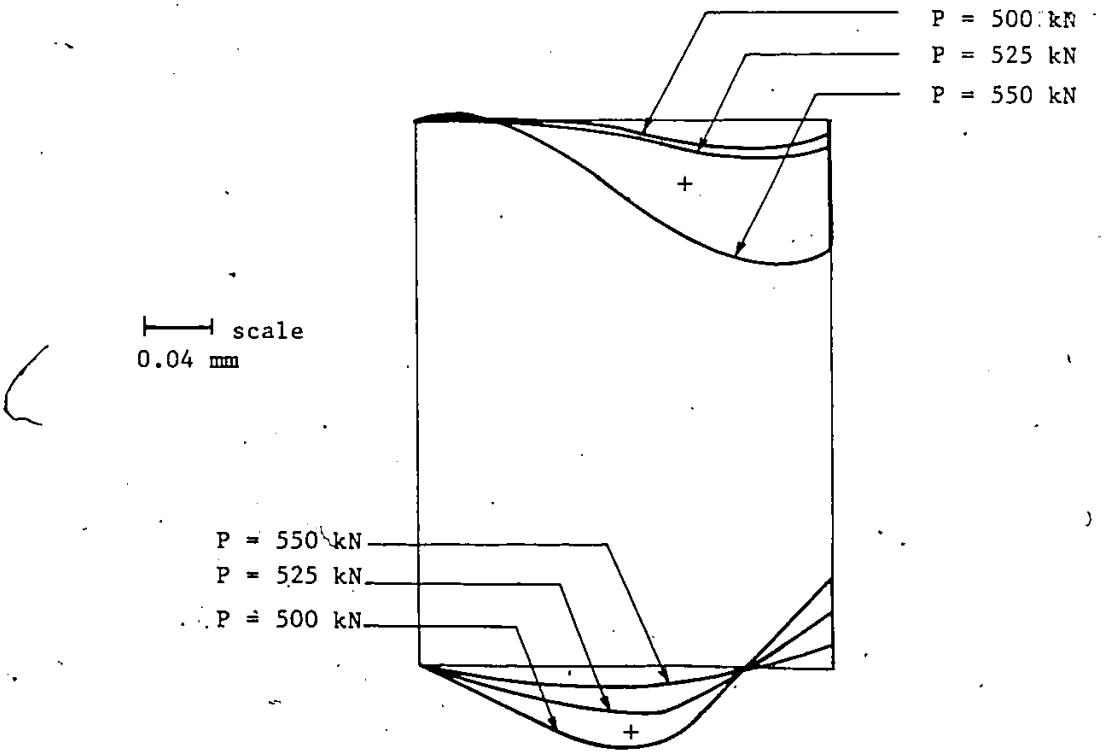

(a) Transverse direction at x=3/8ℓ

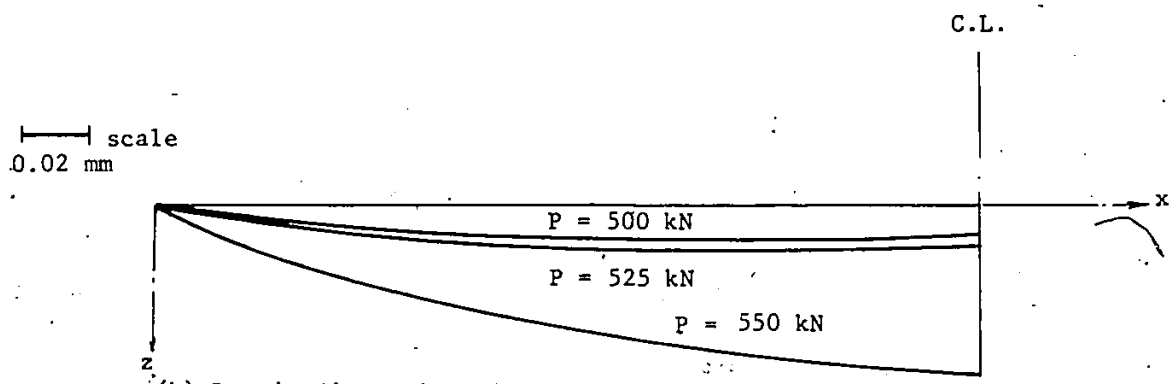

(b) Longitudinal direction along the center of the compression flange.

Fig. 7.6. Distribution of the in-plane displacement in the y-direction.

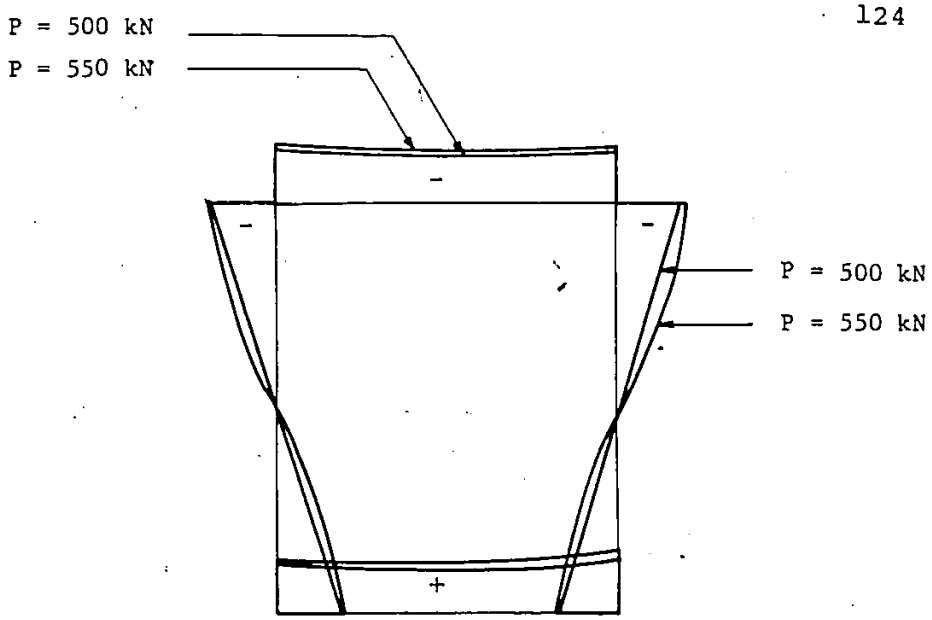

(a) Section at x=3ℓ/8

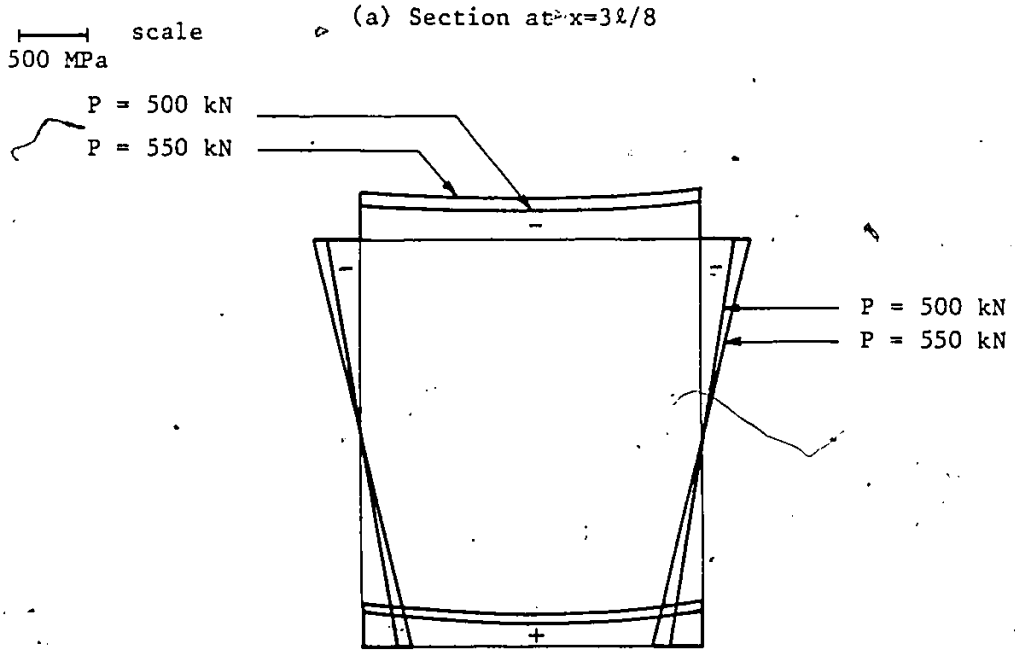

(b) section at x=ℓ/8

Fig. 7.7. Distribution of σ_x for two sections at 1/8 and 3/8 of the span.

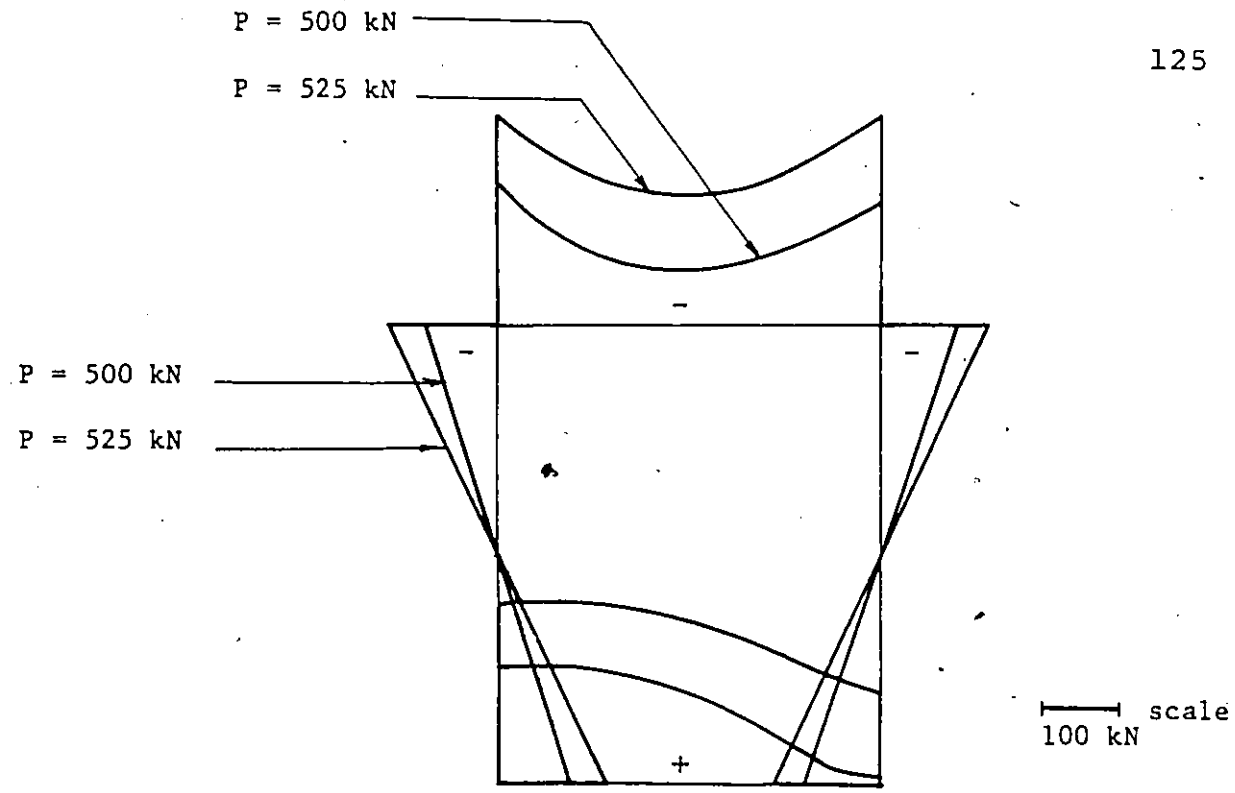

(a) Section at x=3ℓ/8

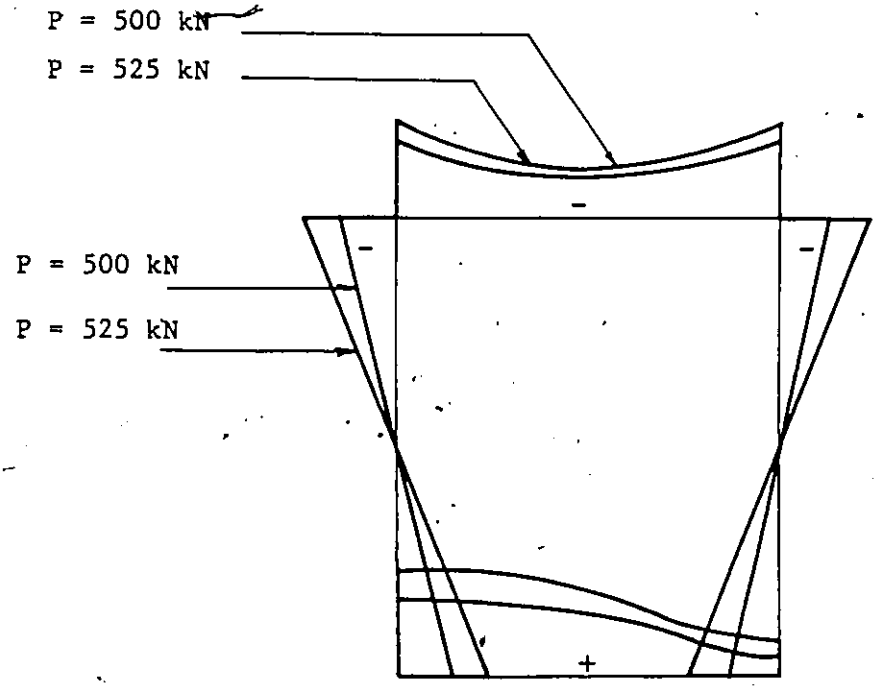

(b) Section at x=ℓ/8

Fig. 7.8. Distribution of σ_y for two sections at 1/8 and 3/8 of the span.

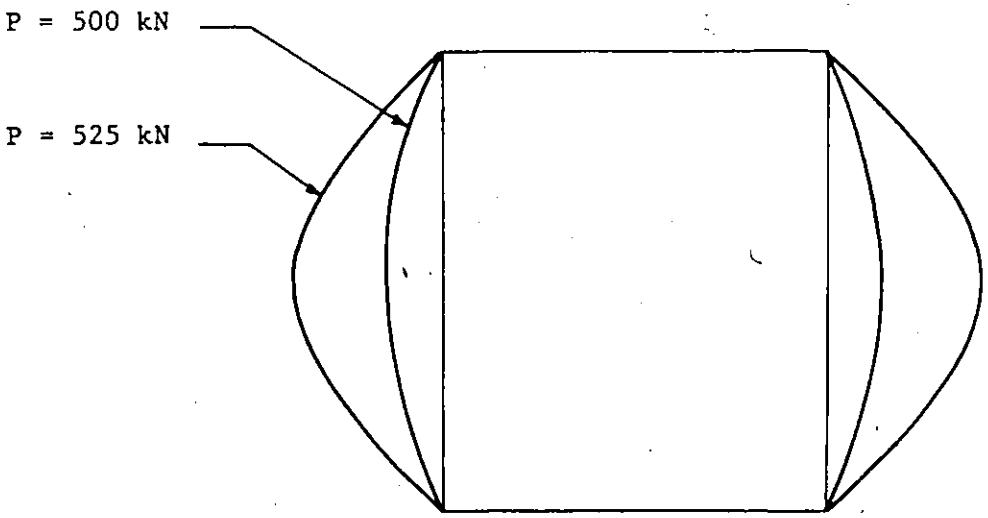

(a) Section at x=3ℓ/8

scale
100 kN

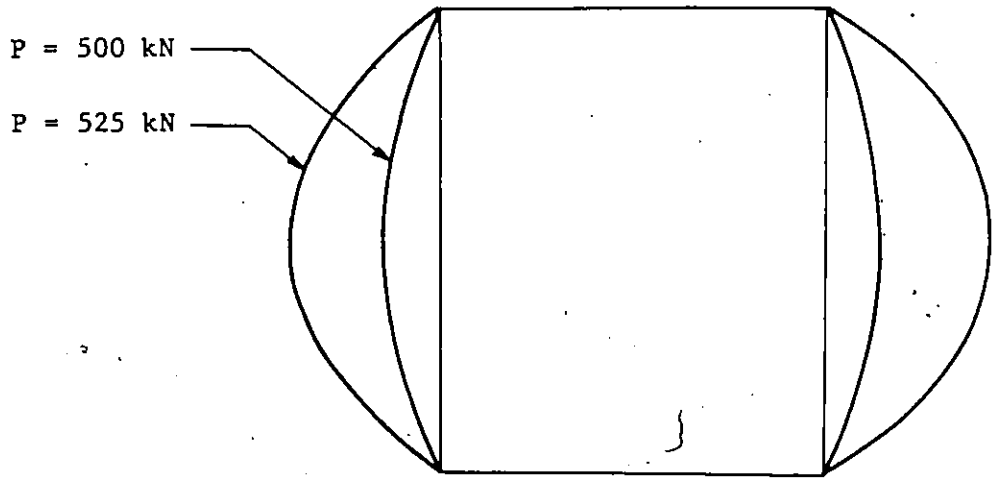

(b) Section at x=ℓ/8

Fig. 7.9. Distribution of τ_{xy} for two sections at 1/8 and 3/8 of the span.

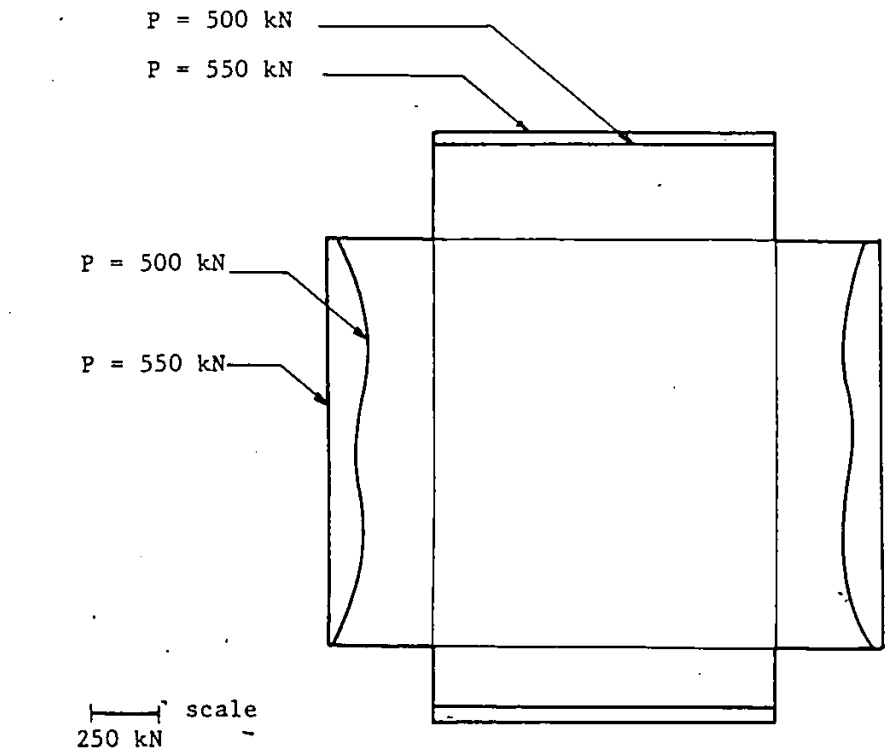

(a) Section at x=3ℓ/8

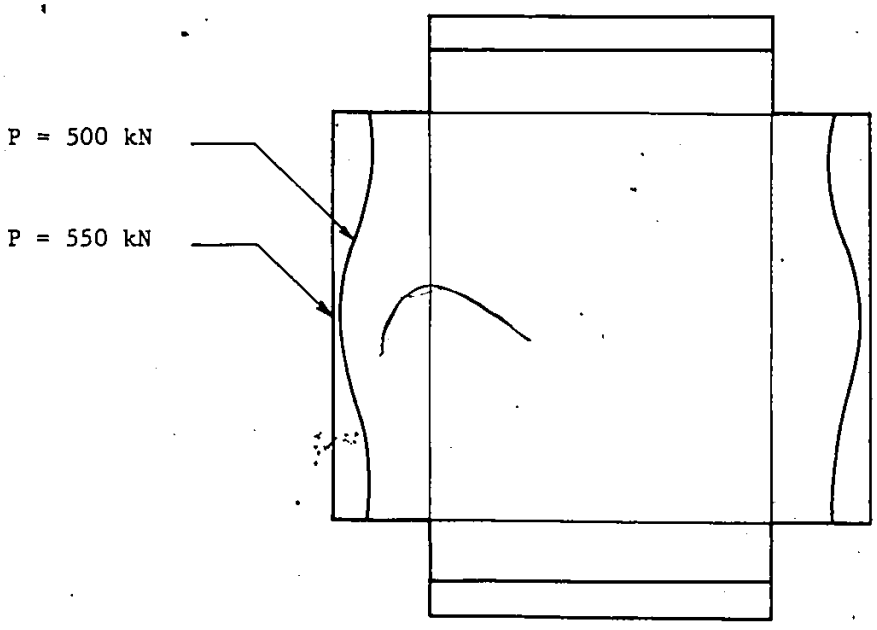

(b) Section at x=ℓ/8

Fig. 7.10. Distribution of σ_e in two sections at 1/8 and 3/8 of the span.

elements are more capable of detecting the initiation and the progression of yielding in the different parts of the model. Thus, this refined modelling will give closer results to the actual values.

The effect of the number of elements is demonstrated by solving the problem explained in section 7.3 with variable number of elements. Mesh subdivision with 32, 64 and 256 elements are used. The deflection of the center line of the beam is calculated at different load values. The relation between the applied load and the maximum deflection at mid-span is shown in Fig. 7.11.

It is clear that as the number of elements increases, the obtained results become closer to the finite element solution. It should also be noted that as long as the model is entirely elastic all of the three mesh subdivisions yielded the same deflection regardless of the number of elements used.

7.6 EFFECT OF FRICTION

Friction forces act in the plane of the flanges of the cross-section as a result of the contact between them and the rollers of the bending machine. In modelling the rolling process the friction forces are included in the analysis when the specimen starts to move during the rolling process.

The effect of friction is studied by solving three

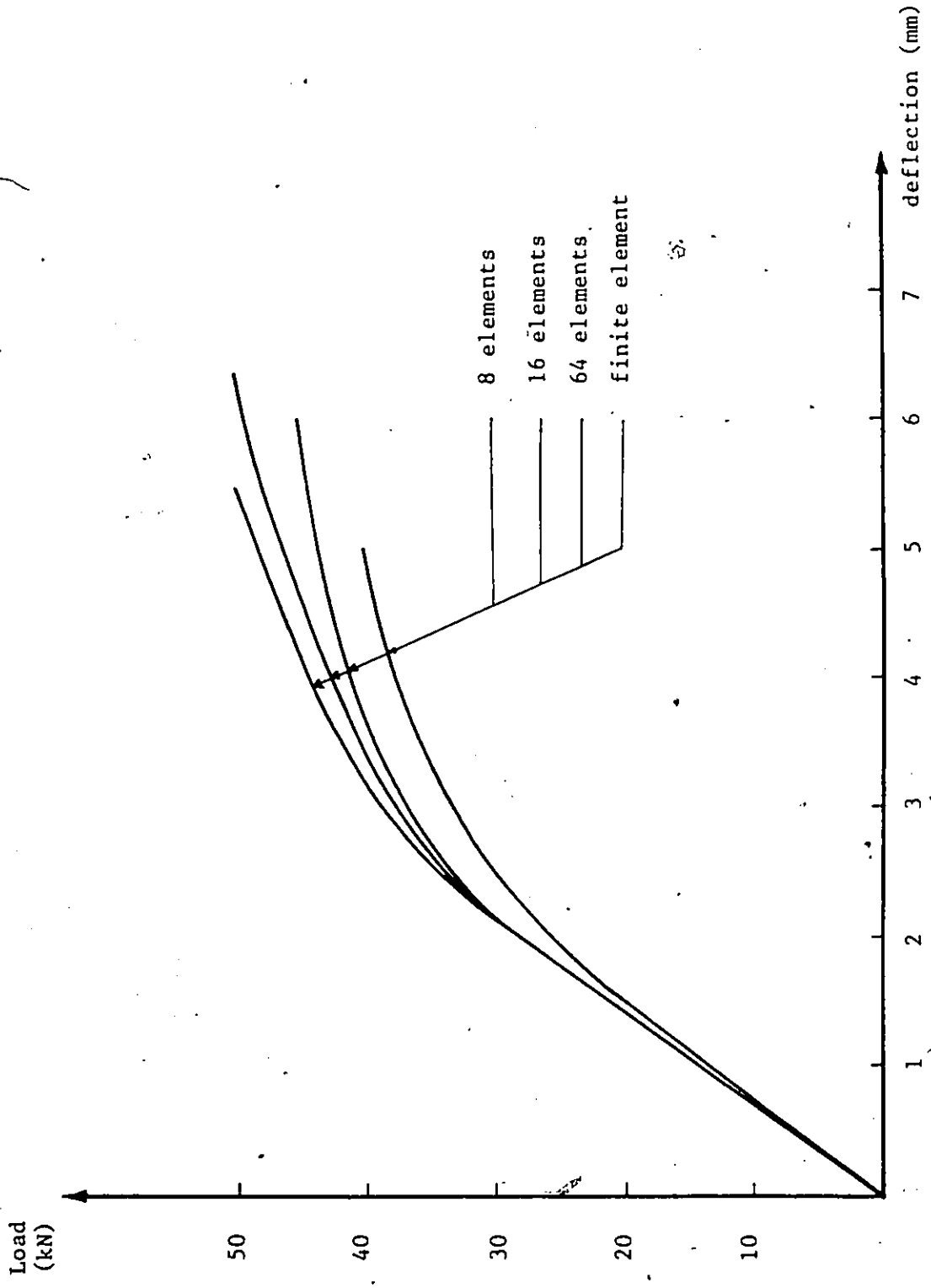

Fig. 7.11. Effect of the number of elements on the overall deflection.

different models, each model is solved twice. The first solution accounted for the effect of friction while the second disregarded that effect. In all cases the effect of friction was too small to affect the final deformations of the model. The change in the magnitude of deformations resulting from accounting for the friction forces was less than 1%. This effect is so small that it can be neglected without considerable error in the results. This conclusion is supported by many studies conducted in the rolling process where the effect of friction was neglected due to its small value (1, 15, 21).

7.7 DISTRIBUTION OF RESIDUAL STRESSES

The magnitude of the residual stresses resulting at different parts of the HSS member due to the rolling process depends on the geometry of the cross-section, its material properties as well as on the imposed radius of bend. The computer program developed herein, predicts the residual stresses at the center and corner points of all the elements in the mesh subdivision of the four plates composing the HSS.

The magnitude of the residual stresses resulting from the rolling process could be quite considerable. To demonstrate, the residual stresses at the center of the compression flange #1 and at the quarter point of the web plate #2 for different profiles of HSS are given in Table 7.3. It can be observed that the effective stresses calculated from

Table 7.3

Residual Stresses in Plates #1 and #2 for Different HSS Profiles

Section			Radius	Plate #1 at x = ℓ/2 and y = 0.0				Plate #2 at x = ℓ/2 and y = h/4			
h (mm)	b (mm)	t (mm)	(m)	σ_x	σ_y	τ_{xy}	σ_e	σ_x	σ_y	τ_{xy}	σ_e
101.6	101.6	4.78	2.44	136	-63	0.0	176	-39	78	52	86
127.0	127.0	4.78	3.05	226	-60	0.0	261	-40	91	78	157
152.4	101.6	4.78	2.44	229	-50	0.0	258	-63	126	55	123
177.8	177.8	7.95	7.32	176	-33	0.0	196	-33	66	61	120
203.2	203.2	6.35	9.14	248	-111	0.0	318	-38	76	93	114

Yield stress = 350 MPa

the residual stresses could be as high as 0.9 times the yield stress. Tighter radii of bend would have resulted in still higher values for the residual stresses. Generally, the residual stresses in the longitudinal direction σ_x in the two flanges, plates #1 and #3, are greater than all the other components of stresses resulting in the section. These longitudinal stresses are generally tensile in plate #1 and compressive in plate #3.

7.8 COMPARISON BETWEEN THEORETICAL AND EXPERIMENTAL RESULTS

The experimental results are presented in terms of the two parameters p_b and p_e at different radii of bend. The analytical procedure was applied to different sizes of the HSS. The results obtained are compared to those measured in the experimental program. This comparison is given in Tables 7.4 and 7.5. Only ten different profiles are used in this comparison. The first five profiles were chosen from those sections bent on the bending machine #1, Fig. 6.3; while the rest were from those bent on machine #2. All the ten profiles were chosen at random from the twenty seven profiles used in the experimental program.

Some profiles were excluded before choosing those used in the comparison because there was doubt in the accuracy of their results. For example, the deformations of the web of the profile 254.0x152.4x6.35 were the same when the member was bent to four different radii. Also the profiles 203.2x101.6x6.35 and 203.2x101.6x9.53 gave the same value for the parameter p_b irrespective of the different thick-

Table 7.4

Comparison Between Theoretical and Experimental Values for p_b

Member Size			Radius	p_b%	
h (mm)	b (mm)	t (mm)	(m)	Experimental	Theoretical
101.6	50.8	3.81	0.84	7.40	7.87
			1.22	6.25	5.82
			1.83	6.25	4.17
			2.44	4.70	2.12
101.6	101.6	4.78	1.52	8.60	4.92
			2.44	5.10	3.91
			3.66	4.70	3.75
			4.88	3.12	3.13
127.0	76.2	9.53	0.91	9.37	6.47
			1.22	6.80	5.72
			1.68	4.70	5.32
			2.44	4.17	4.92
127.0	127.0	4.78	3.07	8.76	6.81
			3.68	6.26	3.86
			4.27	5.00	3.51
			5.49	5.00	2.88
152.4	101.6	9.53	1.22	13.27	9.17
			1.52	12.50	9.05
			2.44	7.02	8.70
			3.66	3.90	6.24
177.8	127.0	6.35	2.44	7.50	7.63
			4.27	7.50	4.70
			6.71	5.00	3.79
			10.97	2.50	2.81
177.8	177.8	7.95	2.44	6.26	5.79
			7.32	5.13	4.31
			10.97	4.47	3.18
			15.24	2.23	1.85
203.2	101.6	4.78	4.88	7.82	6.70
			8.23	7.82	6.12
			12.19	5.47	5.61
			15.24	3.12	5.10

Table 7.4 (cont'd.)

Member Size			Radius	P_b%	
h (mm)	b (mm)	t (mm)	(m)	Experimental	Theoretical
203.2	203.2	6.35	9.14	5.47	4.10
			13.72	4.89	3.63
			18.29	3.91	3.34
			24.38	3.12	2.84
254.0	254.0	9.53	10.97	7.50	4.46
			13.72	7.50	3.75
			18.29	5.63	3.25
			30.48	5.63	2.38

Table 7.5

Comparison Between Theoretical and Experimental Values for p_e

Member Size			Radius	p_e%	
h (mm)	b (mm)	t (mm)	(m)	Experimental	Theoretical
101.6	50.8	3.81	0.84	4.70	4.25
			1.22	3.15	3.61
			1.83	1.55	2.89
			2.44	0.25	2.20
101.6	101.6	4.78	1.52	9.78	7.75
			2.44	7.02	6.10
			3.66	1.57	3.51
			4.88	0.77	1.72
127.0	76.2	9.53	0.91	2.63	1.89
			1.22	2.10	1.61
			1.68	1.03	1.42
			2.44	0.17	1.14
127.0	127.0	4.78	3.07	10.00	7.02
			3.68	8.76	6.50
			4.27	3.76	6.00
			5.49	3.12	5.02
152.4	101.6	9.53	1.22	3.90	5.59
			1.52	3.13	5.37
			2.44	2.72	4.70
			3.66	1.57	4.10
177.80	127.0	6.35	2.44	8.70	6.13
			4.27	5.00	4.90
			6.71	2.50	4.35
			10.97	2.18	3.25
177.8	177.8	7.95	2.44	11.61	7.92
			7.32	4.47	5.52
			10.97	2.23	4.82
			15.24	1.56	4.21
203.2	101.6	4.78	4.88	10.95	7.50
			8.23	7.82	6.05
			12.19	1.57	2.15
			15.24	1.57	1.50

Table 7.5 (cont'd.)

Member Size			Radius	p_e%	
h (mm)	b (mm)	t (mm)	(m)	Experimental	Theoretical
203.2	203.2	6.35	9.14	10.16	6.45
			13.72	6.25	6.00
			18.29	1.56	5.81
			24.38	0.79	4.91
254.0	254.0	9.53	10.97	5.00	6.43
			13.72	3.75	4.30
			18.29	2.50	2.71
			30.48	1.88	2.43

ness in the two profiles. In many cases two different radii gave exactly the same value of deformations which is unlikely to happen. A possible reason for such discrepancies is that the experimental program was carried out in a workshop of a factory where the environment was not as controlled as in a testing laboratory. Also because of the danger involved, the rolling machine had to be operated by a worker who in many cases contributed to an error in the results by altering the test procedure explained in Chapter 6. However, for most specimens used in the comparison reasonable agreement was shown between the theoretical and experimental results.

The disagreement between some of the theoretical and experimental results could be due to several reasons. In addition to those mentioned above, an important source of discrepancy is that the analysis assumes that the rolling process is completed in one pass of rolling. However, in many cases the rolling machine operator has to use several passes of rolling to obtain certain radius of bend, such passes can alter the results considerably.

It should be noted that several passes of rolling were sometimes required to produce a specific radius of bend because the process was done mainly by trial procedure. Depending on the experience of the operator of the rolling machine, the position of the middle roller, which defines the

deflection of the beam under rolling, had to be changed several times to obtain the required radius of bend. However, adopting the procedure explained in section 5.2, that establishes the relationship between the radius of bend and the position of the middle roller, the change in position of the middle roller corresponding to any radius of bend can be predetermined using the developed computer program. Thus, only one pass of rolling will be sufficient to obtain that radius of bend and conclude the rolling process.

It is interesting to note that the mean and the standard deviation of the differences between the measured and the calculated values for p_b were 1.00% and 1.75%, respectively, and those for the differences in p_e were -0.4% and 2.1%, respectively. To check the significance of the differences between the theoretical and experimental results, the T-test was used. The calculated values for t were 3.56 and 1.15 for the differences in p_b and p_e, respectively. In this case the number of degrees of freedom is 39, for a 1% level of significance, the tabulated value of t is 2.71 (23). This means that at 1% level of significance the difference in p_e is not significant and can be attributed to chance, while the difference in p_b is significant. However, since the difference between the calculated and tabulated values for t for the differences in p_b is small and because of the lack of uniformity of the experimental

results, that small difference in t can be neglected and the differences in p_b can be considered attributed to chance.

A multiple regression analysis is applied to the values obtained from the theoretical analysis and given in Tables 7.4 and 7.5. The purpose is to offer a simple and quick method that can be used to give a reasonable estimate to the deformations corresponding to any radius of bend. If the exact magnitude of the deformations is required, the computer program should be used. Otherwise, the following expressions can be used:

$$p_b\% = \left(\frac{1}{R^{0.52}}\right) \times \left(\frac{1}{h^{37.94}}\right) \times \left(b^{22.88}\right) \times \left(\frac{1}{t^{4.66}}\right) \times \left(I_x^{22.51}\right) \times \left(\frac{1}{I_y^{17.48}}\right) \times (14.88) \qquad (7.1)$$

$$p_e\% = \left(\frac{1}{R^{0.67}}\right) \times \left(h^{31.00}\right) \times \left(\frac{1}{b^{30.91}}\right) \times \left(\frac{1}{t^{1.25}}\right) \times \left(\frac{1}{I_x^{19.88}}\right) \times I_y^{20.46} \times (0.0094) \qquad (7.2)$$

The multiple correlation coefficients for equations 7.1 and 7.2 are 0.90 and 0.83, respectively, and their standard errors are 0.19% and 0.32%, respectively. A comparison between the calculated values and those estimated by equations

7.1 and 7.2 is given in Tables 7.6 and 7.7, respectively.

7.9 PARAMETRIC STUDY

The magnitude of distortion resulting in the cross-section is a function of the geometry of such sections. The ratios between the depth (h), the width (b) and the thickness (t) of the cross-section have a significant influence on the resulting distortion. A series of beam models having various such ratios are analyzed assuming that they are bent to the same radius of curvature. The relations between $\frac{h}{t}$ and the two parameters p_b and p_e describing the deformations of the web and the compression flange, respectively, are shown in Figures 7.12 and 7.13, respectively. It is clear that as $\frac{h}{t}$ increases both the deformations of the flange and the web increase. Similar relations could be obtained if the ratio $\frac{b}{t}$ is drawn against the parameters p_b and p_e. The deformations of the flange and the web also increase with increasing either the width (b) or the depth (h) of the cross-section as shown in Figures. 7.14 and 7.15.

Table 7.6

Comparison Between Calculated and Estimated Values for p_b

Member Size			Radius	p_b %		
h (mm)	b (mm)	t (mm)	(m)	Calculated	Estimated*	% Difference
101.8	50.8	3.81	0.84	9.40	7.87	16.27
			1.22	5.82	4.38	24.24
			1.83	4.17	3.54	15.10
			2.44	2.12	3.05	-43.86
101.6	101.6	4.78	1.52	4.92	5.20	5.69
			2.44	3.91	4.07	2.81
			3.66	3.75	3.29	12.26
			4.88	3.13	2.84	9.26
127.0	76.2	9.53	0.91	6.47	8.14	-25.81
			1.22	5.72	7.00	-22.37
			1.68	5.32	5.92	-11.28
			2.44	4.92	4.88	0.81
127.0	127.0	4.78	3.07	6.81	4.81	29.37
			3.68	3.86	4.38	-13.47
			4.27	3.51	4.06	-15.67
			5.49	2.88	3.56	-23.61
152.4	101.6	9.53	1.22	9.17	8.62	6.00
			1.52	9.05	7.68	15.13
			2.44	8.70	6.00	31.03
			3.66	6.24	4.86	22.11
177.8	127.0	6.35	2.44	7.63	7.39	3.14
			4.27	4.70	5.52	-17.44
			6.71	3.79	4.37	-15.30
			10.97	2.81	3.38	-20.28
177.8	177.8	7.95	2.44	5.79	6.58	-13.64
			7.32	4.31	3.72	13.69
			10.97	3.18	3.01	5.34
			15.24	1.85	2.54	-37.30
203.2	101.6	4.78	4.88	6.70	8.11	-21.04
			8.23	6.12	6.18	- 0.98
			12.19	5.61	5.04	10.16
			15.24	5.10	4.49	11.96

*Equation 7.1

Table 7.6 (cont'd.)

Member Size			Radius	P_b%		
h (mm)	b (mm)	t (mm)	(m)	Calculated	Estimated	% Difference
203.2	203.2	6.35	9.14	4.10	4.17	-1.70
			13.72	3.63	3.38	6.89
			18.29	3.34	2.91	12.87
			24.38	2.84	2.50	11.97
254.0	254.0	9.53	10.97	4.46	4.29	3.81
			13.72	3.75	3.82	-1.87
			18.29	3.25	3.29	-1.23
			30.48	2.38	2.54	-6.72

Table 7.7

Comparison Between Calculated and Estimated Values for p_e

Member Size			Radius	p_e%		
h (mm)	b (mm)	t (mm)	(m)	Calculated	Estimated*	% Difference
101.8	50.8	3.81	0.84	4.70	4.25	9.57
			1.22	3.61	3.48	3.60
			1.83	2.89	2.65	8.30
			2.44	2.20	2.19	0.45
101.6	101.6	4.78	1.52	7.75	7.30	5.80
			2.44	6.10	5.31	12.95
			3.66	3.51	4.04	15.10
			4.88	1.72	3.33	-93.60
127.0	76.2	9.53	0.91	1.89	2.62	-38.62
			1.22	1.61	2.15	33.54
			1.68	1.42	1.73	-22.53
			2.44	1.14	1.35	-18.42
127.0	127.0	4.78	3.07	7.02	6.97	0.71
			3.68	6.50	6.17	5.08
			4.27	6.00	5.58	7.00
			5.49	5.02	4.72	5.97
152.4	101.6	9.53	1.22	5.59	4.58	18.07
			1.52	5.37	3.95	14.71
			2.44	4.70	2.87	38.93
			3.66	4.10	2.19	46.59
177.8	127.0	6.35	2.44	6.13	8.52	-38.98
			4.27	4.90	5.84	-19.18
			6.71	4.35	4.31	0.92
			10.97	3.25	3.10	4.61
177.8	177.8	7.95	2.44	7.92	10.38	-31.06
			7.32	5.52	4.96	10.14
			10.97	4.82	3.78	21.58
			15.24	4.21	3.03	28.03
203.2	101.6	4.78	4.88	7.50	5.55	26.00
			8.23	6.05	3.90	35.54
			12.19	2.15	3.00	-39.53
			15.24	1.50	2.58	-72.00

*Equation 7.2

Table 7.7 (cont'd).

Member Size			Radius	p_e%		
h (mm)*	b (mm)	t (mm)	(m)	Calculated	Estimated	% Difference
203.2	203.2	6.35	9.14	6.45	6.54	1.39
			13.72	6.00	4.98	17.00
			18.29	5.81	4.10	29.43
			24.38	4.91	3.38	31.16
254.0	254.0	9.53	10.97	6.43	6.46	-0.47
			13.72	4.30	5.56	-29.30
			18.29	2.71	4.59	-69.37
			30.48	2.43	3.25	-33.74

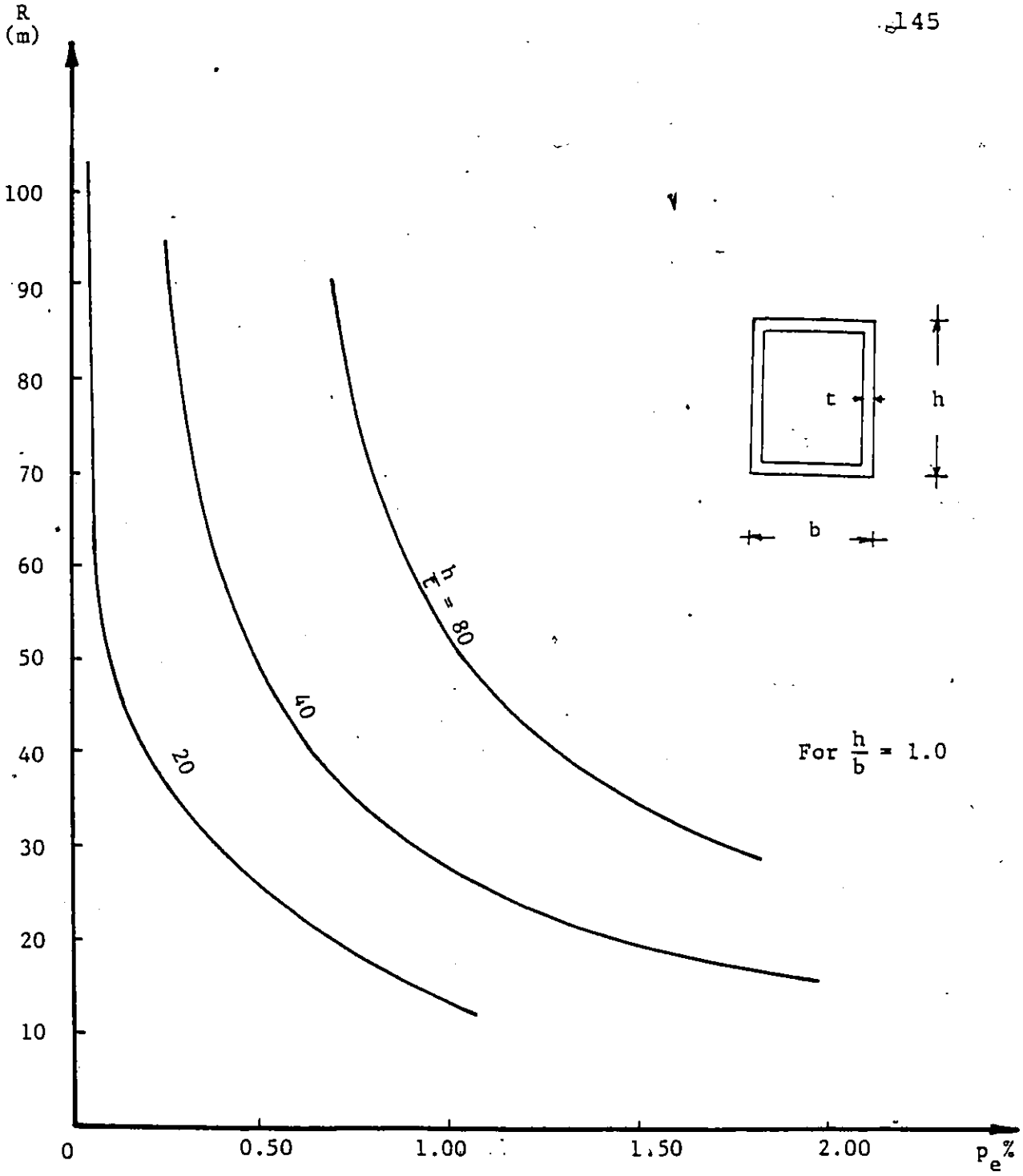

Fig. 7.12 Effect of the ratio $\frac{h}{t}$ on the deformations of the compression flange.

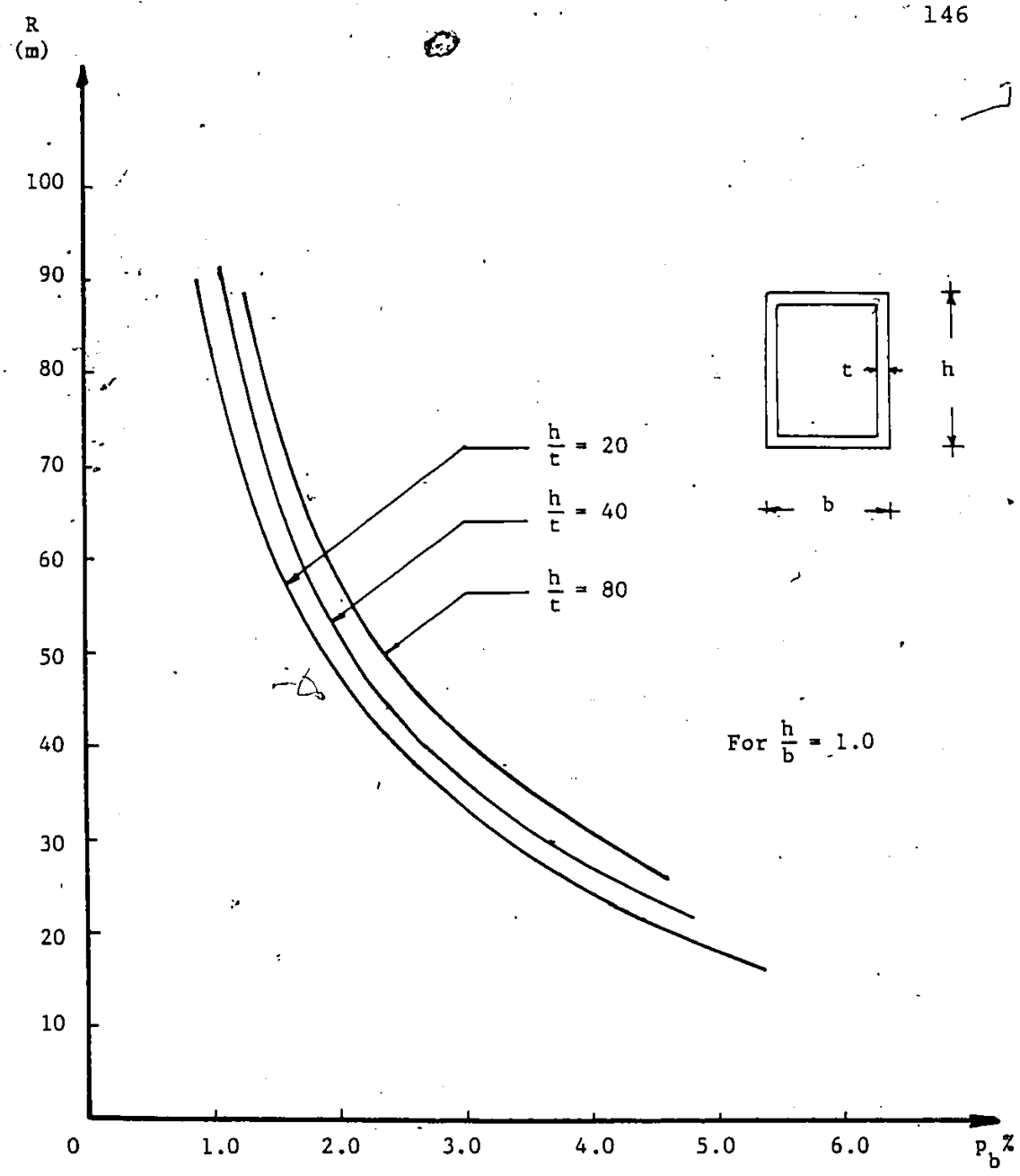

Fig. 7.13 Effect of the ratio $\frac{h}{t}$ on the deformations of the web.

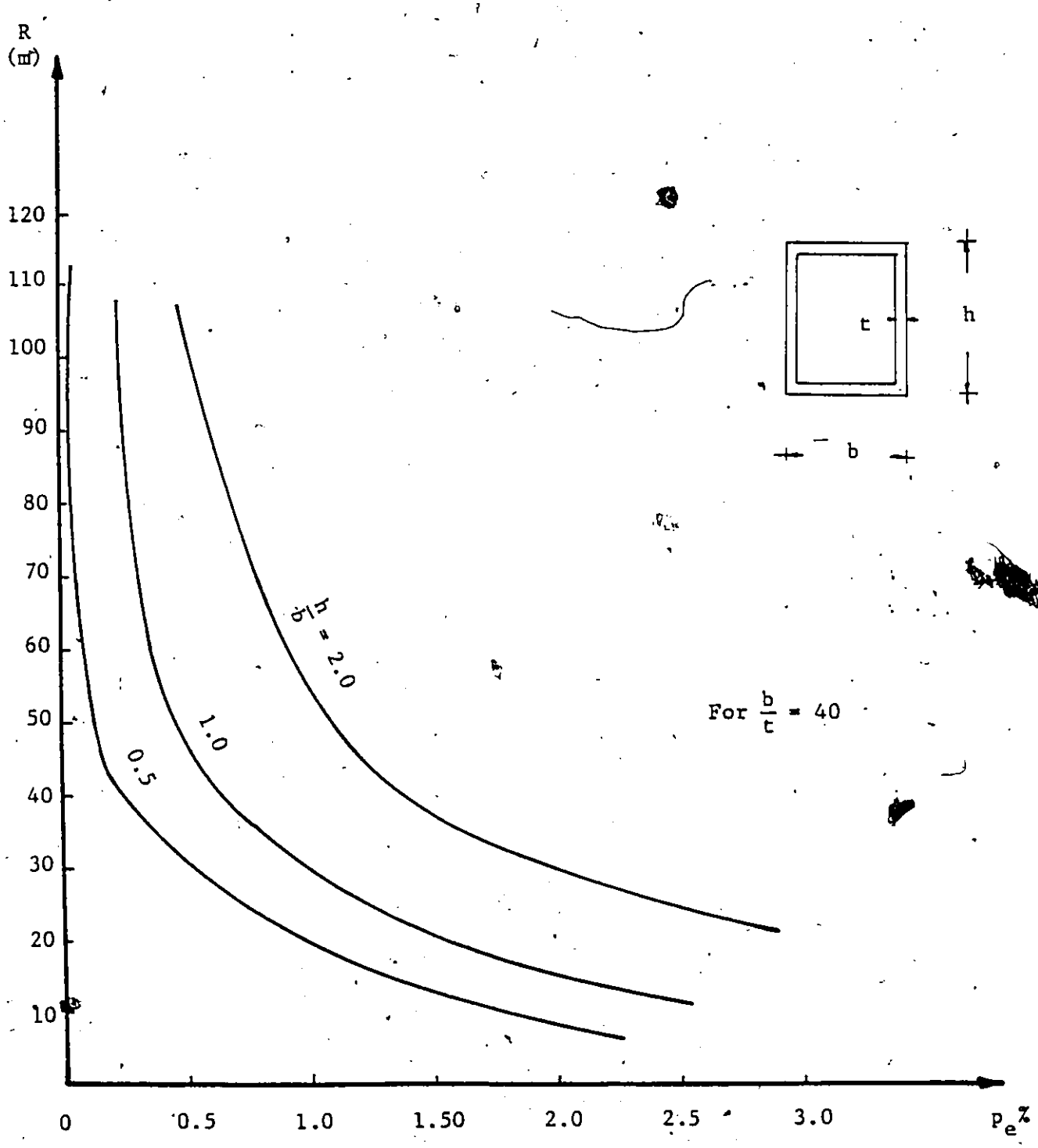

Fig. 7.14 Effect of the ratio $\frac{h}{b}$ on the deformations of the compression flange.

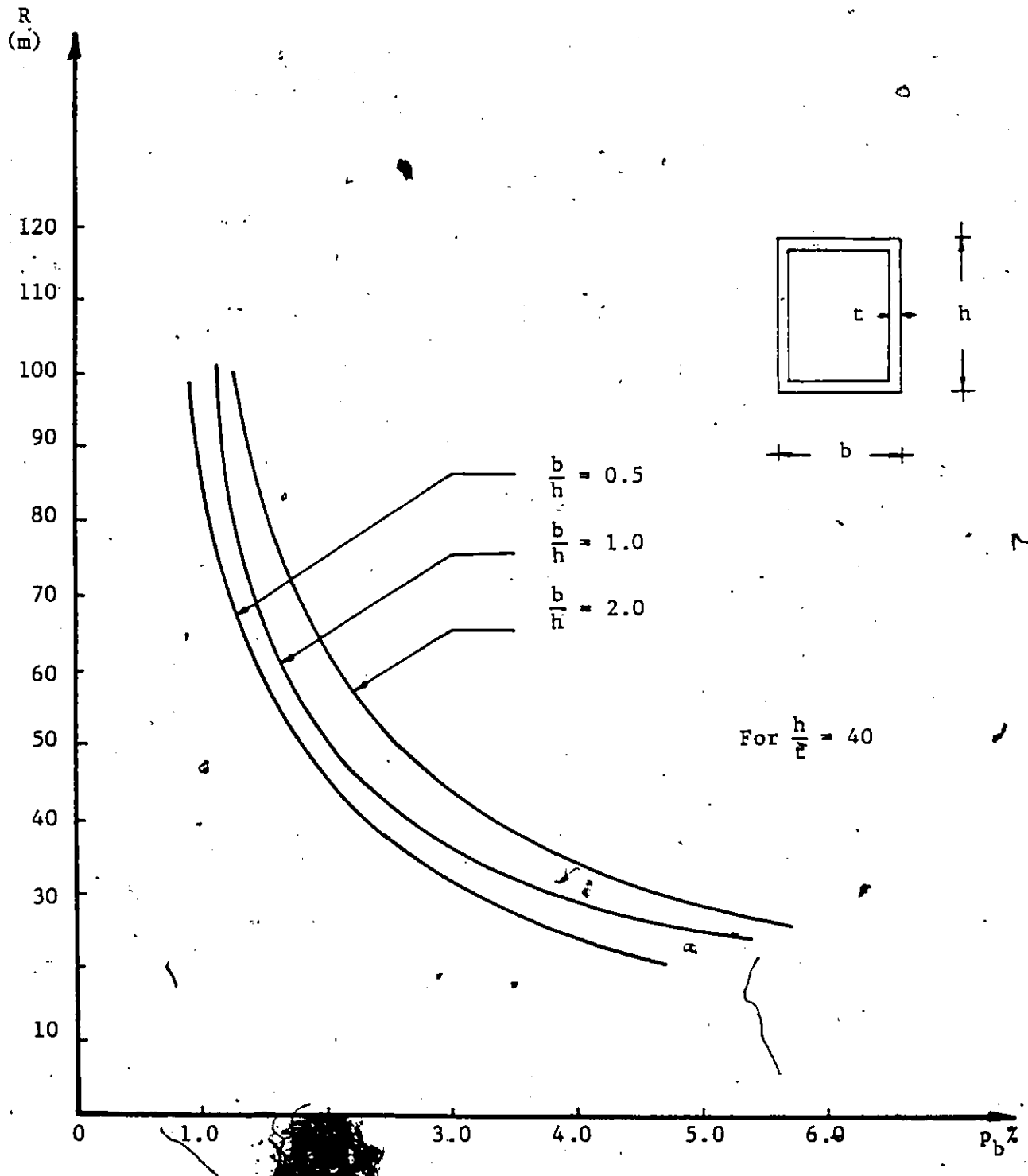

Fig. 7.15. Effect of the ratio $\frac{b}{h}$ on the deformations of the web.

CHAPTER VIII

MINIMUM RADIUS OF BEND

8.1 GENERAL

It is apparent from the results obtained that cold bending of unfilled HSS will cause measurable distortion in the cross-section. The tighter the radius of bend imposed, the larger the amount of distortion that will result. These distortions affect the aesthetic appearance as well as the capacity of the member to carry subsequent load. According to the uses of HSS members after bending, different criteria that define acceptable levels of distortion in the cross-section can be defined. These criteria are used to calculate the minimum radius to which a specific member can be bent.

In this chapter, the minimum radii recommended by three different steel companies for different HSS profiles are reviewed. Based on the results obtained in this study two different levels of acceptable distortion are recommended. Two equations that define these limits are used to calculate the minimum radii of bend recommended for the different sections. A comparison between these recommended

values and those used by the different steel companies is presented.

8.2 MINIMUM RADII RECOMMENDED BY THE STEEL COMPANIES

Different steel companies recommend different values for the minimum radii of bend of the HSS. The values recommended by U.S. Steel, British Steel and Ferrotubi, the steel company of Italy, are given in Tables 8.1, 8.2 and 8.3, respectively. All efforts made to obtain the basis on which these minimum values are calculated failed; these tables were given a long time ago and no records of such basis are now available.

Because of the lack of a common criterion on which the minimum values are calculated, disagreements between these values are likely to happen. Such disagreements can be found when comparing the values given in the aforementioned tables.

8.3 RECOMMENDED MINIMUM RADII

The calculation of the minimum radii of bend for HSS depends mainly on the definition of the acceptable level of distortions in the cross-section of the member. Different criteria can be assumed to define that acceptable level. In this study two criteria are considered likely to be suitable:

(i) Specification of an acceptable level of distor-

Table 8-1

Minimum Radii of Bend Recommended by U.S. Steel

Member Size			Minimum Radius (m)
h (mm)	b (mm)	t (mm)	
50.00	50.00	4.76-6.35	0.46
63.50	63.50	4.76	0.61
		6.35-7.94	0.56
76.20	76.20	4.76	0.76
		6.35-7.94	0.71
88.90	88.90	4.76	0.86
		6.35-7.94	0.81
101.60	101.60	4.76-6.35	0.91
		7.93-12.7	0.86
127.00	127.00	4.76-7.93	1.14
		9.53-12.7	1.07
152.40	152.40	4.76-7.93	1.37
		9.53-12.7	1.27
177.80	177.80	4.76-12.7	1.78
203.20	203.20	6.35-15.8	2.03
254.00	254.00	6.35-15.8	2.54

Table 8-2

Minimum Radii of Bend Recommended by British Steel

Member Size		Minimum Radius*
h (mm)	t (mm)	(m)
12.7	1.8	0.06
15.9	1.8	0.08
19.0	2.0	0.10
25.4	2.0	0.13
38.1	2.6	0.19
50.8	3.2	0.25
63.5	4.0	0.32
76.2	4.9	0.46
88.9	6.3	0.53
101.6	6.3	0.61
114.3	6.3	0.67
127.0	6.3	0.76
152.4	9.5	0.91
177.8	9.5	1.07
203.2	9.5	1.42
254.0	12.5	1.78
308.8	16.0	2.16
355.6	16.0	2.84
406.4	16.0	3.25
457.2	16.0	3.66

*These minimum values do not depend on the flange width dimensions

Table 8-3

Minimum Radii of Bend Recommended by Ferrotubi (Italian Steel Co.)

Member Size			Minimum Radius
h (mm)	b (mm)	t (mm)	(m)
110.0	50.0	2.5	5.00
		3.0	3.80-5.00
130.0	50.0	2.5	6.00
		3.0	5.20-7.25
		3.5	6.00
150.0	60.0	3.0	8.00
		3.5	7.25-8.25
		4.0	7.25
		4.5	6.00
170.0	80.0	3.0	15.00
		3.5	10.15-11.50
		4.5	10.15
190.0	75.0	3.5	18.00
		4.0	16.00
		4.5	14.00
		5.0	13.00-15.00
200.0	100.0	4.0	16.00-18.00
		4.5-5.0	14.00-20.00
250.0	95.0	5.0	25.00
		5.5	20.00
		5.9	20.00-22.00

tion in the flange (p_b).

(ii) Specification of an acceptable level of distortion in the web (p_e).

The choice of a numerical value to define the acceptable level of distortion is a difficult task because it depends on the uses of the HSS member after bending as well as on the engineering judgement of the user. Therefore, these numerical values may change from one case to another. However, based on the visual inspection of the different specimens after rolling, values of 5.0% and 2.5% for p_b and p_e, respectively, seemed to be quite suitable. At these values it was felt that significant levels of distortion were reached (4).

The radius of bend corresponding to the specified values for p_b and p_e were then calculated. These values for the minimum radii were calculated by linear interpolation between the values given in Table 6.3.

The values obtained from the experimental results for the minimum radii of bend were spread over a wide range. Therefore, multiple regression analysis was used to obtain relations that predict the minimum radii at these specified values of distortions. The best relations obtained are (4):

$$R_{(p_{b=5\%})} = 18.16\times10^{-4}\ \frac{h^2}{t} + 11.38\ I_y$$

$$-13.32\times10^{-4}\ \frac{h^2}{t^2} - 1.581 \qquad (8.1)$$

$$R(p_e=2.5\%) = 13.82\times10^{-4}\,\frac{bh}{t} + 1.92\times10^{-8}\,I_y + 5.43\times10^{-4}\,\frac{bh^2}{t} - 1.092 \qquad (8.2)$$

The standard error and the multiple correlation coefficients for equation 8.1 are 0.609 meters and 0.990, respectively, and those for equation 8.2 are 0.372 meters and 0.996. As explained in Chapter 6, the results for the four large sections were excluded from the regression analysis. Therefore, equations 8.1 and 8.2 are only applicable to sections with web depth between 100 mm and 205 mm. Comparison between the actual values for the minimum radii, calculated from the results of the experimental program, and those predicted by equations 8.1 and 8.2 is given in Table 8.4.

It should be noted that there is no relation between the parameters p_b and p_e and it is not necessary that they occur simultaneously. Therefore, the two parameters can be treated separately and the minimum radius of bend could be based on either parameter with the other completely disregarded.

8.4 COMPARISON BETWEEN RECOMMENDED AND PUBLISHED MINIMUM RADII

The minimum radii of bend based on this study are compared to those published by the different steel companies.

Table 8-4

Comparison Between Measured and Predicted Minimum Radii

Member Size			p_b = 5%			p_e = 2.5%		
h (mm)	b (mm)	t (mm)	Actual R (m)	Predicted* R (m)	Difference %	Actual R (m)	Predicted** R (m)	Difference %
101.6	50.8	3.81	2.34	2.44	4.57	1.52	1.54	0.80
101.6	50.8	6.35	0.86	1.10	27.36	0.86	0.49	-43.11
101.6	50.8	7.95	0.98	0.64	-35.03	0.31	0.18	-42.16
101.6	76.2	4.78	1.83	1.89	3.60	1.88	2.07	9.96
101.6	76.2	6.35	1.41	1.22	-13.55	1.32	1.30	-1.78
101.6	101.6	4.78	2.74	2.05	-25.32	3.45	3.14	-9.22
101.6	101.6	9.53	0.81	0.72	-11.32	1.02	1.08	6.70
127.0	76.2	6.35	2.22	2.73	22.96	1.65	2.10	27.47
127.0	76.2	9.53	1.61	1.55	-3.76	0.95	1.06	11.47
127.0	127.0	4.78	4.27	4.24	-0.57	6.35	6.01	-5.43
127.0	127.0	9.53	1.78	2.33	31.25	2.44	2.60	6.48
152.4	101.6	4.78	6.70	6.33	-5.57	6.40	6.14	-4.06
152.4	101.6	9.53	3.23	3.25	0.46	2.74	2.62	-4.38
152.4	152.4	6.35	4.80	5.73	19.33	7.31	7.23	-1.13
177.8	127.0	4.78	8.89	10.00	12.47	9.78	10.24	4.68
177.8	127.0	6.35	6.70	8.21	22.50	6.70	7.56	12.74
177.8	177.8	4.78	10.31	10.41	0.92	14.22	14.74	3.64
177.8	177.8	7.95	9.51	7.80	-18.02	9.24	8.72	-5.69
203.2	101.5	4.78	12.80	13.37	4.47	10.16	9.92	-2.31
203.2	101.6	6.35	9.35	11.00	17.72	7.11	7.35	3.34
203.2	101.6	9.53	7.11	8.62	21.17	4.27	4.79	12.20
203.2	203.2	6.35	12.52	12.43	-0.76	16.26	15.67	-3.60
203.2	203.2	9.53	10.16	10.68	5.09	10.16	10.52	3.55

*by Eq. 8.1

**by Eq. 8-2

Because of the reasonable agreement between the experimental and theoretical results obtained in this study, the comparison can be held between either one of them and the published data. Each steel company uses different profiles of HSS. Calculating the minimum radii for all these profiles using the computer program requires a very large amount of computer time. Therefore, it was decided to use equations 8.1 and 8.2 to obtain the minimum values recommended by this study. The comparisons between these recommended values and those recommended by the different steel companies are given in Tables 8.5, 8.6 and 8.7.

The comparison presented in these tables shows little or no agreement between the minimum values recommended in the present study and those recommended by the different steel companies. The minimum values recommended in the present study are generally larger than those recommended by U.S. Steel and British Steel. However, good agreement is found between the minimum values based on p_b and those recommended by Ferrotubi for the profiles having web depth up to 150.0 mm. For the larger profiles, Ferrotubi's values are much higher than those recommended in the present study.

This discrepancy could be due to the following factors:

(i) The lack of common criteria on which the minimum values are calculated.

Table 8.6

Comparison of Recommended Minimum Radii and that of U.S. Steel

Member Size			Present Study		U.S. Steel
h (mm)	b (mm)	t (mm)	p_b=5% R(m)	p_e=2.5% R(m)	R(m)
101.6	101.6	4.76	2.08	3.16	0.91
101.6	101.6	6.35	1.45	2.12	0.91
101.6	101.6	7.95	1.06	1.51	0.96
127.0	127.0	4.76	4.28	6.04	1.14
127.0	127.0	7.95	2.79	3.29	1.14
127.0	127.0	9.53	2.44	2.62	1.07
152.4	152.4	4.76	7.08	9.89	1.37
152.4	152.4	7.95	5.07	5.69	1.37
152.4	152.4	9.53	4.62	4.66	1.27
177.8	177.8	4.76	10.49	14.81	1.78
203.2	203.2	6.35	12.54	15.69	2.03

Table 8.7

Comparison of Recommended Minimum Radii and that of British Steel

Member Size			Present Study		British Steel R(m)
h (mm)	b (mm)	t (mm)	p_b=5% R(m)	p_e=2.5% R(m)	
101.6	101.6	6.35	1.45	2.12	0.61
114.3	114.3	6.35	2.33	3.13	0.69
127.0	127.0	6.35	3.35	4.31	0.76
152.0	152.0	9.53	4.62	4.65	0.91
177.8	177.8	9.53	7.44	7.28	1.07
203.2	203.2	9.53	10.95	10.56	1.42

Table 8.8

Comparison of Recommended Minimum Radii and that of Ferrotubi

Member Size			Present Study		Ferrotubi R(m)
h (mm)	b (mm)	t (mm)	p_b=5% R(m)	p_e=2.5% R(m)	
110.0	50.0	2.5	4.67	3.27	5.00
110.0	50.0	3.0	4.00	2.54	5.00
130.0	50.0	2.5	7.14	4.34	6.00
130.0	50.0	3.0	6.20	3.44	7.25
130.0	50.0	3.5	5.41	2.80	6.00
150.0	60.0	3.0	8.80	5.51	8.00
150.0	60.0	3.5	7.75	4.57	8.25
150.0	60.0	4.0	6.88	3.87	7.25
150.0	60.0	4.5	6.15	3.32	6.00
170.0	80.0	3.0	11.83	9.39	15.00
170.0	80.0	3.5	10.50	7.90	11.50
170.0	80.0	4.5	8.46	5.92	10.15
190.0	75.0	3.5	13.44	8.77	18.00
190.0	75.0	4.0	12.04	7.55	16.00
190.0	75.0	4.5	10.88	6.60	14.00
190.0	75.0	5.0	9.90	5.84	15.00
200.0	100.0	4.0	13.73	11.33	18.00
200.0	100.0	4.5	12.46	9.97	20.00
200.0	100.0	5.0	11.40	8.88	20.00

(ii) The amount of distortion is affected by the rolling procedure. Therefore, any change in that procedure could lead to different values of the cross-section distortions.

Therefore, as long as there are no specific guidelines for the testing procedure nor a common criterion to calculate the minimum radii, any comparison or judgement on the validity of certain minimum values will not be justified.

CHAPTER IX

SUMMARY AND CONCLUSIONS

9.1 SUMMARY

Curved Hollow Structural Sections (HSS) of rectangular and square geometry are commonly used for many construction purposes. Different bending methods are used to induce permanent curvature in the HSS to produce curved elements. One of the most common methods of cold bending is by the use of pyramid-type rolling machines. Bending of HSS even to a very large radius of curvature results in measurable distortions in its cross-section. The main objective of the present study was to develop an analytical method to predict the relation between the radius of bend imposed on the HSS and the resulting distortion in its cross-section.

The minimization of the total potential energy using the Rayleigh-Ritz approach was used as the method of analysis. It was assumed that at any instant of the rolling process, the hollow specimen is a beam subjected to concentrated load applied at mid-span through the middle roller. The cross-section was decomposed into four

plates, i.e., two flange plates and two web plates simply supported at their extremities. Displacement functions with unknown coefficients were assumed to describe the deformed shape of the cross-section after rolling. In these functions different series were chosen to represent the overall deformation of the HSS, i.e., due to its action as a beam, the local deformations of each plate, the effect of shear as well as the effect of friction between the beam model and the rollers of the bending machine. Expressions for the total potential energy in terms of the different components of displacements were developed in both the elastic and plastic ranges. The unknown coefficients in the displacement functions were then evaluated by minimizing the total potential energy of the structure using the Rosenbrock's method of minimization.

To account for the geometric non-linearity effects, non-linear strain displacement relations were used. A bi-linear stress-strain relation was assumed to describe the material behaviour under loading and the Von-Mises yield criterion was adopted to determine the initiation of yield in the model. The total deformation theory of plasticity was used to obtain the stress-strain relations in the plastic range.

In modelling the rolling process, the relation between the relaxed radius of bend and the deflection at the

point of contact between the model and the middle roller was established. Using this relation, the deflection at this point of contact corresponding to any required radius of bend can be calculated. If the calculated deflection is forced to the specimen, that required radius of bend can be obtained in one pass of rolling. The rolling process was then modelled by assuming that the load is applied at successive points along the length of the model. Therefore, the load was applied incrementally at a certain point until a specific deflection, i.e., specific radius of bend, was attained. The model was then moved to allow the load to be applied at a new location on the model. The stresses were adjusted in all points of the model to suit their new locations with respect to the applied load. The magnitude of the applied load was then changed to force the same specified deflection to occur at the new point. The process continued until a full length equal to the span of the model passed under the applied load.

Because of the loading system, some sections of the model deformed plastically while the others were still elastic. To accommodate such behaviour the model was discretized into a number of elements. The strain energy of each element was calculated separately depending on its stress level and then summed up for the whole model. The solution was carried out using a computer program

developed specially for this problem.

The solution obtained showed that the amount of deformations resulting in the cross-section depends on the imposed radius of curvature as well as the cross-section dimensions. The tighter the radius of curvature, the more is the deformation resulting in the section. Deformations also increased with increase in the width of the flanges and the height of the webs of the cross-section and with decrease in the thickness of both the flanges and the webs. Results are also affected by the number of terms used in each series in the displacement functions and the number of elements in the mesh subdivision used to model the elasto-plastic behaviour of the beam model. An estimate of the residual stresses resulting in the model due to the rolling process was also calculated.

The results of the theoretical analysis were compared to those obtained from an experimental program. In this program, 54 tests were carried out on 27 different sizes of the HSS. Each specimen was bent to four different radii of curvature. The cross-section distortions corresponding to each radius were accurately measured. Multiple regression analysis was used to develop a relationship between the radius of curvature, the cross-section properties and the distortions resulting in the cross-section. Fair agreement was found between the theoretical and experimental

results.

To calculate the minimum radius to which any HSS can be bent, different criteria should be adopted to define the maximum amount of distortions that can be tolerated in the cross-section. Two parameters were used in the present study; namely, the maximum bulging in the web and the maximum bowing in the compression flange. Values of 5% and 2.5% were assumed for these parameters, respectively. Each parameter was treated separately; therefore, two sets of minimum radii were obtained for the different sizes of the HSS. These minimum values were compared to those published by three different steel companies. However, little or no agreement was found. The most probable reason for this disagreement is the lack of a common criterion on which the calculations of the minimum values are based.

9.2 CONCLUSIONS AND RECOMMENDATION

On the basis of the present study the following conclusions may be reached:

1. Cold bending of HSS members of rectangular and square geometry results in permanent distortions in their cross-section. The fair agreement between the experimental and theoretical results estimating the magnitude of these distortions verifies the assumptions on which the theoretical analysis is based and substantiates the validity of

the proposed method for modelling the rolling procedure.

2. The magnitude of the permanent distortions resulting in the cross-section depends on its dimensions, material properties as well as on the imposed radius of bend. These distortions increase with decrease in the thickness of the section, with increase in its depth and/or width, and with decrease in the radius of bend.

3. The stresses at any point in the HSS are a combination between those resulting from the overall deformations of the HSS and those due to the local deformations of each plate. However, the stresses resulting from the overall deformations constitute the major part of these stresses.

4. The rolling procedure has a considerable effect on the magnitude of the distortions resulting in the HSS. Adopting the procedure outlined in the present study, the required radius of bend of an HSS member can be achieved in one pass of rolling.

5. The effect of friction between the rollers of the bending machine and the HSS member being rolled is relatively small and, therefore, can be neglected.

6. The magnitude of the residual stresses resulting in the different parts of the HSS member after rolling

can be relatively large and should be considered in the design of the member when used subsequently after rolling.

The numerical values chosen in the present analysis to describe the maximum allowable deformations in the HSS are based only on engineering judgement. The lack of agreement between the minimum radii calculated based on these values and those recommended by the different steel companies cited is due to the absence of a common criterion defining the maximum distortion allowed in the HSS. This disagreement could also be attributed to the lack of common guidelines that describe the rolling procedure. Therefore, it is recommended that an effort should be made towards unifying the rolling procedure of HSS members and defining different minimum radii of bend that would be tolerable in the various uses of these members after rolling.

REFERENCES

1. Bassett, M.B. and Johnson, W. "The bending of plates using a three-roller pyramid type plate bending machine." J. of Strain Analysis, Vol. I, No. 5, 1966, pp. 398-414.

2. Bleich, F. Buckling strength of metal structure. McGraw Hill Book Co., New York, 1952.

3. Bradfield, C. D. and Chldny, E. "A review of the elastic-plastic analysis of steel plates loaded in in-plane compression." The University of Cambridge, Report CUED/D Struct./TR.77, 1979.

4. Brady, J. F. "Determination of minimum radii for cold bending of square and rectangular hollow structural sections." CIDECT Programme 11B, final report, May 1978.

5. Budiansky, B. "A reassessment of deformation theories of plasticity." J. Applied Mechanics, 26, 1959, pp. 259-264.

6. Cox, H. L. The buckling of plates and shells. The MacMillan Co., New York, 1963.

7. Fletcher, R. and Reeves, C. M. "Function minimization by conjugate gradient." Computer Journal, Vol. 7, 1964, pp. 149-154.

8. Fletcher, R. "Fortran subroutines for minimization by quasi-Newton methods." Report R7125 AERE, Harwell, England, June 1972.

9. Freize, P. A., Dowling, P. J. and Hobbs, R. E. "Ultimate load behaviour of plates in compression." Steel Plated Structures, Proceedings of a Conference. London, 1976, published by Crosby Lockwood Staples.

10. Gerard, G. "Plastic stability theory of thin shells." Journal of the Aeronautical Sciences, April 1957, pp. 269-274.

11. Graves-Smith, T. R. "The ultimate strength of locally buckled columns of arbitrary length." Ph.D. thesis, The University of Cambridge, U.K., 1966.

12. Graves Smith, T. R. "The local buckling of box girders under bending stresses." Int. J. Mech. Sci., Vol. 11, 1969, pp. 603-612.

13. Graves Smith, T. R. "The post-buckled behaviour of a thin-walled box beam in pure bending." Int. J. Mech. Sci., Vol. 14, 1972, pp. 711-722

14. Graves Smith, T. R. "A finite strip method for the buckling of plate structures under arbitrary loading." Int. J. Mech. Sci., Vol. 20, 1978, pp. 685-693.

15. Hansen, N. E. and Jannerup, O. "Modelling of elastic-plastic bending of beams using a roller bending machine." Journal of Engineering for Industry, Transaction of the ASME, Vol. 101, Aug. 1979, pp. 304-310.

16. Harding, J. E., Hobbs, R. E., and Neal, B. G. "Ultimate load behaviour of plates under combined direct and shear in-plane loading." Steel Plated Structures, Proceedings of a Conference, London, 1976. by Crosby Lockwood Staples.

17. Hill, R. The mathematical theory of plasticity. Oxford Engineering Science Series, 1950.

18. Horrocks, D. and Johnson W. "On the anticlastic curvature with special reference to plastic bending: A literature survey and some experimental investigation." Int. J. Mech. Sci., Vol. 9, 1967, pp. 835-861.

19. Ilyushin, A. E. Plasticite. Editions Eyrolles, Paris, 1956.

20. Johnson, W. and Mallor, P. B. Engineering Plasticity Von Nostrand Reinhold Book Co., 1978.

21. Jortner, D., Osterle, J. F. and Zorowski, C. F. "An analysis of cold strip rolling." International Journal of Mechanical Sciences, Vol. 2, 1960, pp. 179-194.

22. Juvinall, R. C. Stress, Strain and Strength. McGraw-Hill Book Co., New York, 1967.

23. Kennedy, J. B. and Neville, A. M. Basic Statistical Methods for Engineers and Scientists. Second Edition. Harper and Row Co., New York, 1976.

24. Kou-Kuang, C. "A triangular plate finite element for large elastic-plastic analysis of automobile structural components." Computers & Structures, Vol. 10, 1979, pp. 203-215.

25. Langhaar, H. L. Energy Methods in Applied Mechanics. John Wiley and Sons Inc., New York, 1962.

26. Little, G. H. "Rapid analysis of plate collapse by live energy minimization." Int. J. Mech. Sci., Vol. 19, 1977, pp. 725-744.

27. McCormich, J. M. and Selvadori, M. G. Numerical Methods in FORTRAN. Prentice Hall Inc., Englewood Cliffs, New Jersey, 1965.

28. Mayers, J. and Budiansky, B. "Analysis of behaviour of simply supported flat plates compressed beyond the buckling load into the plastic range." National Advisory Committee for Aeronautics, Technical Report 3368, 1955.

29. Mendelson, A. Plasticity: Theory and Application. The MacMillan Book Co., New York, 1970.

30. Monforton, G. "Advanced analysis of structures." Course notes given at the University of Windsor, Civil Engineering Department, January 1982.

31. Moxham, K. E. "Compression in welded web plates." Ph.D. thesis, The University of Cambridge, U.K., 1970.

32. Murray, L. A. and Wilson, E. L. "Finite element post-buckling of thin elastic plates." AIAA, Vol. 7, 1969, pp. 1915-1920.

33. Nielsen, K. L. Methods in Numerical Analysis. The MacMillan Co., New York, 1956.

34. Oden, J. T. Mechanics of Elastic Structures. McGraw-Hill Book Co., New York, 1967.

35. Pogner, F. K. "Finite deflection, discrete element analysis of shells." Ph.D. thesis, Case Western Reserve University, Cleveland, Ohio, 1968.

36. Rhodes, J. and Harvey, J. M. "The local buckling and post local buckling behaviour of thin-walled beams." The Aeronautical Quarterly, Nov. 1971, pp. 363-388.

37. Robert, T. M. and Ashwell, D. G. "The use of finite element mid-increment stiffness matrices in the post-buckling analysis of imperfect structures." Int. J. Solids Structures, Vol. 7, 1971, pp. 805-823.

38. Rockey, K. C. In Thin-Walled Structures. Edited by A. H. Chilver. Chatto and Windus, London, 1967, pp. 248-270.

39. Rockey, K. C. and Bagchi, D. K. "Buckling of plate girder webs under partial edge loading." Int. J. Mech. Sci., Vol. 12, 1970, pp. 61-76.

40. Rosenbrock, H. H. "An automatic method of finding the greatest or least value of a function." The Computer Journal, Vol. 3, 1960, pp. 175-184.

41. Shaffer, B. W. and Ungar, E. E. "Mechanics of the sheet bending process." J. of Appl. Mech., Trans. of the AMSE, March, 1960, pp. 34-49.

42. Szillard, R. Theory and Analysis of Plates. Prentice-Hall Inc., New Jersey, 1974.

43. Tien, Y. L. and Wang, S. T. "Local buckling of beams under stress gradient." ASCE, Vol. 105, St. 8, August 1979, pp. 1571-1588.

44. Timoshenko, S. and Gere, J. Theory of Elastic Stability. McGraw Hill Book Co., New York, 1961.

45. Thomsen, E. G., Yang, C. T. and Kobayashi, S. Mechanics of plastic deformation in metal processing. MacMillan Book Co., New York, 1965.

46. Venktraman, B. and Patel, S. A. Structural mechanics with introduction to elasticity and plasticity. McGraw Hill Book Co., 1970.

47. Zienkiewicz, O. C. The finite element method. McGraw-Hill Book Co., 1977.

APPENDIX A

Elastic Strain Energy

The strain energy density is given by:

$$U_o = \int_o^{\varepsilon} \sigma d\varepsilon \qquad (A.1)$$

where σ and ε are the stress and strain, respectively. For a plate element which has three components of stresses and strains, the strain energy density is given by:

$$U_o = \int_o^{\varepsilon_x} \sigma_x d\varepsilon_x + \int_o^{\varepsilon_y} \sigma_y d\varepsilon_y + \int_o^{\gamma_{xy}} \tau_{xy} d\gamma_{xy}$$

$$= \frac{E}{1-\nu^2} \left[\int_o^{\varepsilon_x} (\varepsilon_x + \nu\varepsilon_y) d\varepsilon_x + \int_o^{\varepsilon_y} (\varepsilon_y + \nu\varepsilon_x) d\varepsilon_y \right.$$

$$\left. + \frac{1}{2} (1-\nu) \int_o^{\gamma_{xy}} \gamma_{xy} d\gamma_{xy} \right]$$

$$= \frac{E}{2(1-\nu^2)} \left[\varepsilon_x^2 + \varepsilon_y^2 + 2\nu\varepsilon_x\varepsilon_y + 0.5\ (1-\nu)\gamma_{xy}^2 \right] \qquad (A.2)$$

substituting the strain displacement relations (Equations 4-2) and collecting terms:

$$U_o = \frac{E}{2(1-\nu^2)} \left[u_x^2 + v_y^2 + 2\nu u_x v_y + 0.5\ (1-\nu)(u_y + v_x)^2 \right]$$

$$+ \frac{E}{2(1-\nu^2)} [u_x w_x^2 + v_y w_y^2 + (1-\nu)\, w_x w_y\, (y_u + v_x)$$

$$+ \nu(u_x w_y^2 + v_y w_x^2)]$$

$$+ \frac{E}{2(1-\nu^2)} [0.25\, w_x^4 + 0.25\, w_y^4 + 0.5\, w_x^2 w_y^2]$$

$$+ \frac{Ez^2}{2(1-\nu^2)} [w_{xx}^2 + w_{yy}^2 + 2(1-\nu)\, w_{xy}^2 + 2\nu w_{xx} w_{yy}]$$

$$- \frac{Ez}{2(1-\nu^2)} [u_x w_{xx} + v_y w_{yy} + (1-\nu)\, w_{xy}\, (u_y + v_x)$$

$$+ \nu(v_y w_{xx} + u_x w_{yy})]$$

$$- \frac{Ez}{2(1-\nu^2)} [0.5\, w_{xx} w_x^2 + 0.5\, w_{yy} w_y^2 + (1-\nu)\, w_{xy} w_x w_y$$

$$+ 0.5\nu\, (w_{yy} w_x^2 + w_{xx} w_y^2)] \qquad (A.3)$$

or,

$$U_o = f_1(u,v) + f_2(u,v,w) + f_3(w) + z^2 f_4(w) + z f_5(u,v,w)$$

$$+ z f_6(w) \qquad (A.4)$$

The strain energy is the integration of the strain energy density over the volume. Therefore,

$$U = \int_V U_o dV = \int_A \left[\int_{-t/2}^{t/2} U_o dz \right] dA \qquad (A.5)$$

therefore,

$$U = (f_1+f_2+f_3) \int_{-t/2}^{t/2} dz + f_4 \int_{-t/2}^{t/2} z^2 dz + (f_5+f_6) \int_{-t/2}^{t/2} z dz$$

$$= (f_1+ f_2+f_3)t + f_4 \frac{t^3}{12} \qquad (A.6)$$

substituting the values of f_1, f_2, f_3 and f_4

$$U_e = \frac{D}{2}\int_A \{[u_x^2 + v_y^2 + 2\nu u_x v_y + 0.5\ (1-\nu)(u_y+v_x)^2]$$

$$+ [u_x w_x^2 + v_y w_y^2 + (1-\nu)\ w_x w_y\ (u_y+v_x)$$

$$+ \nu(u_x w_y^2 + v_y w_x^2)]$$

$$+ [0.25\ (w_x^2+w_y^2)^2]\}\ dA$$

$$+ \frac{S}{2}\int_A [w_{xx}^2 + w_{yy}^2 + 2(1-\nu)\ w_{xy}^2 + 2\nu\ w_{xx} w_{yy}]\ dA \qquad (A.7)$$

where

$$D = \frac{Et}{1-\nu^2}$$

$$S = \frac{Et^3}{12(1-\nu^2)}$$

APPENDIX B

Total Strain Energy

The strain energy is the area under the stress-strain curve. In the plastic range the uniaxial stress-strain relation is replaced by the effective stress-effective strain relation. Therefore, the strain energy density is the area under the σ_{eff}-ε_{eff} curve. Assuming the yield stress and strain are σ_o and ε_o respectively (Fig. B.1), the strain energy density will be given by:

$$U_o = U_{01} + U_{02} + U_{03} \tag{B.1}$$

where, U_{01}, U_{02} and U_{03} are the areas indicated by ①, ② and ③ respectively in Fig. B.1;

$$U_{01} = 0.5\ \sigma_o \varepsilon_o \tag{B.2}$$

$$U_{02} = \sigma_o(\varepsilon_{eff} - \varepsilon_o) \tag{B.3}$$

$$U_{03} = 0.5\ E_p(\varepsilon_{eff} - \varepsilon_o)^2$$

$$= 0.5\ E_p(\varepsilon_{eff}^2 - 2\varepsilon_{eff}\varepsilon_o + \varepsilon_o^2) \tag{B.4}$$

therefore,

$$U_o = 0.5\ \sigma_o\varepsilon_o + \sigma_o\varepsilon_{eff} - \sigma_o\varepsilon_o + 0.5\ Ep(\varepsilon_{eff}^2$$

$$- 2\ \varepsilon_{eff}\varepsilon_o + \varepsilon_o^2) \tag{B.5}$$

or,

$$U_o = \sigma_o \varepsilon_{eff} - 0.5\ \sigma_o \varepsilon_o + 0.5\ E_p \varepsilon_{eff}^2$$

$$- E_p \varepsilon_{eff} \varepsilon_o + 0.5\ E_p \varepsilon_o^2 \qquad \text{(B.6)}$$

Integrating over the volume

$$U = (\sigma_o - E_p \varepsilon_o) \int_V \varepsilon_{eff} dv + 0.5\ E_p \int_V \varepsilon_{eff}^2 dV$$

$$+ 0.5\ (E_p \varepsilon_o^2 - \sigma_o \varepsilon_o) V \qquad \text{(B.7)}$$

where

$$\varepsilon_{eff} = \frac{2}{\sqrt{3}} \sqrt{\varepsilon_x^2 + \varepsilon_y^2 + \varepsilon_x \varepsilon_y + 0.25\ \gamma_{xy}^2};$$

and V = volume

Substituting the strain-displacements relations into the expression for ε_{eff} yields:

$$\int_V \varepsilon_{eff}^2 = \frac{4}{3}\ t \int_A [u_x^2 + v_y^2 + u_x v_y + 0.25\ (u_y + v_x)^2]$$

$$+ [u_x w_x^2 + v_y w_y^2 + 0.5\ w_x w_y\ (u_y + v_x)$$

$$+ 0.5\ (v_y w_x^2 + u_x w_y^2)]$$

$$+ [0.25\ (w_x^2 + w_y^2)^2]\ dA$$

$$+ \frac{1}{9} t^3 \int_A [w_{xx}^2 + w_{yy}^2 + w_{xy}^2 + w_{xx}w_{yy}] \, dA \tag{B.8}$$

and

$$\int_V \varepsilon_{eff} = \frac{2}{\sqrt{3}} \int_V \{ [u_x^2 + v_y^2 + u_x v_y + 0.25 \, (u_y+v_x)^2]$$

$$+ [u_x w_x^2 + v_y w_y^2 + 0.5 \, w_x w_y \, (u_y+v_x)$$

$$+ 0.5 \, (u_x w_y^2 + v_y w_x^2)]$$

$$+ [0.25 \, (w_x^2+w_y^2)^2]$$

$$+ z^2 [w_{xx}^2 + w_{yy}^2 + w_{xy}^2 + w_{xx}w_{yy}]$$

$$- z [2u_x w_{xx} + 2v_y w_{yy} + u_y w_{xy} + v_x w_{xy}$$

$$+ u_x w_{yy} + v_y w_{xx}]$$

$$- z [w_{xx} w_x^2 + w_{yy} w_y^2 + w_{xy} w_x w_y$$

$$+ 0.5 \, w_{xx} w_y^2 + 0.5 \, w_{yy} w_x^2]\}^{1/2} \, dV \tag{B.9}$$

Substituting Eqs. B.2 and B.3 in Eq. B.1 yield an expression for the total strain energy.

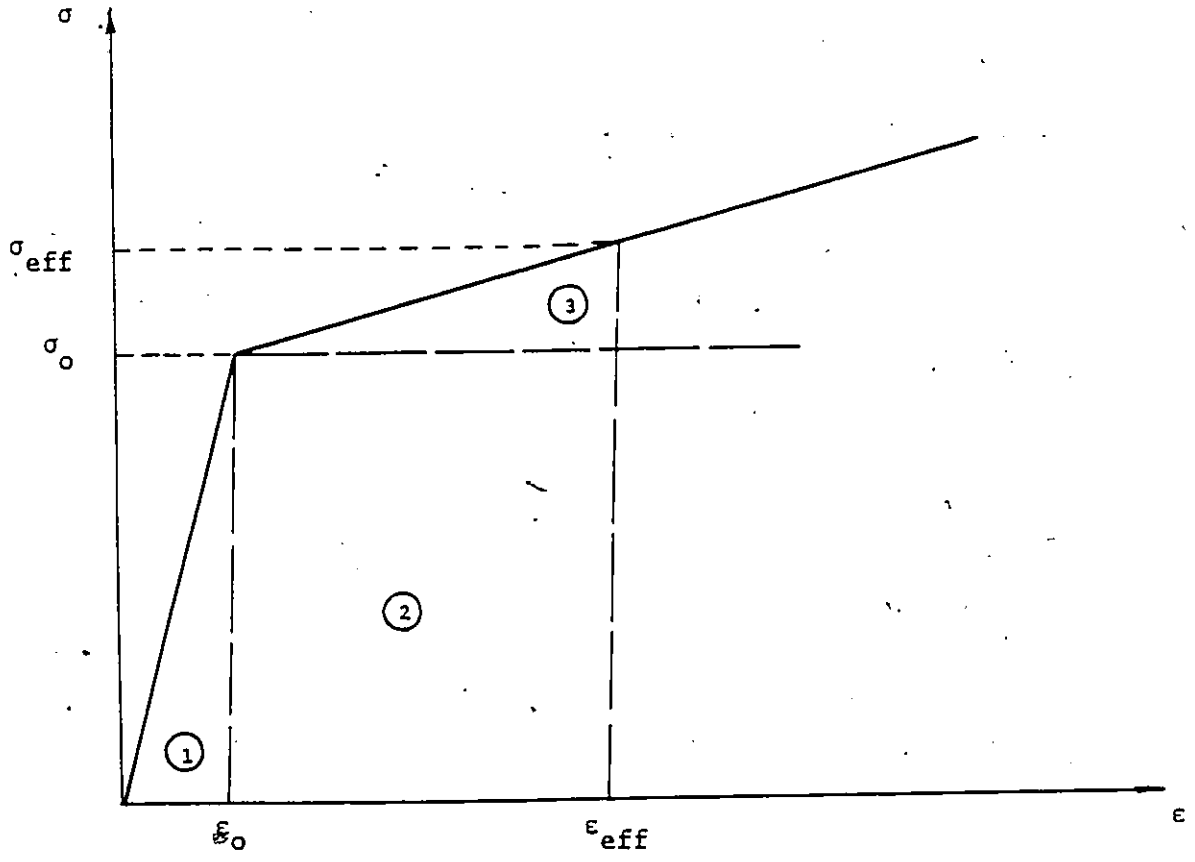

Fig. B.1. Different components of the total strain energy.

APPENDIX C

Derivatives of the Displacement Functions

The displacement functions for plate #1 are:

$$u = \sum_r A_r \frac{h}{2} \sin \frac{r\pi x}{\ell} + \sum_k \beta_k \frac{k\pi}{\ell} \frac{h}{2} \cos \frac{k\pi x}{\ell} + H_q \qquad \text{(C.1a)}$$

$$v = \sum_m \sum_n C_{nm}(y+\frac{b}{2}) \sin \frac{n\pi (y+\alpha\frac{b}{2})}{b} \sin \frac{m\pi x}{\ell} \qquad \text{(C.1b)}$$

$$w = \sum_k \beta_k \sin \frac{k\pi x}{\ell} + \sum_q \sum_p D_{pq}(y+\frac{b}{2}) \cos \frac{p\pi y}{b} \sin \frac{q\pi x}{\ell} \qquad \text{(C.1c)}$$

The derivatives of these functions with respect to x and y are:

$$u_x = \sum_r A_r \frac{r\pi}{\ell} \frac{h}{2} \cos \frac{r\pi x}{\ell} - \sum_k \beta_k (\frac{k\pi}{\ell})^2 \frac{h}{2} \sin \frac{k\pi x}{\ell} \qquad \text{(C.2a)}$$

$$u_y = 0 \qquad \text{(C.2b)}$$

$$v_x = \sum_m \sum_n C_{nm}(y+\frac{b}{2}) \frac{m\pi}{\ell} \sin \frac{n\pi (y+\alpha\frac{b}{2})}{b} \cos \frac{m\pi x}{\ell} \qquad \text{(C.2c)}$$

$$v_y = \sum_m \sum_n C_{nm}[\frac{n\pi}{b}(y+\frac{b}{2}) \cos \frac{n\pi (y+\alpha\frac{b}{2})}{b} + \sin \frac{n\pi (y+\alpha\frac{b}{2})}{b}] \sin \frac{m\pi x}{\ell} \qquad \text{(C.2d)}$$

$$w_x = \sum_k \beta_k \frac{k\pi}{\ell} \cos \frac{k\pi x}{\ell} + \sum_q \sum_p D_{pq} \frac{q\pi}{\ell}(y+\frac{b}{2}) \cos \frac{p\pi y}{b} \cos \frac{q\pi x}{\ell} \qquad \text{(C.2e)}$$

$$w_y = -\sum_q \sum_p D_{pq}\left[(y+\frac{b}{2})\frac{p\pi}{b} \sin \frac{p\pi y}{b} - \cos \frac{p\pi y}{b}\right] \sin \frac{q\pi x}{\ell} \tag{C.2f}$$

$$w_{xx} = -\sum_k B_k (\frac{k\pi}{\ell})^2 \sin \frac{k\pi x}{\ell}$$

$$-\sum_q \sum_p D_{pq} (\frac{q\pi}{\ell})^2 (y+\frac{b}{2}) \cos \frac{p\pi y}{b} \sin \frac{q\pi x}{\ell} \tag{C.2g}$$

$$w_{yy} = -\sum_q \sum_p D_{pq}\left[(\frac{p\pi}{b})^2 (y+\frac{b}{2}) \cos \frac{p\pi y}{b}\right.$$

$$\left. + 2\frac{p\pi}{b} \sin \frac{p\pi y}{b}\right] \sin \frac{q\pi y}{\ell} \tag{C.2h}$$

$$w_{xy} = -\sum_q \sum_p D_{pq} \frac{q\pi}{\ell}\left[(y+\frac{b}{2})\frac{p\pi}{b} \sin \frac{p\pi y}{b} - \cos \frac{p\pi y}{b}\right] \cos \frac{q\pi x}{\ell} \tag{C.2i}$$

For plate #2, the displacement functions are:

$$u = -\sum_r A_r y \sin \frac{r\pi x}{\ell} - \sum_k B_k \frac{k\pi}{\ell} y \cos \frac{k\pi x}{\ell} - \sum_q H_q \sin \frac{q\pi y}{h} \tag{C.3a}$$

$$v = \sum_k B_k \sin \frac{k\pi x}{\ell} \tag{C.3b}$$

$$w = -\sum_m \sum_n C_{nm}\, b \sin \frac{n\pi (y-\alpha\frac{h}{2})}{h} \sin \frac{m\pi x}{\ell} \tag{C.3c}$$

The derivatives of these functions are:

$$u_x = -\sum_r A_r y \frac{r\pi}{\ell} \cos \frac{r\pi x}{\ell} + \sum_k B_k (\frac{k\pi}{\ell})^2 y \sin \frac{k\pi x}{\ell} \tag{C.4a}$$

$$u_y = -\sum_r A_r \sin\frac{r\pi x}{\ell} - {}_kB_k \frac{k\pi}{\ell}\cos\frac{k\pi x}{\ell} - \sum_g H_g \frac{q\pi}{h}\cos\frac{q\pi y}{h} \tag{C.4b}$$

$$v_x = \sum_k B_k \frac{k\pi}{\ell}\cos\frac{k\pi y}{\ell} \tag{C.4c}$$

$$v_y = 0 \tag{C.4d}$$

$$w_x = -\sum_m \sum_n C_{nm} \frac{m\pi}{\ell}\, b \sin\frac{n\pi(y-\alpha\frac{h}{2})}{h}\cos\frac{m\pi x}{\ell} \tag{C.4e}$$

$$w_y = -\sum_m \sum_n C_{nm} \frac{n\pi}{h}\, b \cos\frac{n\pi(y-\alpha\frac{h}{2})}{h}\sin\frac{m\pi x}{\ell} \tag{C.4f}$$

$$w_{xx} = \sum_m \sum_n C_{nm}\left(\frac{m\pi}{\ell}\right)^2 b \sin\frac{n\pi(y-\alpha\frac{h}{2})}{h}\sin\frac{m\pi x}{\ell} \tag{C.4g}$$

$$w_{yy} = \sum_m \sum_n C_{nm}\left(\frac{n\pi}{h}\right)^2 b \sin\frac{n\pi(y-\alpha\frac{h}{2})}{h}\sin\frac{m\pi x}{\ell} \tag{C.4h}$$

$$w_{xy} = -\sum_m \sum_n C_{nm} \frac{nm\pi^2}{h\ell}\, b \cos\frac{n\pi(y-\alpha\frac{h}{2})}{h}\cos\frac{m\pi x}{\ell} \tag{C.4i}$$

For plate #3, the displacement functions are:

$$u = -\sum_r A_r \frac{h}{2}\sin\frac{r\pi x}{\ell} - \sum_k B_k \frac{k\pi}{\ell}\frac{h}{2}\cos\frac{k\pi x}{\ell} \tag{C.5a}$$

$$v = -\sum_m \sum_n C_{nm}(y+\frac{b}{2})\sin\frac{n\pi(y-\alpha\frac{b}{2})}{b}\sin\frac{m\pi x}{\ell} \tag{C.5b}$$

$$w = \sum_r B_r \sin\frac{r\pi x}{\ell} - \sum_j \sum_i G_{ij}(y+\frac{b}{2})\cos\frac{i\pi y}{b}\sin\frac{J\pi x}{\ell} \tag{C.5c}$$

The derivatives of these functions are:

$$u_x = \sum_r A_r \frac{h}{2} \frac{r\pi}{\ell} \sin \frac{r\pi x}{\ell} + \sum_k B_k \left(\frac{k\pi}{\ell}\right)^2 \frac{h}{2} \sin \frac{k\pi x}{\ell} \tag{C.6a}$$

$$u_y = 0 \tag{C.6b}$$

$$v_x = - \sum_m \sum_n C_{nm} \frac{m\pi}{\ell}(y+\frac{b}{2}) \sin \frac{n\pi (y-\alpha\frac{b}{2})}{b} \cos \frac{m\pi x}{\ell} \tag{C.6c}$$

$$v_y = \sum_m \sum_n C_{nm} [\frac{n\pi}{b}(y+\frac{b}{2}) \cos \frac{n\pi (y-\alpha\frac{b}{2})}{b} + \sin \frac{n\pi (y-\alpha\frac{b}{2})}{b}] \sin \frac{m\pi x}{\ell} \tag{C.6d}$$

$$w_x = \sum_k B_k \frac{k\pi}{\ell} \cos \frac{k\pi x}{\ell} - \sum_j \sum_i G_{ij} \frac{J\pi}{\ell}(y+\frac{b}{2}) \cos \frac{i\pi y}{b} \cos \frac{J\pi x}{\ell} \tag{C.6e}$$

$$w_y = \sum_j \sum_i G_{ij} [\frac{i\pi}{b}(y+\frac{b}{2}) \sin \frac{i\pi y}{b} - \cos \frac{i\pi y}{b} \sin \frac{J\pi x}{\ell}] \tag{C.6f}$$

$$w_{xx} = -\sum_k B_k \left(\frac{k\pi}{\ell}\right)^2 \sin \frac{k\pi x}{\ell} + \sum_j \sum_i G_{ij} \left(\frac{J\pi}{\ell}\right)^2 (y+\frac{b}{2}) \cos \frac{i\pi y}{b} \sin \frac{J\pi x}{\ell} \tag{C.6g}$$

$$w_{yy} = \sum_j \sum_i G_{ij} [\left(\frac{i\pi}{b}\right)^2 (y+\frac{b}{2}) \cos \frac{i\pi y}{b} + 2\frac{i\pi}{b} \sin \frac{i\pi y}{b}] \sin \frac{J\pi x}{\ell} \tag{C.6h}$$

$$w_{xy} = \sum_j \sum_i G_{ij} \frac{J\pi}{\ell}\left[\frac{i\pi}{b}(y+\frac{b}{2}) \sin \frac{i\pi y}{b} - \cos \frac{i\pi y}{b}\right]\cos \frac{J\pi x}{\ell} \quad \text{(C.6i)}$$

For plate #4, the displacement functions are:

$$u = - \sum_r A_r y \sin \frac{r\pi x}{\ell} - \sum_k B_k \frac{k\pi}{\ell} y \cos \frac{\pi x}{\ell} - \sum_g H_g \sin \frac{g\pi y}{h} \quad \text{(C.7a)}$$

$$v = \sum_k B_k \sin \frac{k\pi x}{\ell} \quad \text{(C.7b)}$$

$$w = 0 \quad \text{(C.7c)}$$

The derivatives of these functions are:

$$u_x = \sum_r A_r y \frac{r\pi}{\ell} \cos \frac{r\pi x}{\ell} + \sum_k B_k \left(\frac{k\pi}{\ell}\right)^2 y \sin \frac{\pi x}{\ell} \quad \text{(C.8a)}$$

$$u_y = \sum_r A_r \sin \frac{r\pi x}{\ell} - \sum_k B_k \frac{k\pi}{\ell} \cos \frac{k\pi x}{\ell} - \sum_g H_g \frac{g\pi}{h} \cos \frac{g\pi y}{h} \quad \text{(C.8b)}$$

$$v_x = \sum_k B_k \frac{k\pi}{\ell} \cos \frac{k\pi x}{\ell} \quad \text{(C.8c)}$$

All other derivatives are zero.

APPENDIX D

Plastic Moment

The stress-strain relation that describes the material behaviour under loading is bilinear with linear strain hardening. Assuming a beam subjected to pure moment M and loaded above the elastic limit, the stress and strain distribution over the cross-section is as shown in Fig. D-1 . The relations between the stress and strain are as follows:

$$\sigma = E\varepsilon \qquad \text{part OB} \qquad \text{(D.1)}$$

$$\sigma = \sigma_o + \alpha E(\varepsilon - \varepsilon_o) \qquad \text{part BC} \qquad \text{(D.2)}$$

where

σ_o = yield stress;

ε_o = yield strain;

$\alpha = \frac{E_p}{E}$;

E_p = slope of the stress-strain curve in the plastic range; and

E = slope of the stress-strain curve in the elastic range.

For a hollow section, the plastic moment M_p is given by:

$$M_p = M_1 - M_2$$

where

M_1 = plastic moment for a solid section of dimensions $b_1 x 2C_1$; Fig. D.1

M_2 = plastic moment for a solid section of dimensions $b_2 x 2C_2$

An expression for M_1 and M_2 can be derived from the moment of the internal forces on the cross-section. Thus, for

$$M_1 = 2\int_0^{c_1-h_1} \sigma y b \, dy + 2\int_{c_1-h_1}^{c_1} \sigma y b \, dy \qquad (D.3)$$

By similar triangles in the strain distribution diagram, Eqs. D.1 and D.2 can be expressed as follows:

$$\sigma = \sigma_o \left(\frac{y}{c-h}\right) \qquad (D.4)$$

$$\sigma = \sigma_b \left(1-\alpha + \frac{\alpha y}{c_1-h_1}\right) \qquad (D.5)$$

Substituting Eqs. D.4 and D.5 in Eq. D.3 and integrating, the following expression for M_1 is obtained:

$$M_1 = 2\sigma_o b_1 c_1^2 \left\{\left(\frac{1}{3} + \frac{1}{3}\frac{h_1}{c_1} - \frac{1}{6}\frac{h_1^2}{c_1^2}\right) + \alpha\left[\frac{1}{3\left(1-\frac{h_1}{c_1}\right)} - \left(\frac{1}{3} + \frac{1}{3}\frac{h_1}{c_1} - \frac{1}{6}\frac{h_1^2}{c_1^2}\right)\right]\right\} \qquad (D.6)$$

A similar expression is obtained for M_2 if b_1, c_1, h_1 are replaced by b_2, c_2 and h_2, respectively.

To calculate M_p, the ratio $\frac{h}{c}$ that describe the penetration of the plastic zone in the cross-section has to be specified. It should be noted that for beams made of material with linear strain hardening behaviour, the bending moment required to produce full plastic section is equal to infinity. Therefore, the ultimate bending resisence of such beams is set equal to the bending moment which will produce a certain predetermined amount of inelastic strain at the extreme fiber of the beam. The relation between the ratio $\frac{h}{c}$ and the maximum strain at the extreme fiber is obtained by similar triangles in the strain distribution diagram; Fig. D.1 as:

$$\frac{\varepsilon}{\varepsilon_o} = \frac{1}{1-h_1/c_1} \qquad (D.7)$$

where ε is the strain at the extreme fibre of the cross-section and ε_e is the strain at yield.

Based on the stress-strain relation shown in Fig. 3.2 the strain at yield equals 0.0017 while that at failure equals 0.0189. Assuming that the ultimate bending moment produces strain equal to 90% of that at failure, the maximum strain at the extreme fiber of the cross section will be 0.017. Substituting the magnitudes of the strain in equation D.7, the ratio $\frac{h}{c}$ will be 0.9, i.e., 90% of the cross-section is plasticized. It should be noted that a

change of 10% in the magnitude of the ultimate strain will only produce about 1% change in the value of $\frac{h}{c}$, therefore, the ratio $\frac{h}{c}$ is set to be 0.9 throughout the analysis.

Substituting $\frac{h}{c} = 0.9$ in equation D.6 yields:

$$M_1 = 2\sigma_o\, b_1 c_1^2\, [0.498 + 2.835\alpha]; \qquad (D.8)$$

therefore, the plastic moment is given by:

$$M_p = 2\sigma_o\, (b_1 c_1^2 - b_2 c_2^2)\, (0.498 + 2.835\alpha) \qquad (D.9)$$

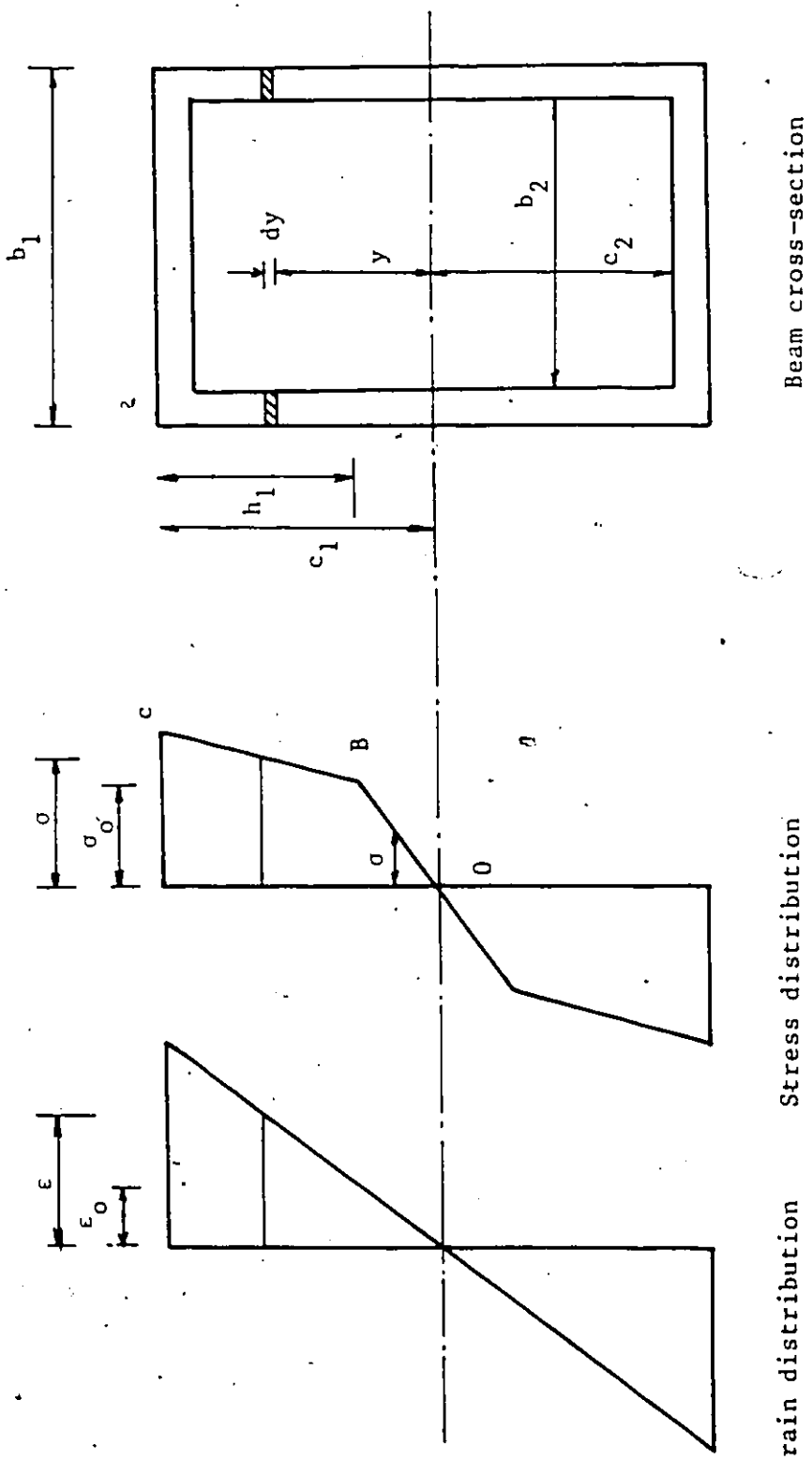

Fig. D.1 Beam loaded above the elastic limit.

APPENDIX E

Radius of Curvature

This appendix is based on the analytical method of Ref. 15. Defining θ as the angle between the x-axis and the center line of the beam model as in Fig. E-1, we find:

$$dx/ds = \cos\theta \tag{E.1}$$

Since the curvature K is equal to $d\theta/ds$, the angle θ can be expressed as follows:

$$\theta = \theta_o + \int_o^s K_1(s)ds \qquad 0 \leq s \leq s_1 \tag{E.2}$$

therefore,

$$\theta_1 = \theta_o + \int_o^{s_1} K_1(s)ds \tag{E.3}$$

and

$$\theta = \theta_1 + \int_{s_1}^s K_2(s)ds \qquad s_1 \leq s \leq s_2 \tag{E.4}$$

therefore,

$$\theta_2 = \theta_o + \int_o^{s_1} K_1(s)ds + \int_{s_1}^{s_2} K_2(s)ds \tag{E.5}$$

Substituting E.1 in E.2 and E.4 and integrating we get:

$$x_1 = \int_o^{s_1} \cos\left(\theta_o + \int_o^s K_1(s)ds\right)ds \tag{E.6}$$

and

$$x_2 - x_1 = \int_{s_1}^{s_2} \cos\left(\theta_1 + \int_{s_1}^{\bar{s}} K_2(\underline{s})ds\right) ds.$$

Therefore,

$$x_2 - x_1 = \int_{s_1}^{s_2} \cos\left(\theta_o + \int_{o}^{s_1} K_1(s)ds + \int_{s_1}^{s} K_2(s)ds\right) ds \qquad (E.7)$$

If the distance between the centers of the fixed rollers is ℓ, the distance $\frac{\ell}{2}$ to the left of the middle roller can be expressed as:

$$\frac{\ell}{2} = r_1 \sin(-\theta_o) + x_1 - r_2 \sin\theta_1$$

therefore,

$$r_1 \sin(-\theta_o) + \int_{o}^{s_1} \cos\left(\theta_o + \int_{o}^{s} K_1(s)\right) ds$$

$$- r_2 \sin\left(\theta_o + \int_{o}^{s_1} K_1(s)ds\right) = \frac{\ell}{2} \qquad (E.8)$$

Similarly $\frac{\ell}{2}$ to the right of the middle roller is:

$$\frac{\ell}{2} = r_2 \sin\theta_1 + (x_2 - x_1) + r_1 \sin\theta_2$$

therefore,

$$r_2 \sin\left(\theta_o + \int_o^{s_1} K_1(s)ds\right) + \int_{s_1}^{s_2} \cos\left(\theta_o + \int_o^{s_1} K_1(s)ds\right.$$

$$\left. + \int_{s_1}^{s} K_2(s)ds\right)ds + r_1 \sin\left(\theta_o + \int_o^{s_1} K_1(s)ds\right.$$

$$\left. + \int_{s_1}^{s_2} K_2(s)ds\right) = \frac{\ell}{2} \qquad \text{(E.9)}$$

In addition to Eqs. E.8 and E.9 two other relations can be obtained by studying the geometry of the specimen in the y-directions:

$$\sin\theta = dy/ds \qquad \text{(E.10)}$$

$$y_o = r_1 \cos(-\theta_o) \qquad \text{(E.11)}$$

$$y_1 = y_o + \int_o^{s_1} \sin\theta \, ds \qquad \text{(E.12)}$$

Substituting Eqs. E.2 and E.11 in E.12 we get:

$$Y_1 = r_1 \cos\theta_o + \int_o^{s} \sin\left(\theta_o + \int_o^{s} K_1(s)ds\right)ds \qquad \text{(E.13)}$$

also

$$y_2 = y_1 + \int_{s_1}^{s_2} \sin\left(\theta_1 + \int_{s_1}^{s} K_2(s)ds\right)ds \qquad \text{(E.14)}$$

but $y_2 = r_1 \cos\theta_2$

$$y_2 = r_1 \cos\left(\theta_o + \int_o^{s_1} K(s)ds + \int_{s_1}^{s_2} K_2(s)ds\right) \qquad \text{(E.15)}$$

Substituting E.13 and E.15 in E.14 we get:

$$r_1 \cos\left(\theta_o + \int_o^{s_1} K_1(s)ds + \int_{s_1}^{s_2} K_2(s)ds\right) - r_1 \cos\theta_o$$

$$- \int_o^{s_1} \sin\left(\theta_o + \int_o^{s} K_1(s)ds\right)ds$$

$$- \int_{s_1}^{s_2} \sin\left(\theta_o + \int_o^{s_1} K_1(s)ds + \int_{s_1}^{s} K_2(s)ds\right)ds = 0 \qquad \text{(E.16)}$$

The position of the middle roller can be related to the deflection of the beam model as follows:

The middle roller position can be defined by y_c where

$$y_c = y_1 + r_2 \cos\theta_1 \qquad \text{(E.17)}$$

$$y_c = r_2 \cos\theta_o + \int_o^{s_1} \sin\left(\theta_o + \int_o^{s} K_1(s)ds\right)ds \qquad \text{(E.18)}$$

The beam deflection δ is equal to:

$$\delta = r_1 + r_2 - y_c \qquad \text{(E.19)}$$

Equations E.8, E.9, E.16 and E.19 are used to obtain the values of θ_o, s_1, s_2 and δ which are required to describe the deformed shape of the beam model during the rolling process.

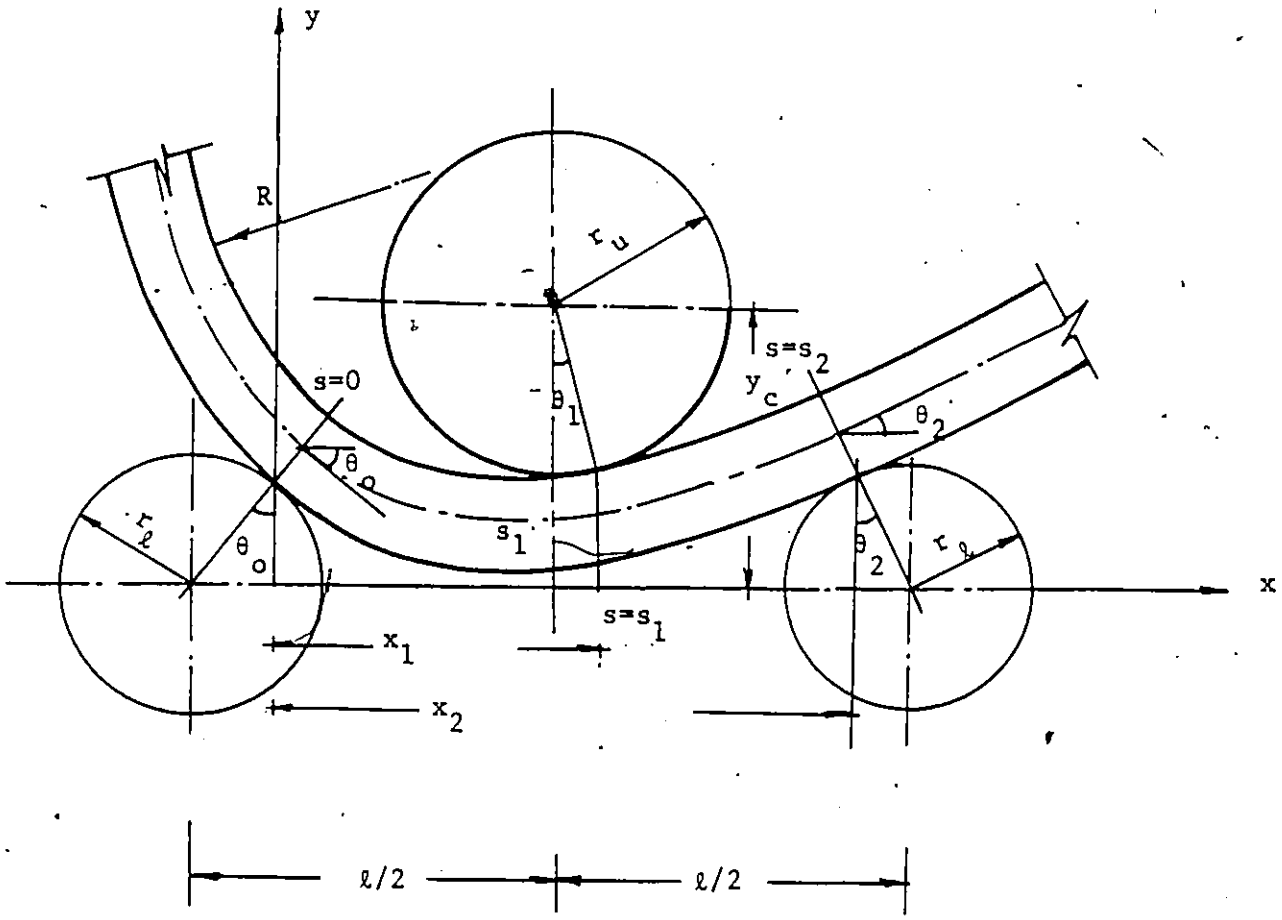

Fig. E.1. Geometry of the deflected shape at any instant of the rolling process.

VITA AUCTORIS

1952 Born on the 18th of May in Cairo, Egypt.

1970 Enrolled in the Faculty of Engineering, Cairo University, Egypt.

1975 Graduated with a Bachelor of Science Degree (honours) in Civil Engineering (Structural Division). Appointed as Teaching Assistant in the Department of Civil Engineering, Cairo University, Egypt.

1978 Enrolled in the Faculty of Graduate Studies, Carleton University, Ottawa, Canada, in a programme leading to the degree of Master of Engineering in Civil Engineering.

1980 Graduated with a M. Eng. in Civil Engineering from Carleton University, Ottawa, Canada.

1981 Enrolled in the Faculty of Graduate Studies, The University of Windsor, Windsor, Canada, in a programme leading to the degree of Doctor of Philosophy in Civil Engineering.